Chapter 19

Oscillations in terrestrial planetary atmospheres

Joseph Michael Battalio[1], Maureen Cohen[2], Peter Read[3], Juan Manuel Lora[1], Timothy McConnochie[4] and Kevin McGouldrick[5]

[1]*Yale University, New Haven, CT, United States*, [2]*Open University, Milton Keynes, United Kingdom*, [3]*Oxford University, Oxford, United Kingdoms*, [4]*Space Science Institute, Boulder, CO, United States*, [5]*University of Colorado Boulder, Laboratory for Atmospheric and Space Physics, Boulder, CO, United States*

19.1 Introduction

While the seasonal and subseasonal oscillations of Earth will always be the most easily studied, many bodies in and beyond our solar system are beginning to reveal the structure of their climates and their associated variability thanks to continued observation, both in situ and from Earth. Here, we focus on terrestrial worlds, defined as planets or moons with a defined solid surface. In the solar system, Venus, Mars, and Titan have substantial atmospheres among terrestrial bodies, though Mars's atmospheric mass is far less than the others. Each has a unique climate with a panoply of climate oscillations at the seasonal and subseasonal timescales in both the tropics (defined as regions where the large-scale circulation has Rossby number greater or equal to 1[1]) and extratropics (defined as regions where the circulation has Rossby number much less than 1[1]). The study of oscillations on other worlds is as critical as of those on Earth, as wave modulation contributes to variations in dust storms on Mars,[2–5] clouds and superrotation on Venus,[6,7] and methane convection on Titan.[4,8] Further, generalizing our understanding of climates across the solar system helps in placing Earth's climate as a member on a continuum of possible climates.[9]

19.1.1 Planetary atmospheres

19.1.1.1 Mars

Before describing climate oscillations in planetary atmospheres, we review the salient properties and general circulation features of each world (Table 19.1). Due to the multidecadal interest in Mars by multiple space agencies, Mars possesses the best-studied non-Earth atmosphere. Mars's atmosphere has been nearly continuously sounded by NASA orbiters since 1996, or Mars Year[14] (MY[114]) 24,[15,16] Companion spacecraft by multiple space agencies enable a wide array of observation modes. As a result, three reanalysis datasets have been released and are constrained primarily with radiances from polar-orbiting satellites.[17–19] However, compared with Earth reanalyses, Mars's are poorly constrained.[20] No direct wind measurements are assimilated, and temporal coverage is confined to approximately 0300 and 1500 local time.

Mars's atmosphere is the thinnest of worlds with documented climate oscillations (Table 19.1). Its surface pressure averages around 610 Pa and has an average surface temperature around 200 K.[21–24] The main constituent is carbon dioxide (approximately 95%), which deposits and sublimates from transient ice caps such that the surface pressure undergoes a doubly periodic cycle of 30%. The transport of mass results in a condensation flow in the mid and high latitudes, but the effects of this flow on the global dynamics are small.[12,13,25,26] Without any species capable of absorbing UV radiation in

1

TABLE 19.1 Planetary parameters for Earth, Mars, Venus, and Titan.[10–13]

	Radius (km)	Surface gravity (m/s^2)	Rotation rate (d)	Length of year (d)	Obliquity (deg)	Orbital eccentricity	Scale height (km)	Surface pressure (bar)
Earth	6378	9.8	1	365.2	23.5	0.017	7	1
Mars	3390	3.7	1.03	687.0	25	0.094	11	0.01
Venus	6052	8.9	243[a]	224.7	177	0.007	15	92
Titan	2575	1.4	15.9	10747[b]	27	0.052	18	1.5

[a] *Venus rotates opposite other planets.*
[b] *Taken as Saturn's.*

the upper levels, Mars lacks a stratosphere, going directly from a troposphere to a mesosphere so that the general circulation extends to altitudes as high as 100 km. Mars's obliquity and rotation rate (a Mars day, or sol, is only 39 minutes longer than an Earth day), combined with low thermal inertia due to a thin atmosphere and a lack of oceans, permit a strong seasonal cycle partly as a consequence of its large orbital eccentricity,[9,27] so Mars's tropospheric seasonal cycle is similar to that of Earth's mesosphere.[28] Perihelion around southern summer solstice (L$_s$=250°[3]) has solar insolation approximately 40% larger than aphelion at northern summer solstice (L$_s$=70°) (Fig. 19.1E–H). As a result, southern summer (Fig. 19.1H) is warmer than northern summer (Fig. 19.1E). The warmest temperatures at solstice are shifted poleward of the subsolar point due to atmospheric dynamics of the mean circulation,[28] thermal tides,[29] and gravity waves.[30–34]

Mars's orbital parameters enforce a dynamical climate regime similar to Earth's.[35,36] The zonal wind on Mars is generally in thermal wind balance with temperatures and is in balance with angular momentum conservation of the overturning circulation.[24,37] Westerly jets occur in the midlatitudes during winter, and easterlies are found in the tropics and the summer hemisphere. The northern winter jet is the stronger, due to the higher meridional temperature gradient caused by Mars's eccentricity.[28] During equinoxes, tropical easterlies weaken as westerlies shift from one hemisphere to the other (Fig. 19.1A–D), but during global dust events, superrotation is possible.[38] Mars has a direct overturning circulation at low latitudes with large scale weather systems at higher latitudes (Fig. 19.1I–L). Despite an 8 km range in terrain with northern lowlands paired with southern highlands, the Martian circulation is similar at both equinoxes. The mass streamfunction exhibits dual Hadley cells during equinoxes, with rising air near the equator and descending air around ±30°N. During solstices, one cell dominates both hemispheres, with the ascending branch in the summer midlatitudes and the descending branch in the winter midlatitudes. The southern summer cell is stronger than the northern summer cell, partly due to the topography.[39,40] Mars has a polar vortex along the edge of the Hadley cell, but unlike Earth, Mars's vortex is annular, with the highest potential vorticity (PV) just off the pole and a local PV minimum at the pole.[37,41,42] This structure appears continually generated by diabatic deposition and sublimation of CO_2 on the polar ice caps,[43,44] though more recent analyses point to dust being the more important driver.[45–47] An annulus of PV is barotropically unstable[48] so is consumed by wave activity.[49–53] Mars only has a weak indirect Ferrel cell during northern winter.

The pairing of barotropic and baroclinic eddies yields prominent high-latitude storm tracks. The strongest eddies occur in the Northern Hemisphere fall and winter[22,41,53–56] (Fig. 19.1P) but are also found throughout the year.[57–60] As Mars has a similar Rossby deformation radius as Earth, the dominant wavenumbers range from 1–4.[3,41,55,61,62] Mars's topography exhibits a wavenumber 3 structure in the north, with wavenumber 2 in the south, and transient eddies amplify within the lowland basins,[53,63,64] with stationary eddies forced by the highlands.[65]

Mars's most apparent difference from Earth is its dust storms, which also follow the seasonal cycle, partly due to the intensification of eddies.[2,3,5,66–77] Because of the thinness of Mars's atmosphere, lofted dust has a dramatic radiative impact on the temperature profile,[78] so that, from a radiative perspective, dust acts much as water vapor does on Earth.[28,36] The dust storm seasonal cycle from a typical year is shown in Fig. 19.2. Dust is always present in the atmosphere, but the second half of the year is more dusty due to stronger meridional and vertical temperature gradients resulting from increased stronger radiative forcing from perihelion. Latitudinally, dust storms and eddies generally track the edge of the

---

3. L$_s$ or areocentric longitude measures the planet's position in orbit defined such that L$_s$=0° corresponds to northern spring equinox, with L$_s$=90°, 180°, and 270° corresponding to summer solstice, fall equinox, and winter solstice, respectively.
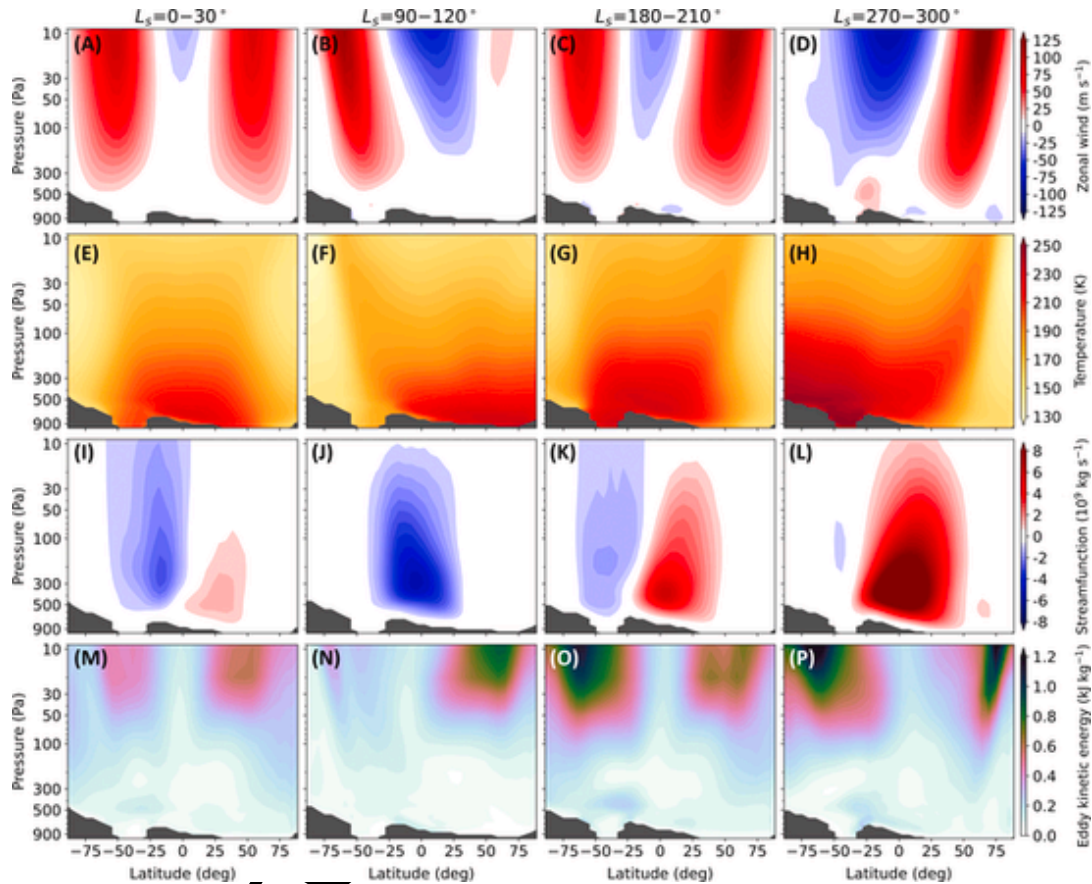
FIGURE 19.1   Seasonal, zonal-mean climatology of the Martian lower atmosphere from the EMARS reanalysis. [18] Shown are (A–D) zonal wind, (E–H) temperature, (I–L) meridional mass streamfunction, and (M–P) eddy kinetic energy for (left column) northern spring, (second column) northern summer, (third column) northern autumn, and (right column) northern winter. Positive streamfunction indicates clockwise motion. Topography is shaded dark gray.
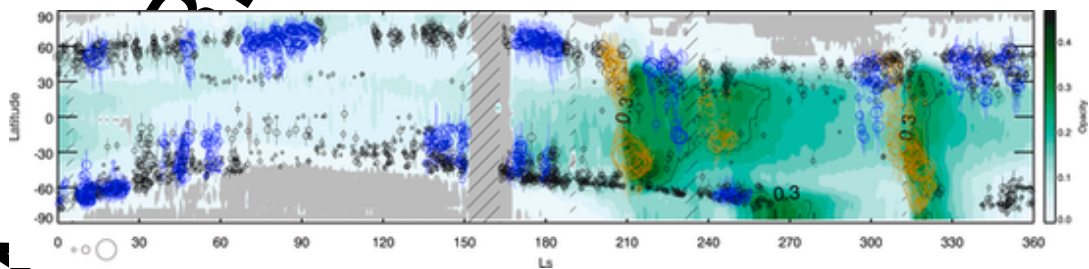

FIGURE 19.2   Representative dust storm climatology from Mars Year 31.   Circles indicate centroid latitudes and L_s of dust storm instances and are scaled by dust storm size. The three circles at bottom left indicate storms of 10^6, 5×10^6 and 10^7 km^2. Vertical lines indicate latitudinal extent. Organized activity is blue; unorganized activity is black, and "major" events are gold. Periods of missing data are hatched. Filled green contours indicate the zonal-mean dust opacity.[79] *Modified from Battalio M, Wang H. The Mars dust activity database (MDAD): a comprehensive statistical study of dust storm sequences. Icarus, 2021;354. https://doi.org/10.1016/j.icarus.2020.114059.*

polar ice cap; however, each year two large regional events "flush"[66] from the Northern to Southern Hemisphere. A northern fall event is called the "A" storm, and the spring event is the "C" storm. A yearly "B" event is confined to the Southern Hemisphere.[80] Between the A and C events, there is a solstitial pause in wave and dust activity—similar to Earth's mid-winter minimum in the Pacific[81]—which is related to stabilization of the atmosphere to baroclinic instability by dust warming.[3,82–85] Mars also has intermittent CO_2 and water ice clouds that are an important radiative driver[86,87] that predominate during the nondusty seasons.

19.1.1.2   Venus

Earth's other planetary neighbor possesses the most massive terrestrial atmosphere of the solar system, despite being only slightly smaller than Earth. Though usually closer to Earth than Mars, the Venusian atmosphere has received less attention. Renewed interest in Venus Express from the European Space Agency[88] and the Akatsuki orbiter from the Japan Aerospace Exploration Agency[89] has enabled continual observation of Venus's atmosphere over the last decade, and work is ongoing to improve general circulation models and generate reanalyses.[90]

Venus's orbit and rotation place its climate in a unique parameter space in the solar system. Venus rotates retrograde compared to the other planets, with a Venusian day of 243 Earth days. This is approximately 10% longer than the Venusian year of 225 days. As such, we pay particular attention to describing only those oscillations relevant to the seasonal to subseasonal time-scale, neglecting the diurnal tides despite the fact that their oscillation frequency can be measured in large fractions of a Venusian year.

At most wavelengths, Venus is enshrouded in clouds composed primarily of photochemically generated H_2SO_4 in several layers: an upper haze layer above 70 km, a uniform cloud layer within 57–70 km, middle cloud layer within 50–57 km, a lower cloud layer 47–50 km, and a lower haze from the bottom of the clouds down to perhaps 35 km.[91–93] The upper layer has uniform coverage, but the lower layer is more variable due to the higher vapor pressure of sulfuric acid that contributes to rapid evaporation at those altitudes.

Venus has minimal obliquity and eccentricity and therefore little seasonal climate variability (Table 19.1). However, the period of the visible clouds at approximately 70 km altitude is approximately 4 days.[94] The dominant dynamical feature of Venus is the superrotation of an equatorial jet stream. The superrotation is westward, in the same direction as planetary rotation, so is defined as a prograde jet. Speeds are consistently on the order of 100 m/s or greater between ±50°N at 50–60 km altitude, then decreasing towards 0 m/s near the poles (Fig. 19.3A).[96,97] Above 70 km, there is an easing of the winds up to 90 km, then increasing upwards. The superrotation arises from the transfer of angular momentum between the tropics and high latitudes, with a menagerie of eddies—including gravity, Rossby, Kelvin waves, and mixed versions of the three,[98–100] along with the thermal tide—playing an important role.[12,101,102]

Venus has a 92 bar surface pressure (Table 19.1) with a resulting 735 K surface temperature.[10] Temperatures generally monotonically decrease up to 100 km, with some exceptions for statically unstable layers around 55 km (Fig. 19.2A, contours), within a so-called "cold collar" around 66 km.[95,103] The cold collar surrounds the warmer polar vortex that has lower cloud heights and a rotation period of 2–3 days.[10,95,103] Venus's meridional circulation is dominated by a pair of Hadley cells at cloud height (Fig. 19.3B).

A panoply of wave modes has been observed on Venus, including a wavenumber 1, high latitude (>40 degrees) mode with a 5–6-day period.[37,104–106] Modeling studies have indicated that this mode is symmetric around the equator with the structure of a planetary Rossby wave.[98,107–109] A 4–5-day period equatorial Kelvin wave is observed as a darkening of
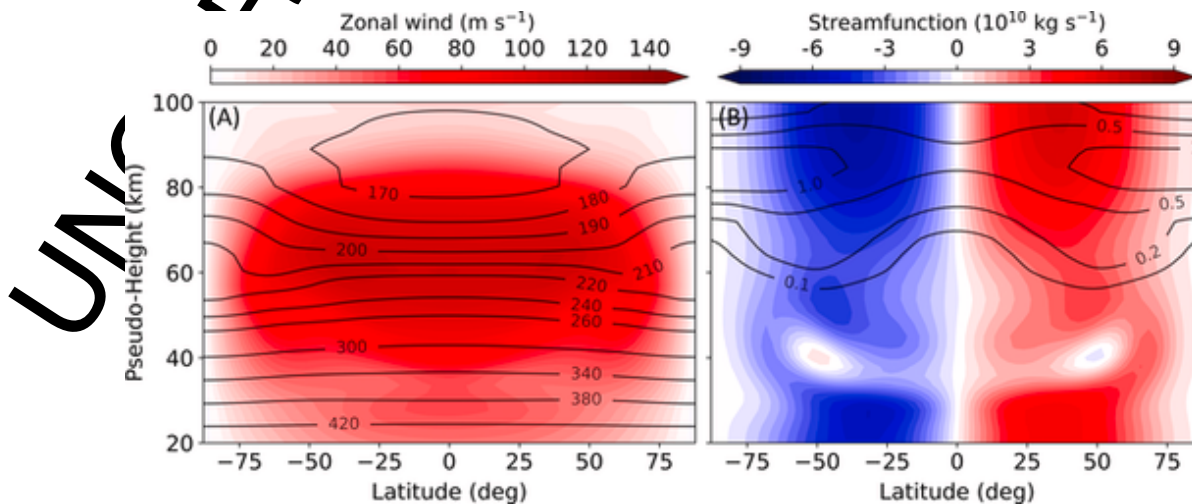

FIGURE 19.3   Venus zonal-mean climatology. Zonal-mean of time-average of Venus over three Earth months (September–December 2018) from an assimilation of Akatsuki observations.[95] Shown are (A) zonal wind, with temperature contoured (K) and (B) meridional mass streamfunction, with eddy kinetic energy contoured (kJ/kg). Positive streamfunction indicates clockwise motion.

the cloud top[110] and is suspected to be a major contributor to the maintenance of superrotation.[104,108,111,112] Their combination seems to contribute to a "Y"-shaped structure often seen at the cloud top.[94,113]

19.1.1.3 Titan

Titan, Saturn's largest moon, is unique in the solar system in being the only satellite with a massive atmosphere, as well as the only other body than Earth known to sustain an active hydrologic cycle and stable surface liquids.[114–117] But, given its distance from Earth, observation of Titan has been limited: Voyager 1 flew by Titan in 1980, and the Cassini-Huygens mission explored the Saturn system between 2004 and 2017. Along with ground-based observations, these data have enabled a thorough understanding of Titan, but nothing like continuous observation is available, precluding the creation of any reanalysis. Instead, climate models of varying complexities have been used to interrogate the principal physical processes operating in its climate system.

In terms of relevant planetary parameters, Titan's characteristics place it somewhere in between Mars (or Earth) and Venus (Table 19.1). First, Saturn's obliquity, and therefore Titan's effective obliquity with respect to the Sun, is similar to Mars's and leads to a strong seasonal cycle mediated in the lower atmosphere by the low thermal inertia surface and efficient heat redistribution,[27,118,119] despite the long radiative timescale of the atmosphere.[116] On the other hand, Titan is tidally locked to Saturn, meaning that its day is approximately 16 Earth days long, placing it into the slow rotation (high Rossby number) category, though not at the same extreme as Venus. Similarly, its atmosphere, which is primarily composed of molecular nitrogen, is considerably more dense at the surface than Earth, but, due to Titan's much lower surface gravity, confers a surface pressure (1.5 bars) only modestly larger.

Like Venus, Titan's middle atmosphere is strongly superrotating,[120] with jet speeds upwards of 200 m/s as well as a seasonal cycle that includes the formation and dissipation of winter polar vortices.[121–123] As on Venus, the superrotation arises from upgradient angular momentum transport by eddies,[124–127] likely involving various wave modes.[128] In the lower atmosphere, modest mid-latitude jets (Fig. 19.4) and weak, presumably largely retrograde flow at low latitudes[131] make up the zonal winds. The meridional flow is comprised of nearly global Hadley cells that reverse seasonally[132] (Fig. 19.4), seemingly flanked by shallow polar thermally indirect cells likely associated with traveling weather disturbances.[116]

Given its distance from the Sun, Titan's atmosphere is cold—the surface temperature is around 93 K. As a result, methane is near its triple point in Titan's environment, and the troposphere is nearly saturated with methane,[133] the replenishment source of which remains somewhat mysterious.[134] The seasonal formation of methane clouds has been thoroughly documented,[135–138] and indicates the latitudinal migration of a region of ascent, and of moist convection, associated with near-surface convergence of moisture in the Hadley circulation.[132] In addition, some observed clouds are thought to have formed because of atmospheric waves,[137,139,140] which appear to communicate their impacts across much of the globe.[8] As such, wave activity pervades Titan's lower as much as its upper atmosphere.

Another consequence of the high methane content of Titan's atmosphere is its ubiquitous haze, which is made up of particles initially formed in Titan's thermosphere from the photochemical products that result from the photodissociation of methane and nitrogen.[141] The particles descend through the atmosphere and grow by coagulation and aggregation[142,143]; in the middle atmosphere especially, they play a major role in the energy budget as they are strong absorbers of sunlight but relatively transparent in the thermal infrared.[144–146] As a consequence, Titan's vertical temperature struc-
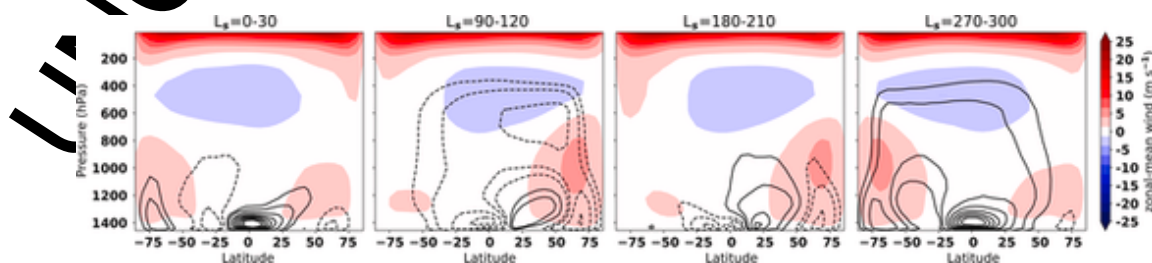

FIGURE 19.4   Seasonal, zonal-mean climatology of Titan's lower atmosphere.   Shown are zonal winds (colors) and meridional mass streamfunction contoured every 10^9 kg/s for (left column) northern spring, (second column) northern summer, (third column) northern autumn, and (right column) northern winter. Solid streamfunction contours indicate clockwise motion. Data taken from the Titan Atmospheric Model[129,130] averaged over 30° of L_s. *Modified from Battalio JM, Lora JM, Rafkin S, Soto A. The interaction of deep convection with the general circulation in Titan's atmosphere. Part 2: impacts on the climate. Icarus, 2022;373. https://doi.org/10.1016/j.icarus.2021.114623.*

ture includes a distinctive stratosphere.[147,148] The haze also obscures the surface from view in the visible and complicates spectroscopic studies of Titan's atmosphere and surface.

19.1.2   Other oscillations

The terrestrial worlds of the solar system all have several types of oscillations within the timescale of subseasonal to seasonal variability. This excludes several climate oscillations that do not have exact Earth counterparts yet fall outside the scope of this chapter. For completeness, it is worthwhile to note those oscillations that cannot be covered in detail here: Due to the short radiative times scales on Mars, diurnal tides achieve large amplitudes over tens of K and have multiple modes, like migrating, sun-synchronous, westward propagating, and nonmigrating Kelvin waves.[43,54,149–171] Venus, too, has diurnal tides of wavenumber 1 (diurnal), 2 (semidiurnal), 3, and 4.[10,172]

Short-period, individual traveling waves on Mars range in wavenumber 1–4 with periods of 2–10 or more Mars days.[3,22,41,53,55–57,59–65,173] Venus has transient wave variability as well, with a wavenumber 1 Kelvin mode over the equator with a period of approximately 4 days that propagates westward at approximately 15 m/s. A second wavenumber 1 mode appears to be an extratropical Rossby wave with an approximately 5-day period that propagates retrograde against the zonal mean winds with a phase velocity over 30 m/s.[7,104,174–178] These are observed in cloud-tracked winds and in brightness variations.[6,112,179,180] Their most obvious influence is in the "Y"-feature in clouds[181–183] and bow wave.[184] Titan also appears to have transient eddies with periods of a few Titan days.[8,116,137,139,140]

Seasonal variability is also important in planetary atmospheres.[11,27,185] Inter-seasonal variability is particularly important on Mars, as Mars's polar vortices have irregular variability,[45] and the Martian storm tracks weaken in each hemisphere's winter in a solsticial pause, which has varying intensity every year.[53,55,56] Titan's atmosphere also varies seasonally, with a winter polar vortex[121–123] and infrequent bursts of cloud cover.[138]

Venus also has longer periodicities, including a 12.5-Earth year cycle in cloud-level winds,[186] but the most obvious multiyear variability in a terrestrial atmosphere beyond Earth is Mars's infrequent global dust events that happen every few Mars years on average but range from twice a year to only one every 7 or 8 Mars years.[67,187–199]

19.2   Annular modes

We begin the discussion of seasonal to subseasonal oscillations in planetary atmospheres with an overview of annular modes (for a discussion of Earth's annular modes, see Chapters 10 and 11). In Earth's, Mars's, and Titan's atmospheres, the variability of the synoptic-interseasonal time scale of the large-scale extratropical atmosphere is dominated by annular modes. Annular modes are zonally symmetric structures of internal climate variability that correlate along lines of latitude.[200] Annular modes arise from the internal dynamics of the atmosphere[201,202] and explain much of the weekly to monthly variability of the jet stream, synoptic-scale wave activity, and precipitation[203–207] so are vital to understanding and forecasting transient weather patterns. The modes are quantified on either the zonal-mean atmosphere or along single hemispheric pressure levels,[201,206–208] using empirical orthogonal function (EOF) analysis.[203,209,210] EOF analysis decomposes a spatiotemporal dataset into multiple functions (of the same spatial dimensions as the analyzed dataset) that are determined by statistical relationships within the dataset. Each EOF of the dataset is paired with a principal component (PC) time series (of the same duration as the original dataset). This PC describes the temporal evolution/amplitude of the EOF at every time step of the dataset.[203]

19.2.1   Barotropic annular modes

Two types of annular modes exist within the atmosphere of Earth, each with multiple spatial structures. The first mode is defined as the first EOF of, equivalently, anomalous (nonseasonal) surface pressure,[206,211] geopotential height,[201,203] or zonal-mean zonal wind between 1000–200 hPa and 20–80 degrees latitude.[204,207] This mode appears separately in both the Northern and Southern Hemispheres: the Northern annular mode (NAM), or Arctic oscillation, and Southern annular mode (SAM), or Antarctic Oscillation, each explain 20%–30% of the variance in the zonal-mean wind, geopotential height, or surface pressure in their respective hemispheres.[201] The NAM/SAM represent shifts in atmospheric mass between the polar regions and the middle latitudes. By convention, the PC, called the annular mode index, is positive when the zonal-mean jet moves poleward, and anomalous low pressure resides over the poles. The negative index specifies times when the jet moves equatorward with anomalously high surface pressure at the pole.

The spatial structure of the annular mode, the EOF, in the zonal-mean zonal wind, [u] (where the square bracket denotes the zonal mean) appears as a vertically uniform dipole, which reflects the poleward and equatorward motion of the

jet. (The second EOF of [u], representing the next most important spatial and temporal pattern of variation, is tri-polar; that is, it has three centers of the action—by convention a positive pole centered on the time-mean jet maximum and negative poles to the north and south—that indicate the strengthening and sharpening of the jet.[207,212,213]) In Earth's atmosphere, the dipoles have maximum action around 300 hPa; the positive node resides around ±60°N, with the negative around ±40°N.[205,214]

Paired with the dipole of [u] is a monopole of eddy momentum fluxes, [u^*v^*] (where v is the meridional wind and asterisks denote deviations from the zonal mean) around ±50°N.[205,215,216] The maximum eddy momentum fluxes precede the PC maximum, generally by one day. The positive polarity of the mode also associated with warm conditions in the midlatitudes and cool conditions at the pole and subtropics.[217] Aloft, warm regions align with anomalous ascent, and cool regions align with descent. However, the NAM/SAM only has a weak signature in eddy fluxes of heat, [v^*T^*], and eddy kinetic energy.[217–219] The vertical uniformity of the wind signature and importance of [u^*v^*] associated with this mode indicate it is a barotropic feature; that is, it is vertically aligned with limited vertical wind shear or meridional temperature gradients.[204,207,216,218] These north-south displacements have important implications for Earth's general circulation,[220] sea ice extent,[221] cloud incidence,[222,223] and storm tracks.[224–231] In the Northern Hemisphere, the NAM is related to the North Atlantic Oscillation as representing the polarity of the annular mode in only the Northern Atlantic sector.[232,233]

The NAM/SAM has two relevant timescales. First, the modes can be modeled generally as red noise with a decorrelation time of approximately 10 days,[220,234] so directly forecasting the mode is difficult. However, recently, the NAM/SAM have been found to have a periodicity of approximately 150 days due to feedbacks between each of leading the two EOFs of the zonal wind on each other [207] but also through cross-feedbacks exerted through the variation of [u^*v^*].[213,235] This timescale is only associated with a mode that propagates with time[236,237] such that the anomalous zonal wind field emerges in low latitudes and propagates coherently poleward. In this regime, EOF 1 and EOF 2 have a sizable correlation at lags of ±10 days, which can be interpreted as one EOF pattern drifting latitudinally with time to overlap the initial time pattern of the other EOF. (Note, by construction, there is no correlation at lag 0.)

19.2.1.1 Mars

19.2.1.1.1 Early modeling analysis and observations

Mars shares many dynamical climate features with Earth, as noted in Section 19.1.2.1, and the seasonal cycles of eddies and dust storms, along with the Martian topography, induce familiar but unique climate oscillations compared to Earth's. The annular modes are one of these shared climate oscillations. The potential for annular oscillations on Mars was first recognized in a pair of modeling efforts. Using the GFDL Mars General Circulation Model (MCGM),[152] the annular modes were calculated on the anomalous logarithm of surface pressure ($\ln p_s$).[238] The first two EOFs of $\delta \ln p_s$ were each dipoles of p_s centered on 70°N, with the second EOF rotated 90 degrees of longitude from the first. Their PCs were offset by a phase of $\frac{\pi}{2}$, meaning the modes were in quadrature for the same mode, with a periodicity of 6–8 sol. This corresponds with the known traveling wavenumber 1 baroclinic wave.[41] Combined EOF 1 and 2 explained over 50% in $\delta \ln p_s$ in the Northern Hemisphere; explained variance in the Southern Hemisphere was small due to topographic effects. The annular mode was similar to the SAM in Earth's atmosphere with a minimum pressure at the pole, but the mode was found in EOF 3, explaining only 6% of the variance. Interestingly, the associated PC of the EOF 3 occasionally achieved a stable state in either polarity for periods of 20–30 sol at a time.

Several years later, a second team addressed the annular mode question using an independently developed model,[238] the Center for Climate System Research (CCSR)/University of Tokyo Mars Global Circulation Model (MGCM).[239] Once again, the first two EOFs of surface pressure selected the traveling wavenumber 1 baroclinic mode as explaining approximately 50% of the variability. EOF 3 contained a mixture of an annular structure and wavenumber 2; EOF 4 was offset in phase from EOF 3 but decayed poleward of 70°N. EOF 3 exhibited a dipole of action on the zonal-mean zonal wind, with the positive pole centered along 50–60°N. This is similar to the NAO on Earth, so EOF 3 was deemed the Martian Annular Oscillation (MAO). With this clear annular signal in the model, the Transformed Eulerian Mean equation was applied to composites of the largest MAO deviations.[240,241] The most salient feature of the analysis was that wave forcing, as diagnosed by the difference in the divergence of Eliassen-Palm flux [216,242] between the positive and negative MAO polarities, exhibited a dipole matching zonal-mean structure of the annular mode in the zonal-mean wind. Further, wavenumber 1 waves generated this forcing, but wavenumber 3 and higher waves contributed little.

These initial indications of annular variability being of lesser importance in Mars's than Earth's atmosphere stem from several unavoidable issues. While the MGCMs were state-of-the-art for the time, their results were hampered by a lack of in-situ data, as they were forced by a prescribed dust climatology. The amplitudes of the traveling waves in the GFDL MGCM showed that wavenumber 1 was overrepresented in the model versus wavenumbers 2 and 3,[238,243] and the sea-

sonality of the modes if they were the wavenumber 1 traveling wave did not match observations of the solstitial pause.[56,238] Additionally, the EOF analysis was performed on 2-sol average data, which would eliminate the approximately 2-sol wavenumber 3 mode. Given the importance of the eddy momentum fluxes for setting the mode in Earth's atmosphere, it may not be surprising that the annular mode appeared unimportant in the MGCM used. The anomalies were calculated as a function of sol-by-year subtracted from only a limited number of years, neglecting that stationary waves on Mars are not completely stationary and instead shift slightly over many tens of sols.[154,244–247] Finally, annular modes should be calculated on data weighted by the square-root of latitude ($\sqrt{\cos\phi}$), instead of $\cos\phi$, since EOF analysis operates on variance. As noted for Earth's modes, weighting by $\cos\phi$ elevates the annular modes to EOF 3,[248] just like the initial Mars modeling studies found. Despite this, these MGCM results demonstrated that annular variability is an important source of climate variability in the Northern Hemisphere of Mars,[238,239] but the seeming reduced importance of the modes has necessitated a reevaluation of their influence on the Martian climate in observations and reanalyses.

The brightness temperatures representative of thermal emission spectrometer (TES) temperature observations were analyzed from the MGCM simulations but lacked annular structures in the top three EOFs.[238] This could be because annular modes are not typically defined from upper-level temperatures; however, the modes should be related to the geopotential height—a quantity derivable from temperature. Further, the nature of the TES dataset limits analysis to only 111 sols in duration, which restricts any long-period variability. Nevertheless, a reevaluation of the TES-retrieved daytime geopotential height between 370–30 Pa for Northern Hemisphere winter during MY 24 and Southern Hemisphere winter during MY 25 points to the existence of annular modes (Fig. 19.5). Anomalous column heights are calculated by removing a 100-sol rolling mean from the timeseries at each location. The Northern Hemisphere annular mode is in EOF 3 (Fig. 19.5A); EOFs 1 and 2 are wavenumber 1 structures like in the MGCMs.[238,239] Yet, the annular mode in TES temperatures explains 17.4% of the variance despite being EOF 3 in the Northern Hemisphere. A minimum in EOF 3 occurs at the pole, and a ring of positive anomalies appears at 60°N. The Southern Hemisphere annular mode in anomalous column heights is in EOF 1 (Fig. 19.5B), explaining a similar 20.8% of the temperature variance. EOF 1 exhibits a ring of positive anomalies around 45–60°S with a minimum at the pole. These annular signatures in the column geopotential height anomalies demonstrate that modes of variability occur prominently in observations and prompt an investigation of modes in Martian reanalyses.
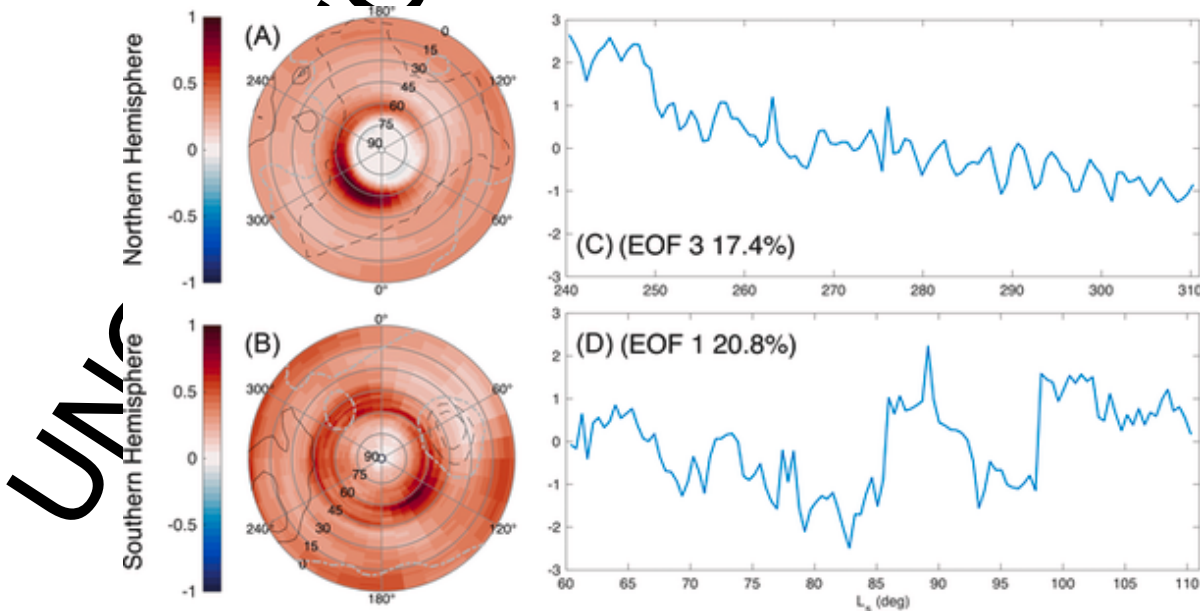

FIGURE 19.5   Spatial signature of Mars's annular mode in anomalous geopotential height between 370 and 30 Pa from the Thermal Emission Spectrometer on Mars Global Surveyor.   (A and B) Empirical orthogonal function and corresponding (C and D) principal components for (A and C) Northern Hemisphere and (B and D) Southern Hemisphere. The PCs are normalized by their standard deviation. The panel titles for (C an D) indicate the percent of variance explained and which EOF contains the annular mode. Topography is shown in 2000 m increments in (A and B), with the 0 m contour dot-dashed in gray and negative contours dashed.

19.2.1.1.2   Reanalysis

Reanalysis datasets are enabling rapid advances in the understanding of Mars's atmospheric dynamics, despite the relatively limited data assimilated compared to Earth's reanalyses. Two have been used to study annular modes on Mars,[4] the Mars Analysis Correction Data Assimilation (MACDA, v1.0)[17] and the Ensemble Mars Atmosphere Reanalysis System (EMARS, v1.0).[18] For MY 24–27, they both assimilate Thermal Emission Spectrometer retrievals [15] from the Mars Global Surveyor. EMARS also contains MY 28–32, generated from Mars Climate Sounder (MCS) retrievals[249] onboard the Mars Reconnaissance Orbiter. The two instrument eras exhibit different abilities to constrain the underlying dynamical cores of each reanalysis, so differences between years of TES and MCS should not necessarily be attributed to interannual variability[45,53,62]; however, averaging the annular modes across both eras for EMARS does not substantively skew the analysis of the annular modes.[4]

With these reanalysis datasets, annular modes can be calculated for Mars in the same way as for Earth. After linear detrending and de-seasoning using a 100-sol running mean, an EOF analysis of the surface pressure or $[u]$ reveals an MAO that explains larger portions of variance of their respective fields than for Earth.[4] The first (and second, not shown) EOF of the anomalous surface pressure exhibits a pressure minimum at the pole in MACDA and both EMARS instrument eras (Fig. 19.6). The Northern Hemisphere has a deeper pressure minimum (Fig. 19.6A, C, and E) than the Southern Hemisphere (Fig. 19.6B, D, and F), partly due to the lower surface pressure in the south as a result of higher topography. The surrounding zonal ring of positive surface pressure anomalies in the Northern Hemisphere is more focused in Utopia (approximately 75°–175°E, approximately 30°–60°N) followed by Acidalia (approximately 300°W–15°E, approximately 30°–60°N) Planitia, not unlike how the NAM on Earth has its zonal ring maximized in the North Pacific and Atlantic.[206] Similarly, the zonal ring in the Southern Hemisphere is maximized around Argyre (330°E) and Hellas (60°E) Basins, with a tertiary peak in Terra Sirenum between 180 and 240°E (Fig. 19.6B, D, and F). Each MAO explains more surface pressure variance than Earth's, between 19% and 39%.
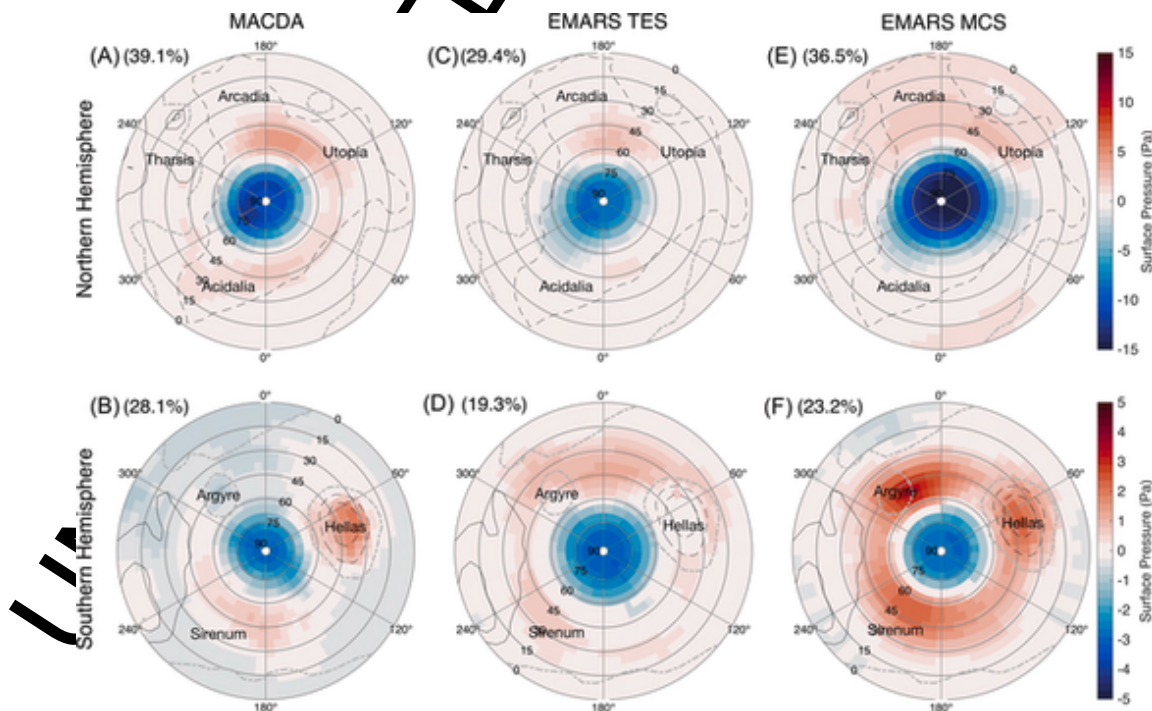

FIGURE 19.6   Annular modes in surface pressure in Martian reanalysis.   Spatial signature of EOF 1 in anomalous surface pressures on Mars for both reanalysis datasets. (A and B) MACDA, (B and D) EMARS-TES and (E and F) EMARS-MCS for (A, C, and E) Northern Hemisphere and (B, D, and F) Southern Hemisphere. The panel titles indicate the percent of variance explained. Topography is shown in 2000 m increments with the 0 m contour dot-dashed in gray and negative contours dashed. Each panel has salient topographical features labeled. Only regressions exceeding 99% confidence are shown. *Adapted from Battalio JM, Lora JM. Annular modes of variability in the atmospheres of Mars and Titan. Nature Astronomy, 2021;5(11): 1139–1147. https://doi.org/10.1038/s41550–021–01447–4.*

The first EOF of $[u]$ in the Northern Hemisphere and second EOF for the Southern Hemisphere for both reanalyses exhibit a dipole feature, similar to that of Earth (Fig. 19.7A–D) which, like Earth's, is barotropic—that is, vertically aligned.[204,207] The dipole bisects the $[u]$ (Fig. 19.7A–D, contours) and represents the movement of the jet north-south so that the poleward motion of the jet is associated with lower surface pressure. The northern MAO in EOF 1 explains 33%–39% of the $[u]$ variance depending on the reanalysis used. The southern MAO in EOF 2 explains somewhat less of the variance, 21%–28%. The centers of action of the annular modes are located at ±70°N for the positive pole and ±40°N for the negative pole, centered at approximately 100 Pa (approximately 20 km altitude). The southern EOF 1 is monopolar but only captures slightly more variance than EOF 2 (approximately 25%–35%). The differences between which EOF of the MAO matches Earth's structure may be due to the dichotomous terrain on Mars that could disrupt the north-south movement of the jet in the Southern Hemisphere. Variations in structure for EOF 1 and 2 are not uncommon for Earth either and may signify differences in the representation of the jet stream.[212,214]

A characteristic of Earth's NAM/SAM is association with anomalous $[u^*v^*]$,[207,217] which the MAO (EOF 1 in the north and EOF 2 in the south) also displays. At 1-sol lag $[u^*v^*]$ is located in the node between the mode's centers of action (±50–60°N). The fluxes are stronger in the MACDA dataset (Fig. 19.7I and J) but are also present in EMARS (Fig. 19.7K and L) (possibly due to differences in jet amplitude in EMARS[37] and stronger in the Northern versus Southern Hemispheres). The divergence of $[u^*v^*]$ corresponds to convergence of momentum in the positive pole and divergence of momentum in the negative pole during positive index and vice versa during the negative index. The southern EOF 1 does not correspond to a barotropic, eddy-related, NAM/SAM-like mode. As it is monopolar, its associated $[u^*v^*]$ divergence
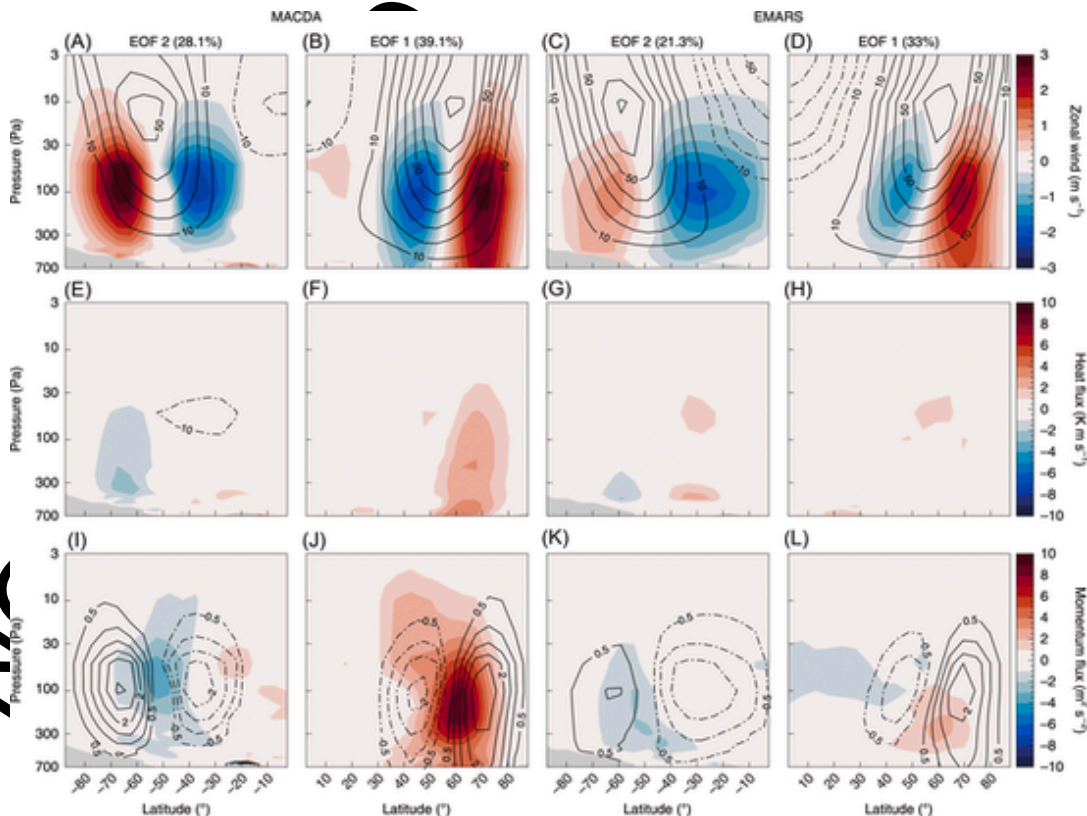

FIGURE 19.7   **Mars barotropic annular mode from reanalysis.**   Spatial signature of the Mars Annular Mode (MAO) as the dipolar EOF in anomalous zonal-mean zonal wind for both reanalysis datasets. (A, E, and I) MACDA Southern Hemisphere, (B, F, and J) MACDA Northern Hemisphere, (C, G, and K) EMARS Southern Hemisphere, (D, H, and I) EMARS Northern Hemisphere. (A–D) Time-average, zonal-mean zonal wind (contours every 10 m/s) and regressions of the MAO onto anomalous zonal-mean zonal wind (shading). The individual column titles indicate which EOF corresponds to the MAO and give the percentage of variance explained. Topography is shaded in gray. (E–H) Regressions of the MAO onto anomalous zonal-mean eddy kinetic energy (contours every 10 m^2/s^2) and anomalous eddy heat flux at -1-sol lag (shading). (I–L) Contours duplicated from shading in the top row (contours every 0.5 m/s, with dashed contours indicating negative values) and the anomalous eddy momentum flux at -1-sol lag (shading). Only regressions exceeding 99% confidence are shown. *From Battalio JM, Lora JM. Annular modes of variability in the atmospheres of Mars and Titan. Nature Astronomy, 2021;5(11): 1139–1147. https://doi.org/10.1038/s41550–021–01447–4.*

cannot drive the changes in jet amplitude. This EOF may be more related to driving of the jet via angular momentum conservation from the Hadley cell[24] so is not strictly related to the internal dynamics of the southern MAO. The MAO (EOF 1 in the Northern Hemisphere and EOF 2 in the Southern Hemisphere) regresses only weakly on the anomalous $[v^*T^*]$ and eddy kinetic energy (Fig. 19.7E–H contours), similarly to Earth's NAM/SAM.[214,219] This is particularly true for EMARS, but for MACDA, there is a weak relationship to poleward $[v^*T^*]$ (Fig. 19.7E–H). The weak association with $[v^*T^*]$ indicates that the MAO, like Earth's NAM/SAM, is not baroclinic.

Up to this point, we have only described the spatial patterns of variability of the MAO, but its index (PC) denotes the intensity and sign. The largest features are spikes due to global dust storms at MY 25, $L_s=180°$ and MY 28, $L_s=270°$ (Fig. 19.8A). The largest regular repeating cycle is the seasonal cycle of the amplitude in the north that maximizes around northern winter at $L_s=270$ degrees, which is clearer in the MCS era. The seasonal changes are the most important cycle in the MAO in the north; a yearly cycle is not evident in the Southern Hemisphere. The time series spectrum of the MAO has a red noise spectrum (Fig. 19.9A) with an average e-folding time of 41.8±1.5 sol, which is considerably larger than
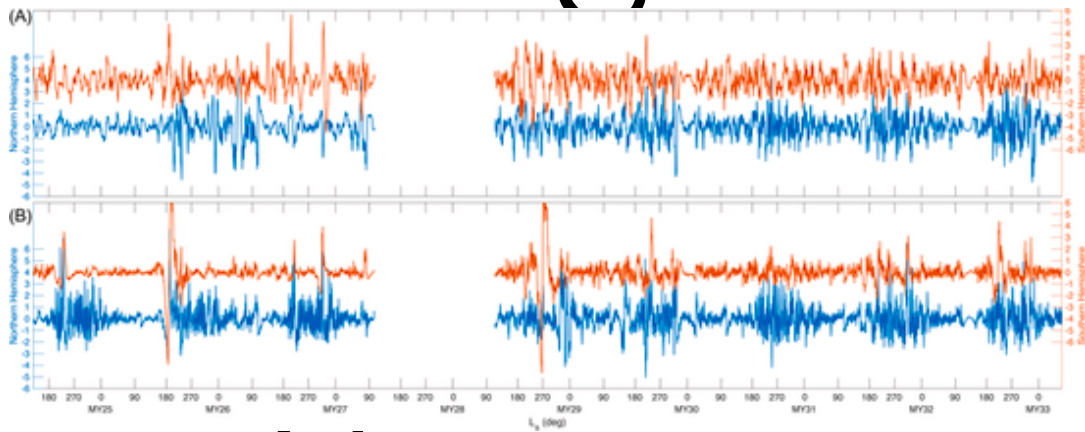

FIGURE 19.8   Principal component time series of the two Martian annular modes. Principal components from the EMARS reanalysis of the (A) MAO and (B) MBAM for the Northern (blue) and Southern (orange) hemispheres. The gap in data during MY 28 is due to the change from the Thermal Emission Spectrometer era to the Mars Climate Sounder era.
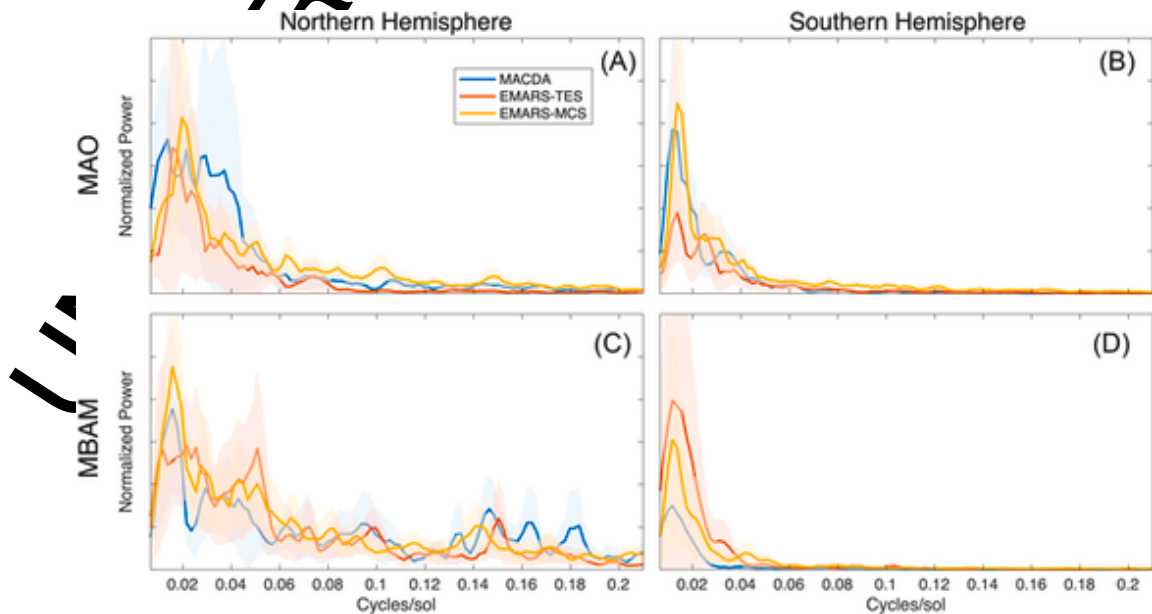

FIGURE 19.9   Power spectra for the Martian annular modes. Power spectra of the principal components associated with the Martian annular modes for the (A and C) Northern hemisphere and (B and D) Southern Hemisphere. (A and B) Spectra of the index of the MAO. (C and D) Spectra of the index of the MBAM. The 95% confidence intervals are shaded.

the NAM/SAM time of 10 days.[207] The spectra are calculated from successive 500-sol timeseries that overlap by 250 sols and are then averaged.[217]

19.2.1.2 Titan

Though Titan inhabits a different regime of atmospheric dynamics than Mars, indications of near-surface baroclinic waves[126,129] and upper-level barotropic waves[124,125,128] suggest the potential for substantial climate variability. Indeed, many seemingly annular structures have been observed in Titan's atmosphere, likely linked to the strongly zonal flow, but nevertheless deserving of further scrutiny.

A readily observable feature of Titan's atmosphere is a strong seasonal north-south axisymmetric asymmetry in the stratospheric haze, which forms and dissipates as a result of transport of aerosols from the spring or summer hemisphere into the fall or winter hemisphere, with a phase that depends on the depth of the atmosphere probed.[250–253] Beyond this phenomenon, various annular structures of different brightnesses than their surroundings have been observed in the haze, including polar bands,[252] equatorial bands,[254] and weaker features at other latitudes.[255–257] The seasonal atmospheric circulation has been implicated in all cases, with, in particular, the upwelling branch of the meridional circulation likely associated with the low-latitude bands.[254,257] At the poles, an additional process of haze scavenging by cloud particles (of various compositions) condensing during polar night is likely important.[252,258–260]

Lower in the atmosphere, clouds composed of methane have been observed for nearly one Titan year with a variety of observatories.[138] While the location of tropospheric methane clouds has been clearly tied to the seasons and is connected to the surface sources of methane,[116,261] a subset of these clouds exhibit banded morphologies reminiscent of annular structures.[138,139,255] Shearing and stretching by the superrotating winds aloft is a likely explanation,[255] but waves of various types have been invoked to explain cloud phenomena,[8,137,140] making the possibility of more organized oscillations an intriguing one.

Though quite different from Mars and Earth, Titan, too, appears to support annular modes of variability in anomalous zonal-mean zonal wind,[4] based on simulations with a state-of-the-art Titan general circulation model.[129,130,261,262] The annular mode in $[u]$ (labeled here as the Titan Annular Oscillation, TAO) is dipolar, but the centers of action are stacked vertically (Fig. 19.10A and B) as opposed to horizontally as on Mars or Earth. The TAO explains approximately 68% of the variability of the $[u]$ in the domain from the surface to 0.05 hPa and ±8–90°N, which is substantively more than for Earth or Mars. The PC of the TAO is defined similarly to Earth's so that the positive polarity indicates anomalously low surface pressure at the pole (not shown). With this convention, the negative polarity pole resides at 300 hPa—just under the tropopause—at ±50°N, while the weaker positive polarity peak resides near the lowest vertical extent of the jet at 1100 hPa and ±70°N. This vertically stacked structure represents vertical shifts of the jet, as opposed to the horizontal oscillations of Earth's and Mars's jet mode. The TAO is characterized by westward $[u]$ anomalies and poleward anomalous eddy momentum flux colocated at the negative polarity pole of the mode but also weaker poleward $[u^*v^*]$ with the eastward $[u]$ anomalies in the positive polarity pole (Fig. 19.10I and J). There is little association between the TAO and eddy kinetic energy, but the TAO does capture poleward $[v^*T^*]$ near the surface in the midlatitudes and equatorward $[v^*T^*]$ around 300 hPa (Fig. 19.10E and F). As well as being associated with anomalously low surface pressure at the pole, the TAO associates with a ring of anomalous mass-integrated eddy kinetic energy between ±30 and 45°N (not shown), which is different from the modes on Mars and Earth and may be related to nonbaroclinic waves modulating the jet.

The time series of Titan's modes are unique from those of Mars and Earth in being characterized by brief and infrequent peaks (Fig. 19.11A). The TAO is especially distinguished by rare bursts, happening only two or three times over a 20-Saturn year simulation; the variability of the TAO is red with an e-folding time-scale of 43.9±0.9 Titan days, possibly owing to the long duration of the Titan year and day.

19.2.2 Baroclinic annular modes

The second type of annular mode—the Baroclinic annular mode (BAM)—has only more recently been documented.[217,263,264] The BAM is described by the first EOF of anomalous zonal-mean eddy kinetic energy (EKE), $[K_e] = \frac{1}{2}\left[u^{*2} + v^{*2}\right]$, where square brackets denote the zonal-mean, and asterisks indicate departures from the zonal-mean. The BAM has a clearly zonally symmetric component and comes in northern and southern flavors, explaining 43% and 34%, respectively, of the variance in the EKE for Earth.[214,217,219] This mode associates with anomalous $[v^*T^*]$ and varies nonmonotonically with height, indicating a baroclinic nature; that is, the mode structure has strong vertical wind shear and meridional temperature gradients. Earth's BAM is associated with anomalous warm temperatures between ±50° and 60°N that correspond to warming driven by poleward $[v^*T^*]$, and the BAM projects weakly onto the anomalous
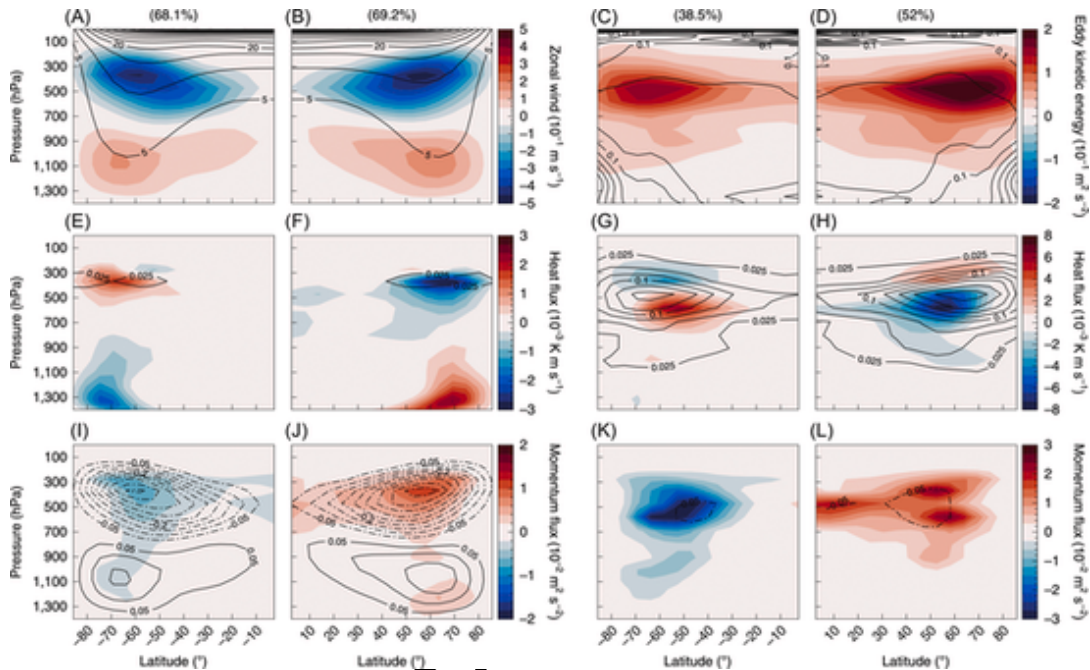
FIGURE 19.10   Annular modes for Titan from the Titan atmospheric model. Zonal-mean structure of the annular modes in zonal-mean zonal wind (TAO, left two columns) and eddy kinetic energy (TBAM, right two columns) on Titan from the Titan atmospheric model. (A and B) Time-average, zonal-mean zonal wind (contours every 5 m/s) and regression of the TAO onto the zonal-mean zonal wind (shading). (C and D) Time-average, zonal-mean eddy kinetic energy (contours every 1×10^{-2} m²/s²) and regression of the TBAM onto the zonal-mean eddy kinetic energy (shading). The individual column titles give the percentage of variance explained. (E–H) Regressions onto the anomalous zonal-mean eddy kinetic energy (contours every 2.5×10^{-2} m²/s²) and the anomalous eddy heat flux at 0-day lag (shading) for the TAO (E and F) and TBAM (G and H). (I–L) Regressions onto the anomalous zonal-mean zonal wind (contours every 1×10^{-2} m/s) and anomalous eddy momentum flux at −1 day lag for the TAO (I and J) and TBAM (K and L). Only regressions exceeding 99% confidence are shown. *From Battalio JM, Lora JM. Annular modes of variability in the atmospheres of Mars and Titan. Nature Astronomy, 2021;5(11): 1139–1147. https://doi.org/10.1038/s41550–021-01447–4.*
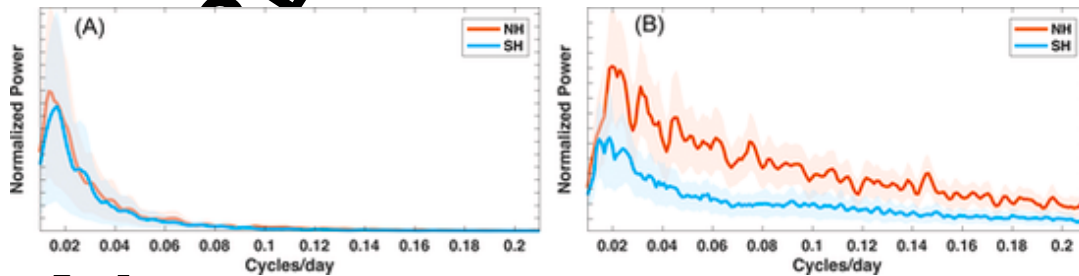

FIGURE 19.11   Power spectra of the principal components of Titan's annular modes. Spectra of the principal component time-series of the (A) TAO and (B) TBAM from the Titan Atmospheric Model simulation. The 95% confidence intervals are shaded.

$[u^*v^*]$.[212-265] The BAM PC index associated with the EOF spatial structures is defined such that positive values correspond to increased anomalous $[K_e]$, and negative values correspond to decreased $[K_e]$. Earth's BAM, as defined from zonal deviations of EKE, and NAM/SAM are essentially uncorrelated at any lag. Further, Earth's BAM is only weakly correlated to $[u^*v^*]$, and the NAM/SAM is uncorrelated to $[v^*T^*]$.[212,214,219] However, if the BAM is instead defined from EKE using transients (deviations in time instead of deviations from the zonal mean), a weak relationship between the BAM to $[u^*v^*]$ and to the NAM/SAM appears[398,399], indicating that processes with strong zonally asymmetric components within the storm tracks, like downstream development[266-270] are important to connecting the barotropic and baroclinic modes.[271]

19.2.2.1 Mars

The first indications of a BAM on Mars came from an analysis of dust storm activity.[5,74] A recurring path of storms in the Aonia-Solis-Valles Marineris (ASV) (0°–45°S, 0°–100°W) region exhibits a curious repeatability at approximately 20 sol during late winter in the Southern Hemisphere.[2] This periodicity is reminiscent of the periodicity in Earth's storm tracks due to the BAM. An analysis of $[K_e]$ during Southern Hemisphere spring from MACDA revealed an annular mode[2] exhibiting a monopole at 50°–60°S during L_s=120°–195° (not shown) and sharing many characteristics with Earth's BAM. The mode exhibits a periodicity remarkably similar to that of the terrestrial BAM of approximately 20 sols and matches the pulses in the ASV dust storm track[2] (Fig. 19.12). Individual years, indicated by the thin colored lines in Fig. 19.12, show a great deal of variability, but the average spectrum, shown in black, peaks at approximately 20 sol. The slightly different timescale for the ASV annular mode compared to Earth's BAM may result from the different radiative and dynamical time scales of Mars and Earth. This observational evidence motivated more extensive analysis of the BAM on Mars.

The first EOF of the anomalous zonal-mean EKE mode resembles Earth's BAM,[214,219] which we denote the MBAM (Mars BAM). The MBAM exhibits a monopole structure that overlaps the maximum time-average EKE. The first EOF explains 48%–65% of the anomalous zonal-mean EKE (Fig. 19.13A–D), which is substantially more than the BAM on Earth.[214,219] The MBAM maximizes within ±60°–70°N and 10–150 Pa and is robust across both hemispheres and reanalysis datasets.

Like Earth's BAM, the MBAM links to anomalous poleward eddy heat fluxes (Fig. 19.13E–H). The fluxes vary with height, indicating that the MBAM is a baroclinic mode. The northern MBAM in both reanalyses relates to intense $[v^*T^*]$ along 60°N, though the heat fluxes in MACDA are stronger at the surface (Fig. 19.13F) than EMARS (Fig. 19.13H), potentially due to the stronger representation of baroclinic eddies near the surface by the TES instrument versus MCS,[53,62] which is not included in MACDA. The southern EMARS has similarly intense poleward $[v^*T^*]$ as the Northern Hemisphere (Fig. 19.13G), but the southern MACDA has substantively weaker $[v^*T^*]$ that are absent at the surface (Fig. 19.13E), potentially due to the reduction in baroclinic eddies during global dust events.[51] Mars years with a global dust event represent a larger portion of the MACDA (approximately 1/3 of all years) dataset than EMARS (approximately 1/4 of all years).

While the BAM must be defined with a particular type of EKE—transient EKE ($[K_e']$)—to directly relate to eddy momentum fluxes,[271,272] the MBAM possesses a more general relationship to the MAO. The MBAM has a strong association to $[u^*v^*]$ (Fig. 19.13I–L); this association is double that between $[u^*v^*]$ and the MAO (Fig. 19.7I–L). There are several potential reasons why the MBAM, regardless of the type of EKE used, takes barotropic characteristics. First, the Mars transient storm tracks are generated by baroclinic and by barotropic processes, potentially due to the unstable polar vortex.[45,48,51,52,273] Second, stationary waves on Mars are especially amplified due to topography[245,247] and contribute to an EKE defined using anomalies from a zonal mean. Third, the Martian storm track is particularly zonally symmetric,[53,55] so EKE defined from anomalies from a zonal mean captures more of the storm track processes as for EKE defined from time deviations compared to Earth.
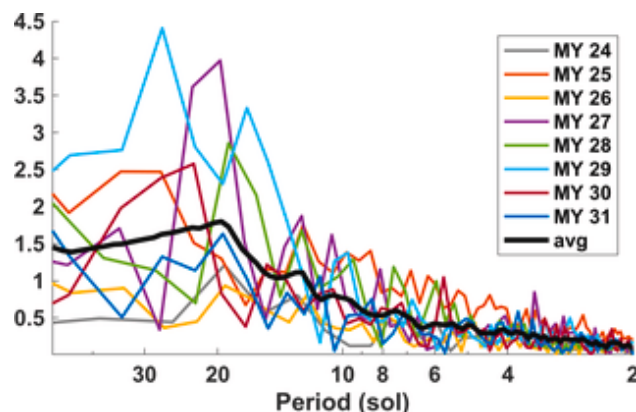

FIGURE 19.12   Power spectrum of Mars's dust activity.   Power spectrum derived from the time series of dust storm area from the Aonia-Solis-Valles Marineris (0°–45°S, 0°–100°W) storm track in Mars's Southern Hemisphere. Colors indicate different Mars years. The averaged spectrum is depicted with a thick black line. The peak occurs at approximately 20 sol. *Modified from Battalio M, Wang H. The Aonia-Solis-Valles dust storm track in the Southern Hemisphere of Mars. Icarus, 2019;321: 367–378. https://doi.org/10.1016/j.icarus.2018.10.026.*
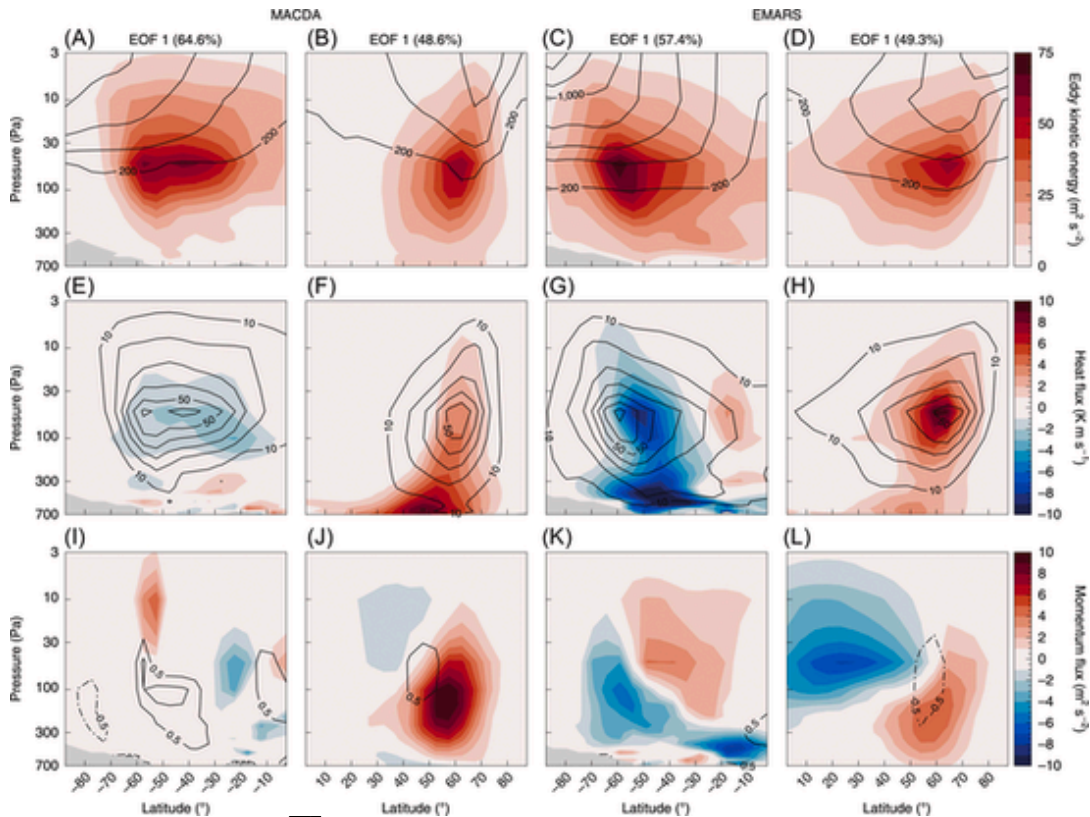
FIGURE 19.13 **Mars Baroclinic annular mode from reanalysis.** Signature of the Mars Baroclinic annular mode (MBAM) for the MACDA (left two columns) and EMARS (right two columns) reanalysis datasets. (A, E, and I) MACDA Southern Hemisphere, (B, F, and J) MACDA Northern Hemisphere, (C, G, and K) EMARS Southern Hemisphere, (D,H,I) EMARS Northern Hemisphere. The individual column titles indicate which EOF corresponds to the dipolar mode and give the percentage of variance explained. Topography is shaded in grey. (A–D) Time-averaged zonal-mean eddy kinetic energy (contours every 200 m² s⁻² and regressions onto the anomalous zonal-mean eddy kinetic energy (shading). (E–H) Contours duplicated from shading in the top row (contours every 10 m²/ s²) and the anomalous eddy heat flux at 0 sol lag (shading). (I–L) Regressions of the mode onto zonal-mean zonal wind (contours every 0.5 m/s with dashed contours indicating negative values) and the anomalous eddy momentum flux at 0 sol lag (shading). Only regressions exceeding 99% confidence are shown. *From Battalio JM, Lora JM. Annular modes of variability in the atmospheres of Mars and Titan. Nature Astronomy 2021;5(11): 1139–1147. https://doi.org/10.1038/s41550–021–01447–4.*

Given that, the MBAM is defined here from a purely zonal-mean field, the annularity of the mode warrants investigation through analysis of the vertically integrated EKE:

$$\langle EKE_{\lambda,\phi}\rangle = \frac{1}{2g}\int_{p_t}^{p_s} \left(u^{*2} + v^{*2}\right) dp, \tag{19.1}$$

where p_s is the pressure at the surface, $p_t = p_s \times 1.5 \times 10^{-3}$ is the pressure at the top of the Martian reanalyses, $g = 3.71$ m/s², λ is longitude, and ϕ is latitude.[3] In regressing the PC from the MBAM in each hemisphere onto anomalous $\langle EKE_{\lambda,\phi}\rangle$ (with anomalies as the deviations from de-trended, <100-sol timeseries), the Martian storm tracks are prominently distinguished. The anomalous $\langle EKE_{\lambda,\phi}\rangle$ peaks within 45°–75°N and 15°–60°S (Fig. 19.14A and B). While these are clearly annular structures, individual sectors stand out, like how Earth's BAM associates most strongly with individual storm tracks over the Pacific and Atlantic Ocean.[214,274–276] In the Northern Hemisphere, the association between the MBAM and $\langle EKE_{\lambda,\phi}\rangle$ is strongest near Acidalia (330°E), Arcadia (210°E), and Utopia (120°E) Planitiae. In the Southern Hemisphere, $\langle EKE_{\lambda,\phi}\rangle$ in Argyre Basin (330°E) in particular but also Hellas Basin (60°E) exhibits a strong link to the southern MBAM. All three planitiae in the north and two basins in the south have pronounced transient waves,[2,3,51–53,55,63,277] so the northern and southern MBAM describe the zonal-mean intensity of the collective storm track—the MBAM is annular.

Earth's BAM is related not just to the EKE that quantifies storm intensity but also to the impactful weather resulting from transient eddies, like precipitation.[214,223,278] Similarly, the MBAM describes the connection between transient ed-

Mars (MACDA/EMARS)

(A) Northern Hemisphere

(B) Southern Hemisphere

Titan (TAM)

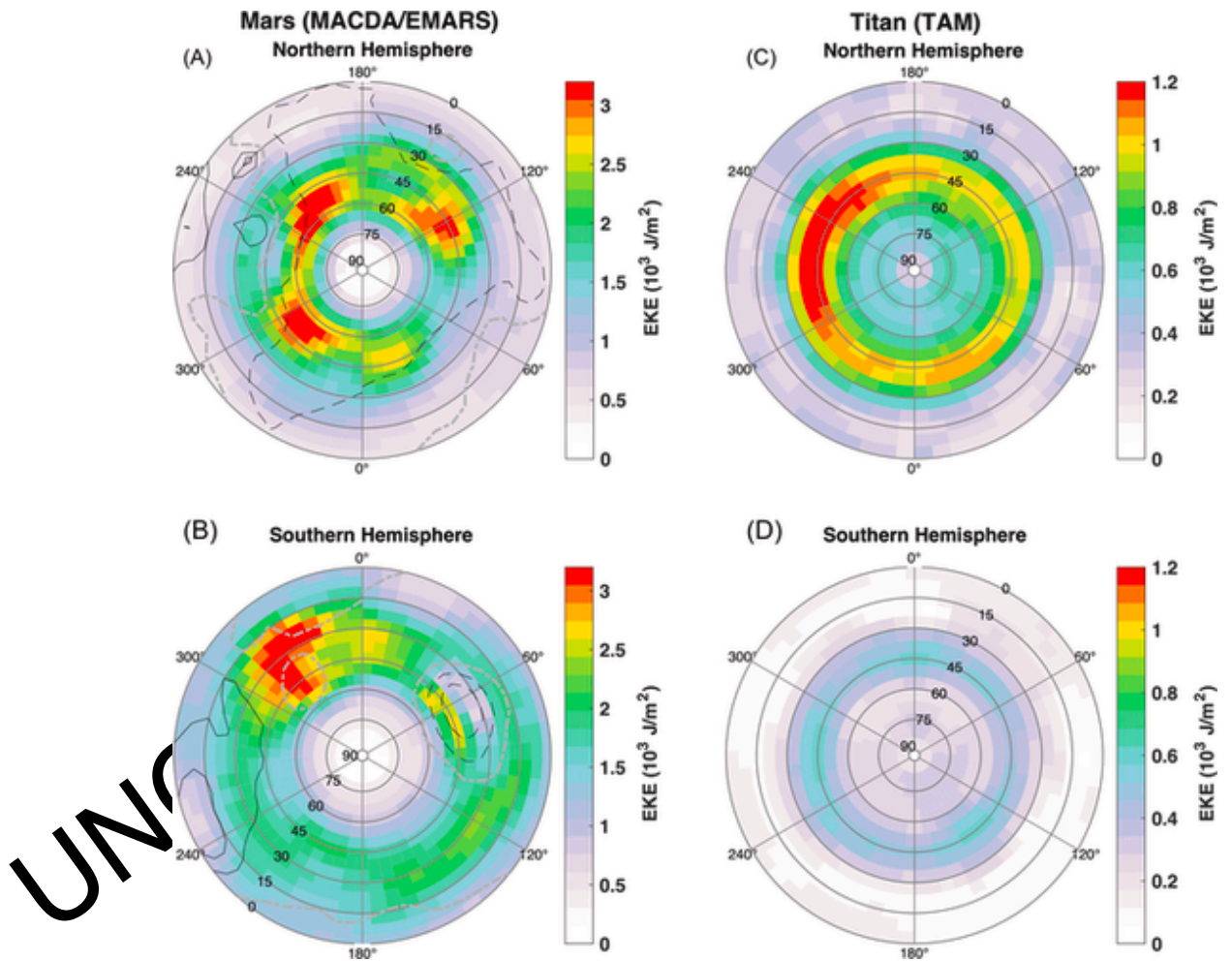(C) Northern Hemisphere

(D) Southern Hemisphere

FIGURE 19.14   Signature of the MBAM and TBAM on eddy kinetic energy.   Polar plots of vertically integrated eddy kinetic energy regressed onto the MBAM a   TB Hemisphere. (B and D) Southern Hemisphere. For Mars (A and B), topography is shown in 2,000 m increments with the 0 m contour dot-dashed in gray and negative contours shown for Titan (C and D). Only regressions >99% confidence are shown. *Modified from Battalio JM, Lora JM. Annular modes of variability in the atmospheres of Mar and 2021;5(11): 1139–1147. https://doi.org/10.1038/s41550–021-01447–4.*

dies and their most impactful weather feature: regional dust storms.[4,5,73,74] The three planitiae where large, regional dust activity originates each fall, which are the same regions where transient waves maximize, are identified when the northern MBAM is regressed to lag four sols behind the dust activity (Fig. 19.15A). That is, dust storms initiate before the MBAM—therefore $[K_e]$ —maximizes. When the timing relationship between the northern MBAM and dust activity is reversed so that the MBAM leads dust storms by four sols, the areas in the Southern Hemisphere, like the highlands between Argyre and Hellas Basins, where dust storms flush into from the Northern Hemisphere, are highlighted (Fig. 19.15B) at a rate of over 1 dust storm per 10 sols. This indicates that only after transient eddies in the north maximize does dust activity propagate into the south, a result confirmed by individually investigating regional dust events.[3,279]

The lead/lag relationship between sensible weather and the MBAM is like how Earth's BAM lags precipitation by one day.[214] The difference between the one-day versus four-sol lag could be related to the residence time for dust. Precipitation on Earth is relatively rapid compared to the multisol growth required to achieve a large dust event,[5,280,281] while dust can remain in the atmosphere for months,[79,198] so the amplification of the northern MBAM induces consequences for the atmosphere for potentially months afterwards. The fact that the intensity of the MBAM has predictive capabilities versus the lagging relationship for the BAM on Earth suggests that eddies must be of sufficient amplitude preceding the dust growth in the Southern Hemisphere to permit cross-equatorial flushing.[3,66] This may enable rudimentary predictive capabilities if Mars's northern transient waves can be monitored sufficiently well in real-time. Further research is required to determine the generality of the relationship for the northern MBAM and if a relationship exists beyond the ASV track for the southern MBAM.[2]
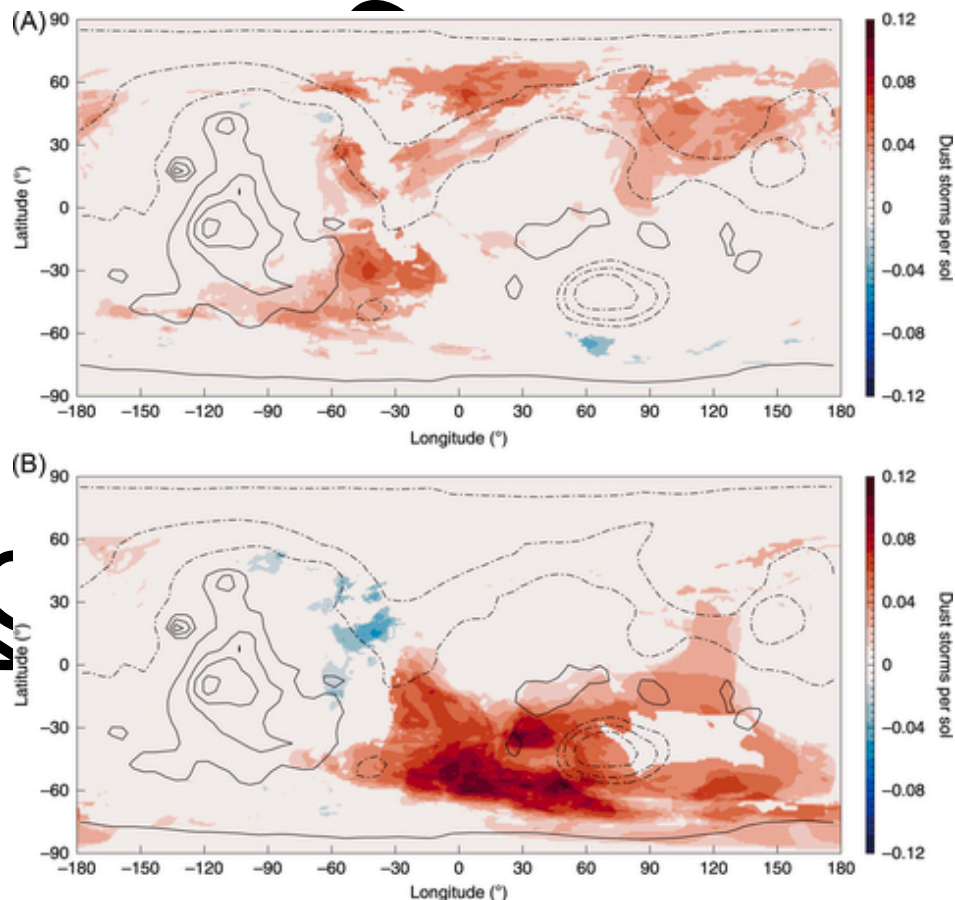

FIGURE 19.15   Signature of the MBAM on Mars dust storms.   Regression of the northern MBAM on the Mars Dust Activity Database for MY 31 during the dusty season (L_s=180°–360°). (A) Dust activity leading the MBAM by 4 sols. (B) Dust activity lagging the MBAM by 4 sols. Regressions are shown at >95% confidence. Topography is shown in 2000 m increments with the 0 m contour and negative contours dot-dashed. *From Battalio JM, Lora JM. Annular modes of variability in the atmospheres of Mars and Titan. Nature Astronomy, 2021;5(11): 1139–1147. https://doi.org/10.1038/s4155 0–021-01447–4.*

A yearly cycle is most evident in the northern MBAM, which becomes most amplified when transient wave activity is maximized during the fall and winter and displays a lull during the solstitial pause.[3,52,53,55,56] The northern MBAM spectrum is also approximately red, with an e-folding time of 13.9±1.1 sol (Fig. 19.9C), like Earth's BAM. There are some indications of elevated power at higher frequencies at 20 sol (0.05/sol),[2] with additional power around the periods of individual baroclinic waves, or 5–7 sol. The southern MBAM is dominated by long-period power, with a time-scale of 115±3 sol, arising from the rare occurrence of global dust storms (Fig. 19.9D). Combined with the finding that the spatial patterns of variability during global dust storms are highly correlated to the patterns without global storms ($r>0.95$), this indicates that global dust storms merely amplify existing spatial patterns of annular variability instead of generating additional modes. If the MAO and MBAM are calculated using only the fall and winter seasons then comparing them to the full-reanalysis calculated structures, they are correlated at $r>0.95$, but this is not the case during the spring and summer seasons. Thus, annular variability appears more important in the autumn and winter for Mars, as apparent from the magnitude of the PCs during those seasons.

19.2.2.2   Titan

Again analyzing a 20-Saturnian year simulation from the Titan Atmospheric Model,[4] Titan's BAM (TBAM) is somewhat different from baroclinic modes elsewhere in the solar system. The TBAM has a monopole of action near 500 hPa and ±60°N (Fig. 19.10C and D) that is displaced from the maximum of the time-average $[K_e]$, which is above 100 hPa (Fig. 19.10C and D, contours). Nevertheless, the TBAM explains 38.5% and 52% of the Southern and Northern Hemisphere variability in $[K_e]$. A second difference of the TBAM from Earth's or Mars's BAM is that the regression of the TBAM onto anomalous eddy heat fluxes, $[v^*T^*]$, exhibits a vertical dipole of action, so that above the TBAM monopole, heat is fluxed poleward, and below the TBAM heat is transported equatorward (Fig. 19.10G and H). This means that below the TBAM's center of action, any waves providing EKE at these levels are not baroclinic.[265,270,282] Instead, these waves might be barotropic or tropical-like since the TBAM regresses more strongly on eddy momentum fluxes, $[u^*v^*]$, (Fig. 19.10K and L) than the TAO (Fig. 19.10I and J). This is more similar to Mars's MBAM than Earth's BAM, which may be due to the zonal symmetry of Titan's storm track[130] owing to the lack of large-scale topography.[283] That the TBAM also projects strongly onto $[u]$ (Fig. 19.10K and L, contours) indicates that the waves involved with the TBAM may not force the superrotating jet.

Like Earth's BAM and Mars's MBAM, the TBAM is truly an annular structure as evidenced by projecting the TBAM on $\langle EKE_{\lambda,\phi}\rangle$ (Eq. 19.1). This exhibits a ring around each pole around ±35–65°N (Fig. 19.14C and D), which is noted to be a latitudinal corridor for baroclinic waves.[8,261]

The TBAM operates on shorter timescales than the TAO, with an e-folding time-scale of 8.0±0.2 Titan days (Fig. 19.11B). This suggests that timescales for the annular modes follow dynamical and radiative timescales across worlds. Interestingly, like the TAO, the TBAM is distinguished by rare bursts that occur several times per year. Each of the mode-correlated events represents the occurrence of large-scale overturning of the troposphere by a large methane storm.[8] Moist convection on Titan has long been expected to be infrequent but intense,[284,285] an expectation seemingly borne out by observations[286] and simulations.[287] Indeed, a so-called relaxation-oscillator convection regime appears to operate on Titan[288] as has been proposed for Earth-like hothouse climates.[289] These storms are connected to the thermodynamic buildup of Convective Available Potential Energy that is periodically released by traveling wavenumber 1, baroclinic Rossby waves at the high latitudes.[8] The convective initiation then triggers a cascade of tropical wave modes, as well as gravity waves to completely overturn the boundary layer, whereupon the potential energy begins slowly building again. Thus, Titan's modes have a clear connection to moisture, like Earth's modes,[290] whereas Mars's do not because Mars is dry.

In summary, Earth, Mars, and Titan all experience annular modes; given the ubiquity of annular features elsewhere in the solar system, like Venus's cold collar[92,95,103,291] and Jupiter's prominent jet structure,[292–296] future simulations may continue to further the understanding of annular modes, jets, and storm tracks throughout the solar system.

19.3   Other oscillations

Beyond the annular modes, Mars and Venus each have additional atmospheric oscillations at subseasonal to yearly timescales. Mars has a SAO, as well as long-period waves. Venus has oscillations at approximately 255, 150, and 50 days.

19.3.1   Mars

19.3.1.1   Semiannual oscillation

The possibility that Mars exhibits a cyclic oscillation in its zonal wind analogous to the semiannual (SAO) or quasi-biennial oscillations (QBO) in the Earth's stratosphere and mesosphere was first examined using a MCGM[297] that found evidence for cyclic variations in the zonal mean temperature on the equator, as measured by the TES instrument on Mars Global Surveyor,[298] with a period of half a Mars year.

Like the QBO in the Earth's stratosphere, Earth's SAO manifests as a cyclic reversal of the zonally averaged zonal wind, but with a period of just 6 months (in contrast to the QBO's mean period of around 27 months[299,300] and a typical peak amplitude of around 30 m/s[299,301,302]). Both the SAO and the QBO were discovered from observations (mainly rocket soundings) in the Earth's tropics in the 1960s[303] and are widely understood to arise largely from the nonlinear effects of upward-propagating waves from the troposphere as they grow in amplitude with the decrease in density, encounter critical layers and dissipate, depositing momentum and accelerating zonal velocity.[300,301] The direction of the resulting zonally symmetric flow is determined by the horizontal phase speed of the dominant waves at the altitude where they are dissipated, and the cyclic variation arises through a competition for dominance at different altitudes between eastward and westward propagating waves. In the case of Earth's SAO, however, the westward phase of each cycle is also strongly influenced by the zonally symmetric overturning circulation in the stratosphere and mesosphere, which is partly diabatically driven and is strongly controlled by the seasonal cycle.[304] This leads to a close synchronization of the oscillation to the seasonal cycle with a period of precisely 6 months, with peak westward winds occurring around each solstice when the cross-equatorial meridional flow is strongest. This is in contrast to Earth's QBO, which seems to be almost entirely wave-driven in both its eastward and westward phases, though some evidence exists for its partial and sporadic synchronization with rational multiples of the annual cycle.[305] The tropical SAO on Earth actually exhibits two distinct maxima in amplitude, one near the stratopause at around 45 km altitude and another near the mesopause at an altitude of around 80 km,[301] though both seem to be mutually phase-coherent. Although it is strongest close to the equator, its influence is observed to extend at least into midlatitudes.

In common with many other studies of wave-zonal flow interaction,[301,306] the maintenance of the zonally averaged zonal flow can be understood with reference to the Transformed Eulerian Mean (TEM) zonal momentum equation, which can be written as

$$\frac{\partial \overline{u}}{\partial t} = \left(f - \frac{1}{a\cos\phi} \frac{\partial}{\partial \phi} (\overline{u}\cos\phi) \right) \overline{v^*}^{[1]} - \overline{\omega^*} \frac{\partial \overline{u}}{\partial p}^{[2]} + \frac{1}{\rho_0 a\cos\phi} \nabla \cdot \mathbf{F}^{[3]} + \overline{\mathbf{X}}^{[4]}$$

(19.2)

where $f = 2\Omega \sin\phi$ is the Coriolis parameter, a is the planetary radius, ϕ is latitude and the overbar denotes a zonal average. (v^*, ω^*) represents the TEM meridional circulation velocity (in pressure coordinates) with components defined by $[\omega^+] = \left[\omega] + \frac{\partial}{\partial\varphi} \left(\frac{[v^*\theta^*]}{\frac{\partial[\theta]}{\partial p}} \cos(\varphi) \right) \right]$; $[v^+] = \left[v] - \frac{\partial}{\partial p} \left(\frac{[v^*\theta^*]}{\frac{\partial[\theta]}{\partial p}} \right) \right]$

$F = \left(F^\phi, F^p \right)$ is the Eliassen–Palm (EP) flux representing the stress-induced upon the zonal mean wind by waves and eddies, with components given by

$$F^\phi = \rho_0 a\cos\phi \left(\frac{\partial[u]}{\partial p} \left(\frac{[v^*\theta^*]}{\frac{\partial[\theta]}{\partial p}} \right) - [u^*v^*] \right); \qquad F^p$$

$$= \rho_0 a\cos\phi \left(\left[f - \frac{1}{a\cos\phi} \frac{\partial}{\partial\phi} ([u]\cos\phi) \right] \left(\frac{[v^*\theta^*]}{\frac{\partial[\theta]}{\partial p}} \right) - [u^*\omega^*] \right).$$

$\overline{\mathbf{X}}$ represents a residual due to nonconservative forces such as friction or other forcings. Analyses of observations (mainly via assimilated reanalyses) and numerical model simulations indicate that Earth's SAO is mainly driven via the zonal mean advection terms [1] and [2] in Eq. (19.2) during the westward phase of the oscillation and the eddy stress convergence during the eastward phase, dominated by fast equatorial Kelvin modes and others such as shorter wavelength

gravity waves.[304,307,308] The identification of which waves make the most significant contributions to driving the SAO, however, is still not well established because of difficulties in obtaining suitable observations at these altitudes.

Another study[297] analyzed simulations of the Martian atmospheric circulation using their version of the Center for Climate System Research/National Institute of Environmental Studies (CCSR/NIES, Japan[309]) GCM.[310] Their analysis focused on variations in circulation ±10°N of the equator during the seasonal cycle in a multiannual run that imposed variations of the total dust loading that emulated observations during the TES observational period. Their results confirmed the presence of a semiannual period oscillation in the zonal wind, $[u]$, over the equator with an amplitude of up to 20 m/s, and with a reversal of phase above 5 Pa, somewhat similar to what is observed on Earth with the mesospheric SAO. The oscillation exhibited some seasonal asymmetry with significant differences occurring between the northern and southern summer solstices, especially during the MY 25 planet-encircling dust storm. This was attributed largely to the effects of hemispheric differences in Martian surface topography[39] which induces significant differences in the strength of the equator-crossing Hadley circulation between solstices by mechanically blocking the cell in some longitudinal sectors. Seasonal variations in dust loading also have an impact, especially during major dust storms, both of which were confirmed in simulations that used either uniform dust or flat topography.

Their analysis of the terms in Eq. (19.2) above for the latitude band ±10°N of the equator confirmed the major contribution to the westward forcing by the zonal mean TEM meridional circulation, peaking at the solstices. This was mainly associated with the correlation between $[v^{+}]$ and the northward gradient of $[u]$ and was substantially enhanced when dust loading was increased to emulate the MY 25 planet-encircling storm. The eddy forcing of $[u]$ by the EP flux divergence or convergence by waves resolved in their model [term [3] in Eq. (19.2)] was further decomposed by zonal and temporal Fourier harmonic, with notable contributions from (i) stationary planetary waves (i.e., those with periods >30 sols), (ii) westward propagating harmonics with a diurnal period representing the diurnal tides and (iii) eastward propagating Kelvin modes with diurnal period that result from interactions between the diurnal tide and zonally varying topography.[155] The stationary planetary waves were seen to contribute mostly eastward forcing at altitudes below 50 Pa with an annual period but with semiannual forcing at higher altitudes that opposed that due to the zonal mean circulation. This contrasts significantly with the role of stationary planetary waves on Earth. The westward thermal tides provided most of the eastward semiannual forcing via the mechanism found for Earth,[311] peaking during the equinoxes, in which eastward zonal momentum is deposited where the diabatically driven waves are generated and westward momentum deposited where they dissipate. The diurnal period Kelvin modes were found to contribute weak westward forcing more or less all the time. The latter is somewhat surprising given that Kelvin waves propagate eastwards and are usually assumed to be driven from below, dissipating at higher altitudes. The reason for this is not clear, though may be an artifact from the use of a fixed dust loading for the run analyzed, which may underrepresent the forcing of Kelvin waves in the lower atmosphere.

A similar analysis using the fully assimilated MACDA reanalysis for MY 24–27[17] was performed[312] based on the same TES temperature and dust observations as used by the MGCM analysis.[297] This provided more comprehensive coverage in both space and time than considered by previous MGCM studies[297] with a model that was more closely constrained by the available synoptic observations. This dataset also revealed a clear signal of a SAO in each of the 3 Mars years covered by the reanalysis. Fig. 19.16 shows a time-height series of $[u]$ in each of 7 latitude bands covering the entire planet. The SAO is clearly seen not only in the equatorial band (Fig. 19.16D) but also in the mid-latitude bands up to ±60°N, though mostly at high altitudes (above 1 Pa or 60 km in the 40°–60° latitude bands). This indicates a somewhat similar spread of influence of the SAO across the planet on Mars as seen on Earth.[301] In line with the MGCM study,[297] zonal winds are broadly westward around the solstices at most latitudes except towards the north polar regions and below 100 Pa in midlatitudes. Eastward flow prevails at most latitudes during equinoxes though with a significant bias towards stronger eastward winds in the north and some significant interannual variability.

Analysis of the forcing of $[u]$ based on Eq. (19.2) has also been performed for the MACDA reanalysis.[312] Fig. 19.17 summarizes these results for the tropical latitude band within 10° of the equator. Similar to the MGCM study,[297] the TEM meridional circulation (Fig. 19.17A) dominates the forcing of the westward phases of Mars's SAO at the solstices in the tropics, with the southern summer forcing being much stronger than in northern summer. The strongest westward forcing occurs in MY 25 during the major dust storm event in southern summer. This is also somewhat offset by the vertical advection term [Eq. (19.2), term [2]; Fig. 19.17B]. The total eddy forcing [Eq. (19.2), term [3]; Fig. 19.17C] also exhibits a strong semiannual signal at most altitudes from 100 to 1 Pa which is largely in antiphase with Eq. (19.1), term [1]. The EP flux divergence term was decomposed into several components with the addition of a transient eddy term representing time-varying waves and eddies that have periods unrelated to the diurnal cycle [312] (Fig. 19.17E). This contribution in the tropics is relatively weak (a few m/s/sol) but with a definite semiannual signal with eastward forcing around solstices
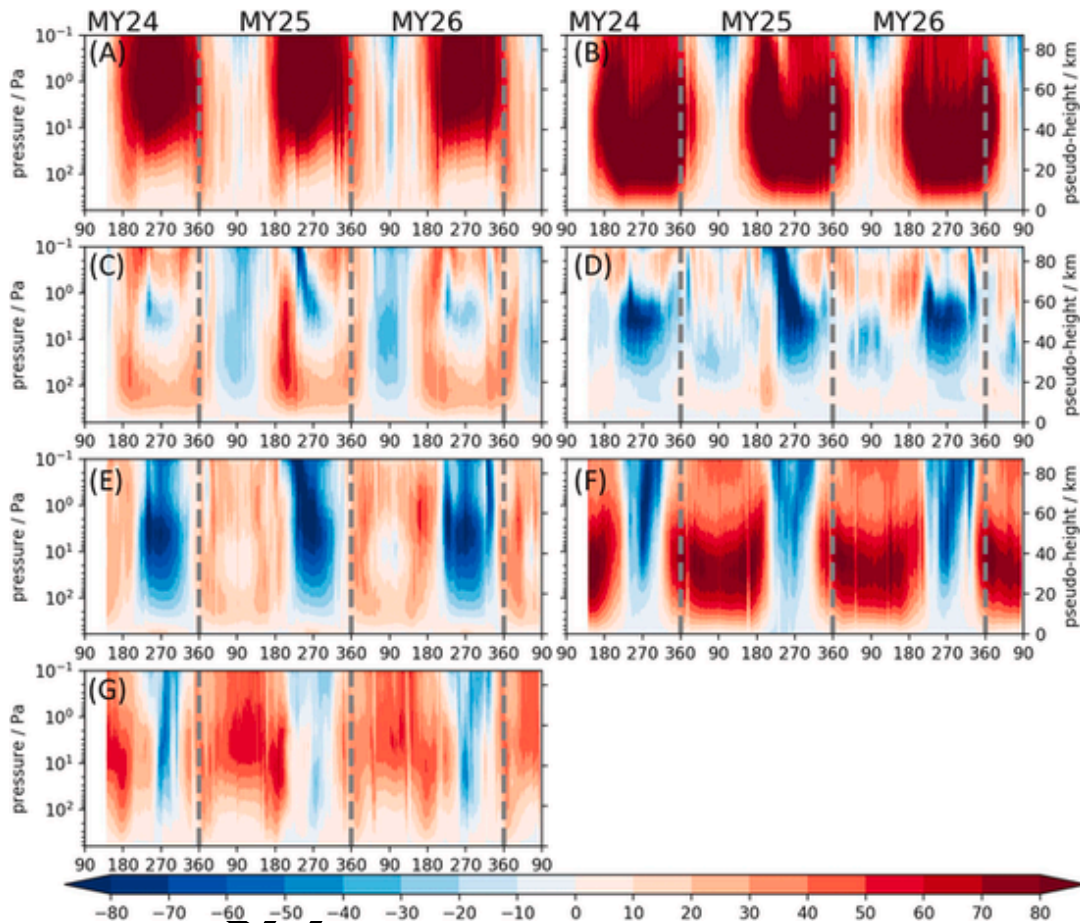
FIGURE 19.16   Zonal-mean wind on Mars in seven latitudinal bands. The zonal-mean of daily-averaged zonal winds (m s^{-1}) in different latitude bands, (A) 60°– 90°N, (B) 40°–60°N, (C) 10°–40°N, (D) 10°N–10°S, (E) 10°–40°S, (F) 40°–60°S, (G) 60°–90°S, obtained from the MACDA reanalysis.[17] *From Ruan T, Lewis NT, Lewis SR, Montabone L, Read PL. Investigating the semiannual oscillation on Mars using data assimilation. Icarus, 2019;333: 404–414. https://doi.org/10.1016/j.icarus.2019.06.012.*

over most altitudes. Forcing by stationary waves and diurnal thermal tides (Fig. 19.17D and F) were somewhat similar to those found by the previous MGCM study [297] though with some differences. The stationary wave forcing was similar between 100 and 10 Pa but without the reversal of sign at higher altitudes seen previously.[297] Eastward tidal forcing also aligned fairly closely with solstices though with substantial interannual variability, peaking strongly during the MY 25 major dust storm, and with broadly westward forcing at altitudes above 2 Pa. Kelvin wave forcing in this analysis, however, was very different to the MGCM findings,[297] with weak or eastward forcing at most altitudes, becoming relatively strong at altitudes above 5 Pa.

The residual term [4] in Eq. (19.2), (Fig. 19.17H) represents effects of unresolved eddies and missing physics in the model used for the assimilation, and was generally small compared with other, more dominant, components at altitudes below 10 Pa. This term does show some stronger features at higher altitudes, however, as evident in Fig. 19.17H, indicating that the terms considered in Eq. (19.2) do not capture all of the observed variability in [u]. This is attributed partly to errors in the diabatic forcing,[312] though it is notable that observational increments in the assimilation were only applied at altitudes below about 40 km (10 Pa), which is the highest altitude covered by the TES nadir observations. It is possible, therefore, that the large residuals during southern summer include an unphysical response of the model to the absence of assimilation increments to temperature and related fields at altitudes above 40 km.

Overall, however, it seems reasonably clear from these studies that Mars does exhibit a robust SAO that resembles the Earth's stratospheric SAO in some respects, notably dominated by zonal mean advection during westward phases around solstices and by eddies during eastward phases near equinoxes. But the wave modes contributing this forcing are somewhat different from Earth, with a more prominent role for thermal diurnal tides on Mars. Like its terrestrial counterpart, the Martian SAO also extends its influence beyond the tropics, but a number of uncertainties remain. In particular, it
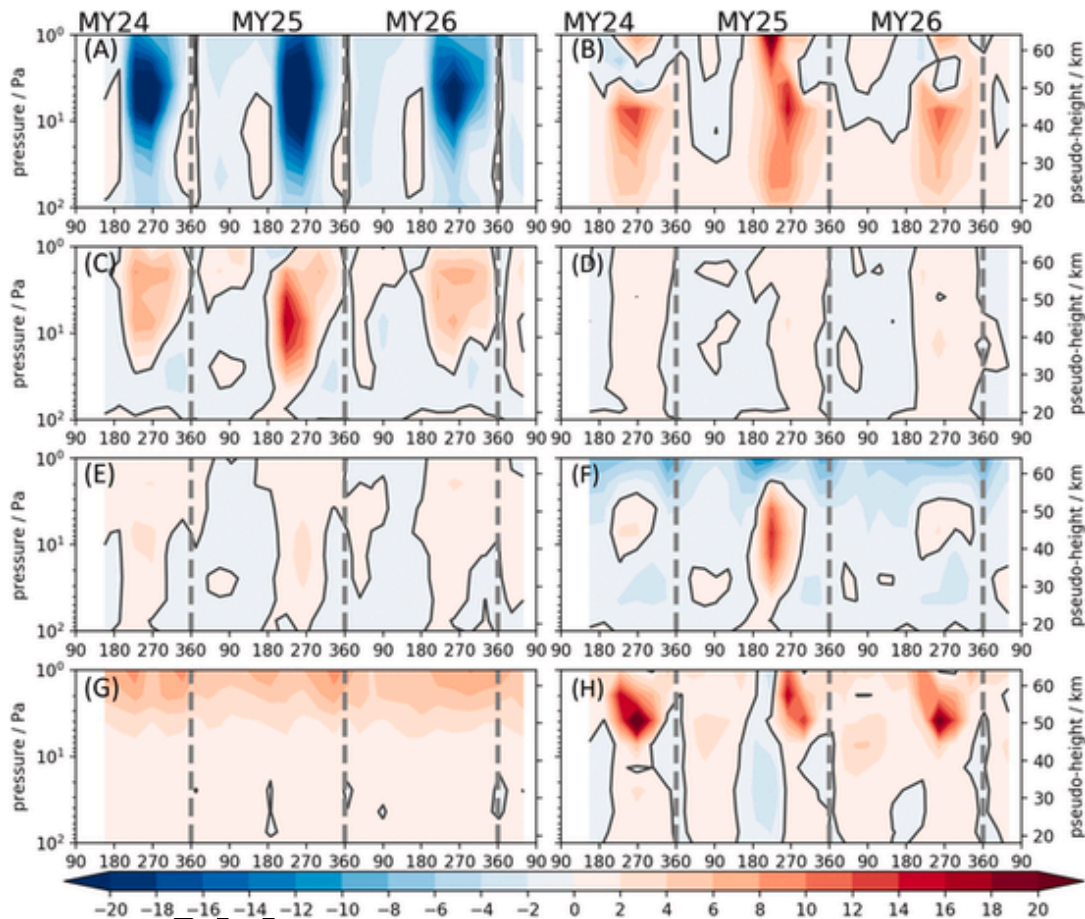
FIGURE 19.17   Transformed Eulerian Mean diagnosed forcing of the Martian semiannual oscillation. The forcing terms on the zonal-mean zonal wind in the MACDA analysis, decomposed from the Transformed Eulerian Mean (TEM) zonal momentum Eq. (19.2) and averaged, using a 60-sol time window, ±10°N. The panels show tendencies (in units of m/s/sol) due to (A) meridional advection, (B) vertical advection, (C) total forcing from different groups of zonal wavenumber-frequency components, (D) quasistationary waves only, (E) transient waves only, (F) westward thermal tides only, and (G) eastward Kelvin waves. Panel (H) shows the calculated residual of the actual zonal-mean acceleration (also averaged with a 60-sol time window) minus the sum of Eq. (19.1), terms [1–3]. All terms are in units of m/s/sol, and only the zero contour line is shown in order to distinguish the eastward (red) and westward (blue) accelerations. *From Ruan T, Lewis NT, Lewis SR, Montabone L, Read PL. Investigating the semiannual oscillation on Mars using data assimilation. Icarus, 2019;333: 404–414. https://doi.org/10.1016/j.icarus.2019.06.012.*

would be desirable to extend this kind of analysis to the Mars Reconnaissance Orbiter era, for which observational coverage is more extensive in altitude and time and with higher vertical resolution.[16] It would also be of interest to explore how the SAO signal is maintained at midlatitudes on Mars by extending the analysis of Eq. (19.2) at higher latitudes.

19.3.5.2   Subseasonal tropospheric oscillations

Like Earth, Mars has multiple subseasonal wave modes embedded amongst the short wave period and seasonal and longer oscillations. Indeed, Mars's subseasonal waves have some similarities to the quasibiweekly mode (QBM), the 30–60 day oscillation [313,314] and even the Madden-Julian oscillation.[315] In the extra-tropics, amplitudes of waves with subseasonal periods ($15 < P < 60$ sol) generally fall below 5 K but waves associated with dust storms can obtain amplitudes as much as 20 K, as observed in retrieved TES and MCS temperatures and in reanalyses.[41,53,54,56,62,316,317] The largest observed temperature amplitudes for these subseasonal waves occur up to 40 km above the surface and tend to not be surface-based.[41,56,318] Overall, the subseasonal waves are found at higher latitudes, with the strongest waves happening in the Northern Hemisphere during the winter solsticial pause of low-altitude, short-period ($1.5 < P < 10$ sol) baroclinic waves,[3,53,55,56,85,319] which shares many commonalities with the Pacific mid-winter minimum of storm track amplitudes on Earth.[81,320–323] The short-period eddies seem to subside due to a reduction in low-level baroclinicity,[51,82–84] which is caused in part by the direct effect of dust on the gradients of temperature [51,82,324] and an indirect effect of dust strengthen-

ing the Hadley cell to adiabatically warm the polar region and therefore amplify the jet.[44,45,319,320,322,325] This effect is similar to Arctic amplification causing weakening of baroclinic storm tracks on Earth.[326–331] Sub-seasonal waves outside this time correlate with large dust storms that exhibit cross-hemisphere flushing motion [3,5,66,71,73,74] Mars's waves generally travel eastward, but westward propagation is also noted, particularly in response to large dust storms [318,332,333] in the Southern Hemisphere, though subseasonal waves are rarer in the Southern than Northern Hemisphere. Almost all subseasonal waves are wavenumber 1 exclusively and have a mixed baroclinic/barotropic character, but the majority of wave forcing comes from barotropic conversion of kinetic energy from the zonal mean to the eddies.[3,41,49–53,324] This conversion may be related to the unstable annular polar vortex.[48,273] The complexity of extratropical modes may be due to instability on each side of the polar vortex annulus,[37,41,273] and further modeling efforts are needed to disentangle the relationship between wave modes and their forcing with the jet and the polar vortex.

Many extratropical wave modes extend to the tropics, which has been speculated to be enabled by inertial instabilities.[54,334] However, subseasonal tropical modes are also consistent with a coupled Rossby-Kelvin wave propagating westward relative to the eastward mean flow near the pole and eastward relative to the westward mean flow in the tropics.[41] Cloud observations of tropical subseasonal waves ($20 < P < 30$ sol) every year confirm the orbital measurements.[335] While these observations are limited to only northern spring, the detection of waves is dependent on observations of clouds at approximately 1500 local time, and clouds have a preferred season in northern late winter to spring as part of the Aphelion Cloud Belt,[336–338] so additional waves may exist outside of the observational constraints. The wave mode implicated for the cloud propagation is hypothesized to be a wavenumber 1 Kelvin wave, as diagnosed from the OpenMARS reanalysis.[335] The wave is symmetric around the equator with little vertical tilt below 20 km altitude, and cloud radiative effects may adiabatically heat the waves from above, consistent with an observed phase reversal at 20 km.[169,335] Surface-based observations corroborate the orbital observations; Mars Science Laboratory (MSL) in Gale Crater at 137°E, 5°S[57] and Mars 2020 in Jezero Crater at 77°E, 20°N[58] have noted long-period eddies. By comparing the leading behavior of presure between MSL and Mars 2020, waves have both baroclinic and barotropic components.[59] Nevertheless, the barotropic Rossby wave combined with Kelvin wave structure is similar to Earth's QBM.[313,314]

Also of note is the absence of a QBO in Mars's atmosphere. This is due to the lack of a stratosphere on Mars, since the QBO is forced on Earth by the flux of vertical momentum into the stratosphere by gravity, Kelvin, and mixed Rossby-gravity waves.[300,339–341] Without a stratosphere, waves on Mars continue to propagate upwards, though it is unclear if there is a so-called mesospheric QBO[300,342] on Mars, which may be due to the intermittency of a mesospheric QBO,[343] as determined from Earth's.

Finally, while Earth is replete with modes identified via teleconnections, like the North Pacific Oscillation, Pacific-South American Pattern, and East Atlantic Pattern and Scandinavian Pattern,[344,345] the field of Mars teleconnections is only just starting to be explored.[55,243,346] There may also be teleconnections between reservoirs of surface dust that control the timing of global dust storms,[347] so further interrogation of the observed radiance datasets and derived reanalyses is required.

19.3.2   Venus

The observation of subseasonal to seasonal oscillations on Venus is more recent despite cloud tracking efforts since the Venus Pioneer missions in the early 1980s.[348] While suggestions of oscillations appeared in those early tracking efforts,[104] gaps in the sampling limited the robustness of any detected oscillations.[6] Within the last ten years, increased interest in the atmosphere of Venus via new orbital missions has enabled more continuous cloud tracking.

19.3.2.1   255-day oscillation

The European Space Agency's Venus Express captures cloud motions around 70 km with the Venus Monitoring Camera (VMC), which observes in the UV.[349] Six years of nearly continuous data centered on the equatorial regions around local noon were analyzed using an automated cloud tracking method to estimate winds.[6] Variations in the zonal winds up to 20 m/s and in the meridional winds up to 8 m/s are apparent between 18° and 24°S. Using a least-squares sinusoidal analysis (LSSA) to account for gaps in data, power spectra of the observed zonal wind pinpoint an oscillation of 255 days, with a full-width at half maximum (FWHM) of 20 days at an amplitude of 11 m/s. This clearly separates this periodicity from the Venusian tides, which have a diurnal period of 225 days (Table 19.1). Some variability in the period of the oscillation is found at different latitudes, ranging from 255 days at 18°S, steadily increasing with latitude up to 267 days at 42°S. At higher latitudes, the winds decorrelate from the low latitudes, but equatorward of 30°S, the mode is in phase across latitudes.

Clouds are not necessarily passive tracers, but the LSSA method detects the 4.2-day Kelvin wave during periods of slower superrotation and the 4.8-day Rossby wave during the faster phase of the superrotation, as evidenced by a 90° phase difference between the meridional and zonal winds, which lends credence to the assumption that observed cloud speeds approximate ambient winds.[6] The Rossby and Kelvin modes are not constant over the entire observation period, indicating subseasonal variation in their amplitudes. The 255-day oscillation relates to which type of wave dominates. The Kelvin wave occurs during periods of slower superrotation, and the Rossby wave dominates the faster phase of the superrotation.[6] The correlation between wave mode and wind speed suggests a relationship like that which forces Earth's QBO. Additional ground-based observations have indicated that the switch between one mode dominating occurs on multiyear timescales, up to 540 days or approximately 2.4 Venus years. Kelvin waves transport positive angular momentum upwards, but Rossby waves transport momentum downwards. The combination of these wave modes and their amplitude of oscillations in time suggest an alternating eastward and westward forcing mechanism, which is how the QBO is forced.[300,342] The absence of oscillations lower in the atmosphere at 45 km [350] indicates that the cloud-top oscillation in the Venusian superrotation must be excited within the cloud layer. However, higher vertical resolution observations will be required to source the forcing mechanisms, and continued cloud-top observation will be required for continued monitoring of the 255-day oscillation.

19.3.2.2   150-day oscillation

A shorter Venusian climate oscillation was found using the Visible and Infrared Thermal Mapping Spectrometer (VIRTIS-M-IR) on Venus Express.[88] A 150-day oscillation was detected using LSSA over 921 orbits in the optical depth of the upper cloud layer at spectral windows at 1.74 and 2.30 μm, corresponding to 50–57 km altitude.[351] Its absence in geometric observation parameters indicates that this oscillation is real and not an instrumentation artifact. The oscillation has an amplitude comparable to the day-to-day variability of the average radiance, but the FWHM is about 20 days, which suggests the 150-day period varies somewhat. Interestingly, while both spectral observation windows separately exhibit the oscillations, a size parameter calculated using their combined effect that measures the cloud particle population does not exhibit an oscillation, indicating that the cloud particle population does not cause the oscillation.

The cause of the 150-day period is unclear, though may be related to several factors. A QBO-like explanation, as with the 255-day oscillation, seems unlikely given the absence of evidence of wave modes capable of depositing alternating eastward and westward angular momentum within the 50–57 km layer. Instead, the oscillation may be the manifestation of a 3:2 resonance between the Hadley circulation and diurnal variations, like the tide.[351] More concretely, the oscillation may result from interactions in the particle physics within clouds rather than dynamics of waves or the general circulation. Assuming a reasonable distribution of cloud particle sizes, the sedimentation rate for cloud particles through a hypothetical 10 km cloud layer is 0.11 cm/s.[352] Further, eddy diffusion could drive the increased radiance (cloud reduction) phase of the oscillation. An 8–15 m^2 s eddy diffusion coefficient fully mixes a 7–10 km cloud layer in approximately 75 days, which is also consistent with a radiative-dynamical cloud model that is driven by radiative heating at the cloud base and radiative cooling of the cloud tops.[92] The radiative cooling timescale for clouds at 50 km is then estimated to be 76 days. The combination of 75 days of warming via eddy diffusion and 75 days of radiative cooling may account for the 150-day oscillation. Additional cloud modeling efforts and continued observation are warranted to ascertain the longevity and cause of the 150-day mode.

19.3.2.3   Sub-50 day oscillation

Finally, a variation of Venus's cloud albedo at the subseasonal scale has been found, resulting from changes of the Kelvin-like (3.5–4.3 day) equatorial mode and Rossby-like (4.5–5.5 day), extratropical (poleward of approximately ±30°N) modes.[7] Previous ground-based observations of the Kelvin and Rossby modes revealed periodic variations in the waves but were limited by the Earth-based view of Venus.[105] Using observations from the UV Imager (UVI) on the Japanese Venus Climate Orbiter Akatsuki,[353] multiple wave modes are apparent even in single image captures at 365 nm (Fig. 19.18A). Images processed to remove light scattering reveal a chevron wave structure composed of a plethora of wave modes (Fig. 19.18B). The combination of 291 images over June to October 2017 (Fig. 19.18C and D) exposes planetary-scale variations with time. The periodicities of the UV brightness and meridional winds demonstrate robust 5-day period waves at 99% confidence over 30–50°N due to the Kelvin and Rossby modes (Fig. 19.18E), but the subseasonal variation of the Rossby waves is substantively larger in amplitude than the waves themselves. The meridional wind (Fig. 19.18E, red line) experiences a 20-day amplification representing an acceleration of 0.18 m/s/day. After reaching a maximum, 50 days of relaxation is required for the intensity to return to normal.
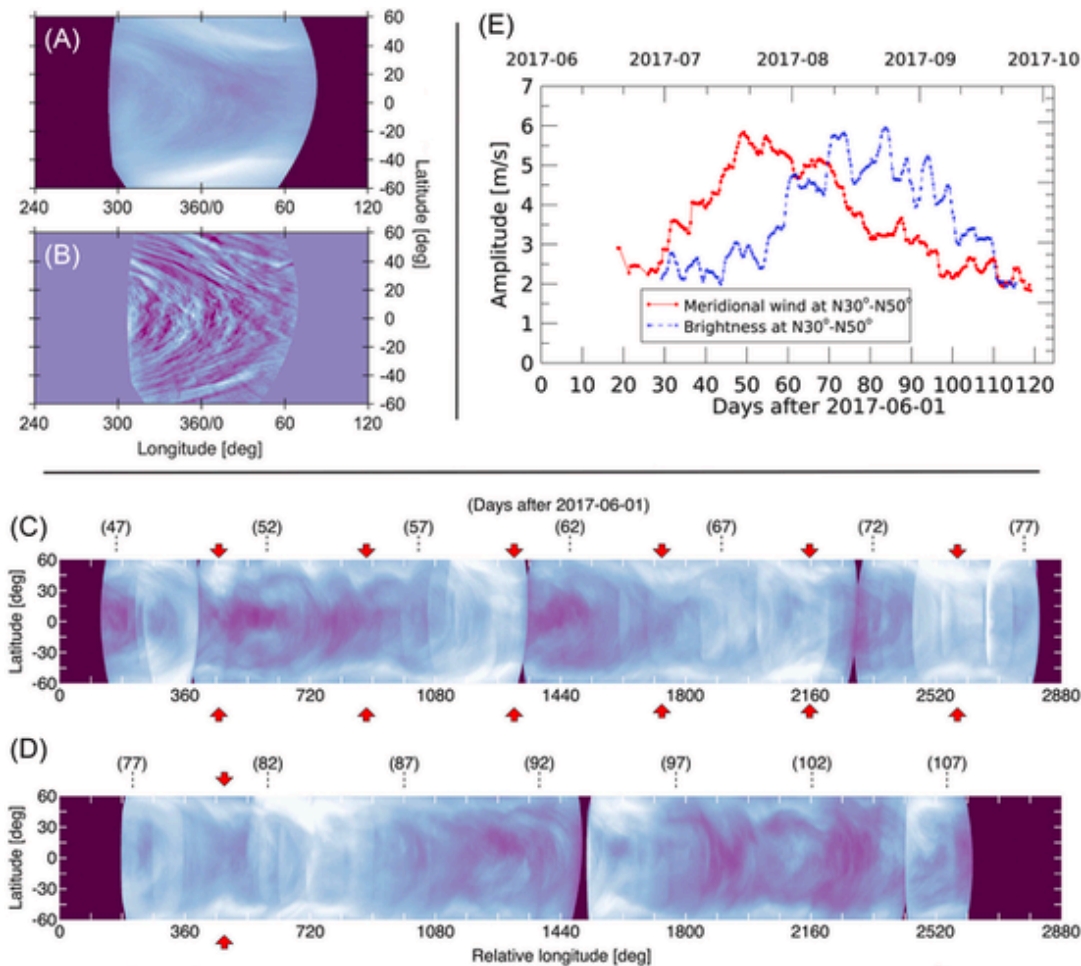
FIGURE 19.18   20-day and 50-day oscillations in Venusian clouds.   Observation of the 20- and 50-day, subseasonal oscillations in the Venusian atmosphere from the Akatsuki climate mission. (A) Projected and processed image from the 365-nm UV Imager Im- ager obtained on 2017–07-30T23:04:74 (B) Band-pass filtered version of UV image from (A) showing the widespread wave activity at cloud-top level of 70 km. (C, D) Projected, composited UV images at 0.25 degrees resolution at (C) 1000–1200 local time for days 47–77 and (D) 1200–1400 local time for days 107–137 days after June 1, 2017. Numbers in parentheses show the days after June 1, 2017. The subseasonal variation of the embedded Rossby and Kelvin waves (red arrows) is apparent. (E) Temporal changes in the meridional wind amplitude (red dots) and UV brightness (blue crosses) within 30°–50°N. *Modified from Imai M, Kouyama T, Takahashi Y, Yamazaki A, Watanabe S, Yamada M, Imamura T, Satoh T, Nakamura M, Murakami S, Ogohara K, Horinouchi T. Planetary-scale variations in winds and UV brightness at the Venusian cloud top: periodicity and temporal evolution. Journal of Geophysical Research: Planets, 2019;124(10): 2635–2659. https://doi.org/10.1029/2019je006065.*

These modulations could be related to variations in the Rossby wave source mechanism and/or the ability of Rossby waves to propagate upwards. To try to determine which of these possibilities contributes to the changing winds, an estimate of the time required for vertical propagation and subsequent damping of a Rossby wave can be obtained from the vertical group velocity of a beta-plane Rossby-wave.[301] This yields a velocity of 1.7 km/day[7] so that 3 days are required to travel a Venusian scale height (H =5 km, Table 19.1). Taking a radiative cooling timescale of 6–10 days[354] means Rossby waves should not be hindered in vertical propagation. This suggests that the changes in 20-day amplification and 50-day damping of winds could be indicative of the timescales of the Rossby wave source.[7] Additionally, the UV brightness also experiences a subseasonal variation that lags the wind changes by about 30 days. With this variation, the Kelvin mode drops in amplitude as the Rossby mode intensifies and does not recover after the Rossby mode completes its 50-day observed damping.[7] The varying population of subseasonal oscillations may be caused perhaps by variations in Kelvin waves, Rossby waves, and cloud radiative effects like the 150-day oscillation.

The convection recharge-discharge model has also been proposed for Venus.[355] The periodicity of the oscillation depends on the exact eddy mixing timescales used, but in general, the variability of sulfur dioxide (SO_2) abundances at the cloud tops of Venus has a 3–9 Earth-year period. This timescale has a planet-relative longer timescale than the Titan-

recharge timescale due to the shortened year on Venus compared to Titan so is beyond the timescales considered here. A high water abundance weakens cloud-level forcing and decreases convective layer height and vertical mixing; in response to the reduced vertical mixing, water abundances decreases to repeat the cycle. Simulations indicate this oscillation may occur on the order of Earth years but is highly dependent on the parameters selected. Additional and continued observation both in orbit and from the ground will be required to determine the provenance of each of these Venusian oscillations.

19.3.3 Tidally locked exoplanets

Advances in astronomy have made it possible to detect terrestrial planets in other solar systems. As techniques for characterizing exoplanet atmospheres continue to develop, the study of these worlds could vastly expand our inventory and understanding of atmospheric oscillations. As of the time of writing, no such oscillations or indeed an atmosphere has yet been detected on any terrestrial exoplanet, but simulations have already begun to point towards interesting future questions.

Most of the discovered rocky exoplanets are likely tidally locked, with one hemisphere always facing the star, or at least in some form of synchronous rotation.[356,357] Close-in planets are easier to detect with both the radial velocity method and the transit method, and this observing bias has skewed the known population.[358,359] As no solar system planets are tidally locked, our knowledge of the atmospheric dynamics of these worlds is so far based solely on theory. Yet tidally locked planets will remain a focus of scientific interest even as new methods develop to detect planets more similar to Earth. This is because we expect most terrestrial planets orbiting in the habitable zone[360] to be tidally locked to an M-class host star.[356,361] M-class stars make up roughly 70% of the stellar population of the galaxy,[362,363] and enough data is available to estimate the prevalence of planets around this type of star. For example, about 0.48 to 0.53 habitable zone terrestrial planets are estimated per M-class host depending on the definition of the habitable zone.[364] Subsequent analyses have supported this general range.[365–368] These figures raise the prospect of billions of terrestrial planets in the Milky Way galaxy.

General circulation models offer theoretical predictions of the atmospheric dynamics of tidally locked rocky worlds. Several studies have examined how the circulation regime of a tidally locked planet depends on its rotation rate.[369–374] Most of these simulations tend toward one of two states, referred to as the single-jet and double-jet regimes.[374] In the single-jet regime, the atmosphere forms a single superrotating equatorial jet, two nightside Rossby gyres in each hemisphere associated with a standing tropical Rossby wave of zonal wavenumber 1, and an overturning circulation consisting of hot air rising on the dayside and subsiding on the nightside.[375] In the double-jet regime, the simulations maintain the overturning component of the circulation but instead develop two mid-latitude jets associated with smaller, higher latitude Rossby gyres near the planet's eastern terminator.[374] These highly idealized simulations typically assume an aquaplanet with no obliquity or eccentricity. The lack of a day-night cycle or seasons in these simulations might lead one to assume that such planets should display little to no variability. However, even these simple set-ups have developed atmospheric and climate oscillations with features contingent on the tidally locked state.

Early work has indicated that tidally locked planets may be subject to greater climate variability than nonsynchronous ones. A dynamical systems perspective[376] has been used to study the persistence of atmospheric patterns in simulations of a tidally locked TRAPPIST-1e,[377] compared to an exoplanet Earth analogue and to the ERA5 reanalysis.[378] This study carried out three simulations each of TRAPPIST-1e and an exo-Earth with varying amounts of carbon dioxide. In the high CO_2 simulation (1 bar of CO_2), both TRAPPIST-1e and the exo-Earth showed high atmospheric persistence, but in the low (10^{-2} bar) and medium (10^{-1} bar) CO_2 simulations, TRAPPIST-1e displayed much more atmospheric and climate variability than either the exo-Earth or the ERA5 data. Further study is required to determine why, but we can speculate that the extreme and permanent difference between the dayside and nightside irradiation on a tidally locked planet, combined with dynamical, radiative, and chemical timescales governing the atmosphere's tendency to seek an equilibrium, could lead to periodic changes in climate state or even circulation regime unknown from nonsynchronous rotators. Even tidally locked planets without obliquity may have "climate variability at the level that is usually produced by seasons."[377]

A few studies have begun to examine atmospheric and climate oscillations specific to tidally locked planets. A phenomenon resembling Earth's QBO has been simulated on the tidally locked Proxima Centauri b,[379] a terrestrial planet orbiting an M-dwarf star with a rotation period of 11.2 days. QBO-like phenomena have also been observed on Jupiter and Saturn, so it is possible that they occur in other extraterrestrial environments (Chapter 18: Equatorial Stratospheric Oscillations in Planetary Atmospheres). In the tidally locked case, the planet's circulation regime, characterized by a single superrotating equatorial jet, leads to longitudinal asymmetries in the oscillation that do not appear on Earth. Fig. 19.19 shows a schematic representation of how wind speed and direction vary with longitude and height around the equator. In general, the QBO manifests as a pattern of stacked stratospheric jets flowing in opposite directions which descends down-
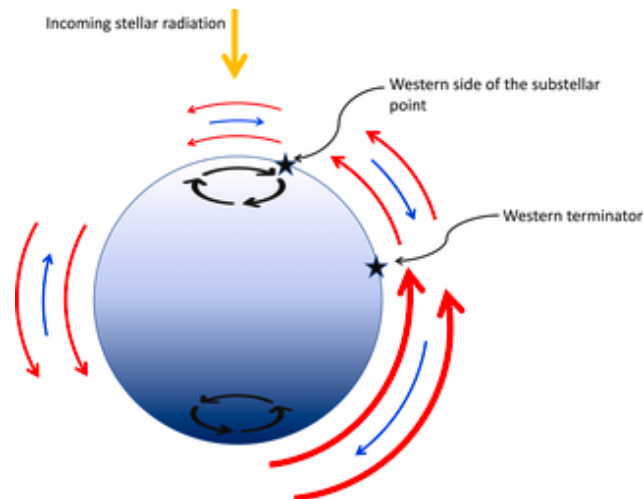
FIGURE 19.19   Schematic of an analog of the Quasi-biennial oscillation on a tidally locked planet.   Schematic diagram of a QBO-analog on a tidally locked planet showing the location and interaction of standing Rossby waves, equatorial jets, and gravity wave sources. The perspective is looking downward from the north pole. The lighter side of the sphere is the dayside and the darker is the nightside. Red (blue) arrows indicate eastward (westward) air flow, with larger arrows representing faster wind speeds. Black spirals represent Rossby gyres. The star symbol indicates gravity wave sources. *From Cohen M, Bollasina MA, Palmer PI, Sergeev DE, Boutle IA, Mayne NJ, Manners J. Longitudinally asymmetric stratospheric oscillation on a tidally locked exoplanet. The Astrophysical Journal, 2022;930(1). https://doi.org/10.3847/1538–4357/ac625d.*

ward over time. In the tidally locked simulation, the westward phase of the nightside oscillation is damped: eastward jets reach speeds upwards of 100 m/s on the nightside and extend over more altitudes, while the westward jets are shallower and rarely reach 20 m/s. The dayside oscillation is more balanced. The planet's dayside-to-nightside overturning circulation leads to downward vertical wind on the nightside which may inhibit the upward propagation of the gravity waves whose pseudomomentum deposition drives the oscillation. In addition, the superrotating jet is faster on the nightside than on the dayside throughout the atmosphere. Gravity wave propagation and breaking are shaped by this asymmetrical background flow to form an asymmetrical oscillation. The asymmetry extends also to the switching time of the jet direction. On Earth, the wind direction at a given altitude appears to change at roughly the same time across all longitudes.[380,381] As shown in Fig. 19.20, in the Proxima Centauri b simulation, the wind direction at a given altitude switches first at the western terminator (a turbulent region where the nightside wind flows onto the dayside and loses speed), then on the dayside, and last on the nightside.

Tidally locked planets could also exhibit atmospheric and climate oscillations without any Earth analog. An oscillation of the general circulation and planetary climate caused by cloud radiative feedback has been described in simulations as well.[382] The mechanism is reminiscent of the moisture-mode hypothesis of the Madden-Julian oscillation,[383] but the phenomenon takes a unique form related to the existence of the permanent dayside and nightside. In simulations of tidally locked, water-rich planets, the substellar region on the dayside forms a persistent cloud layer that reflects light and acts as a stabilizing factor against the runaway greenhouse effect.[384] Fluctuations in the amount of cloud allow more or less radiation to reach the surface at different times. Variations in this cloud radiative feedback influence the location of the planet's Rossby gyres.[382] In a simulation of TRAPPIST-1e, the gyres shift from the dayside to the nightside and back on a 20-day cycle, in tandem with an oscillation in the zonal wind speed at the gyre latitude. An analogous cycle in a simulation of Proxima Centauri b has a 160-day period but remains confined to the nightside. This Rossby gyre cycle is also associated with variability in the global mean surface temperature and cloud water path.[385] Moreover, analysis of simulation results has shown that the overturning circulation on tidally locked planets could funnel atmospheric tracers, in both gas and solid phases, into the Rossby gyres, as demonstrated for ozone.[386] Periodic exposure of the gyres to photolysis when on the dayside could lead to significant oscillations in the planet's atmospheric chemistry. Tidally locked planets could thus experience dynamical "seasons" with not only the magnitude of Earth's seasonal cycle, but stable periodicities.

19.4   Summary and future prospects

Seasonal to subseasonal oscillations are found on terrestrial worlds throughout the solar system beyond Earth. Mars and Titan have barotropic (in the zonal-mean zonal wind, $[u]$) and baroclinic (in the zonal-mean eddy kinetic energy $[K_e]$) annular modes. Mars's annular modes exhibit many structures similar to Earth's modes, namely that the mode in $[u]$ de-
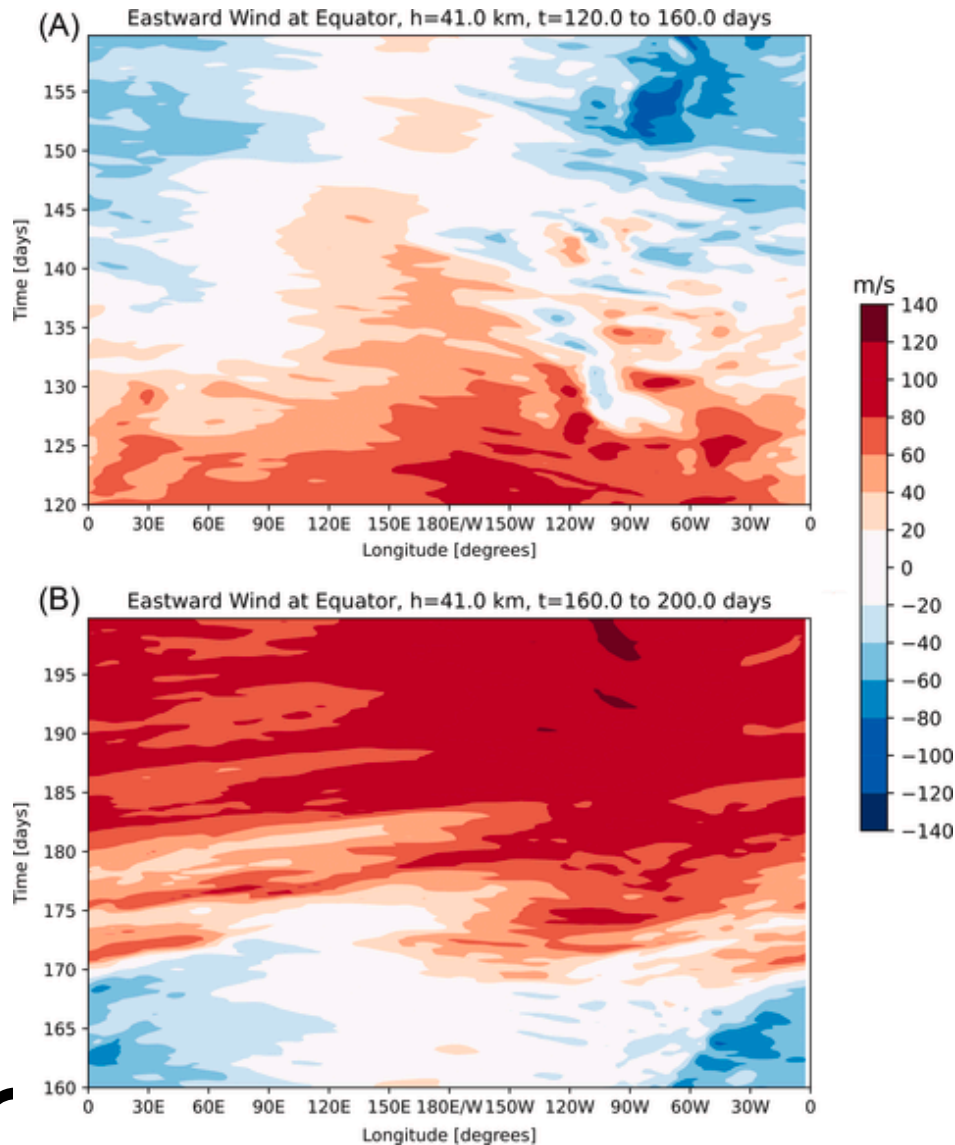
FIGURE 19.20   Oscillation between equatorial eastward and westward zonal winds on a simulated tidally locked planet.   Equatorial zonal wind speeds at 41 km over two 40-day periods in a simulation of Proxima Centauri b. The data has a six-hourly resolution. (A) The transition from eastward to westward winds. (B) The transition from westward to eastward winds. Plots are centered on the antistellar point to highlight the tendency to resist westward flow in this region. *Modified from Cohen M, Bollasina MA, Palmer PI, Sergeev DE, Boutle IA, Mayne NJ, Manners J. Longitudinally asymmetric stratospheric oscillation on a tidally locked exoplanet. The Astrophysical Journal, 2022;930(2). https://doi.org/10.3847/1538–4357/ac625d.*

scribes shifts in the jet stream north-south and associates with eddy momentum flux divergence, but Titan's mode describes vertical jet shifts. Both Mars's and Titan's modes in $[K_e]$ capture zonally symmetric strengthening of the storm tracks and are related to eddy heat fluxes but also capture changes in eddy momentum fluxes. These modes also seem to carry some predictive relationships to dust storms on Mars and methane convection on Titan; fully describing and quantifying these relationships will be an exciting avenue for research.

Mars also has a Semi-annual (SAO) with clear similarities to the stratospheric SAO on Earth. The zonal-mean wind shifts between relative westward and eastward phases during solstice and equinoxes, respectively. Thermal tides are important in forcing Mars's SAO, unlike its counterpart on Earth. Examining these relationships on new reanalysis datasets will be important to quantify the extent of the SAO from the tropics towards the poles. Other long period wave modes on Mars from Kelvin and Rossby waves play an important role in the global dust cycle on subseasonal time scales.

Venus has three subseasonal/seasonal modes. A 255-day oscillation in tracked cloud winds appears to be forced in the same way as Earth's Quasi-Biennial Oscillation as times of slower superrotation align with times that Kelvin modes dom-

inate, while faster superrotation coincides with Rossby wave modes. A 150-day oscillation in cloud optical depth at 50 km may be related to cloud particle physics processes oscillating between eddy diffusion mixing for half a cycle and radiative cooling for the other half. Finally, a <50-day oscillation is expressed in the cloud albedo in amplifications in the Kelvin and Rossby wave modes and appears to be related to changes in the source of the Rossby waves below the clouds.

As modes of climate variability are identified, two important facets require explication. First, mechanistic understanding of planetary atmosphere oscillations will be vital to ensure that future observations of atmospheres are not mis-interpreted or mis-identified, particularly since quality in situ observation requires so much preparation. Secondly, interactions between oscillations will be increasingly important. Modulation of different types of modes on Earth is vital to characterizing their variability,[387–394] so we must also assume that mode interactions are important on Mars, Titan, Venus, and elsewhere. Quantifying those interactions will be critical to understanding their variability as observational datasets increase in duration. By demonstrating the ubiquity of variability in the solar system, yet at the same time being woefully limited in the observations available, we hope to motivate new and renewed interest in climate monitoring of the solar system.

Understanding the variety of subseasonal to seasonal oscillations or other irregular periodicities that exist on Mars, Venus, and Titan and what dynamics are responsible for their variability requires regular, concerted observations. Mars is the only planetary body where such long-term orbital or in situ observations are available, but current orbital assets are aging; the primary instruments constraining the reanalysis are on the 2007 Mars Reconnaissance Orbiter and 2001 Mars Odyssey. Barring the development of new orbiters in the next few years,[395] the nearly continuous record started with Mars Global Surveyor is in jeopardy. New interest in Venusian missions is encouraging, but to ascertain the drivers of the three subseasonal Venus modes will require a dedicated spacecraft monitoring the whole planetary atmosphere for several years to help with the development of Venusian reanalyses.[90] Finally, we are on the cusp of a revolution in the variety of observable climates in the galaxy thanks to JWST and WFIRST.[396,397] Together, we can hope for continued examination of non Earth climates in the coming decades.

Acknowledgment

References

1. A.P. Showman, R.D. Wordsworth, T.M. Merlis, Y. Kaspi In: S.J. Mackwell, A.A. Simon-Miller, J.W. Harder, M.A. Bullock, eds. Atmospheric Circulation of Terrestrial Exoplanets. Tuscon: University of Arizona; 2013:277–326. 10.2458/azu_uapress_9780816530595-ch12.
2. M. Battalio, H. Wang The Aonia-Solis-Valles dust storm track in the southern hemisphere of Mars. Icarus.. 2019;321:367–378. https://doi.org/10.1016/j.icarus.2018.10.026.
3. M. Battalio, H. Wang Eddy evolution during large dust storms. Icarus. 2020;338. https://doi.org/10.1016/j.icarus.2019.113507.
4. J.M. Battalio, J.M. Lora Annular modes of variability in the atmospheres of Mars and Titan. Nature Astronomy.. 2021;5(11):1139–1147. https://doi.org/10.1038/s41550-021-01447-4.
5. M. Battalio, H. Wang The Mars dust activity database (MDAD): a comprehensive statistical study of dust storm sequences. Icarus. 2021;354. https://doi.org/10.1016/j.icarus.2020.114059.
6. T. Kouyama, T. Imamura, M. Nakamura, T. Satoh, F. Yoshifumi Long-term variation in the cloud-tracked zonal velocities at the cloud top of Venus deduced from Venus express VMC images. Journal of Geophysical Research: Planets. 2013;118(1):37–46. https://doi.org/10.1029/2011je004013.
7. I. Watanabe, K. Toru, T. Yukihiro, et al. Planetary-scale variations in winds and UV brightness at the venusian cloud top: periodicity and temporal evolution. Journal of Geophysical Research: Planets. 2019;124(10):2635–2659. https://doi.org/10.1029/2019je006065.
8. J.M. Battalio, J.M. Lora Global impacts from high-latitude storms on Titan. Geophysical Research Letters.. 2021;48(18). https://doi.org/10.1029/2021GL094244.
9. Y. Wang, P.L. Read, F. Tabataba-Vakili, M.B. Young Roland Comparative terrestrial atmospheric circulation regimes in simplified global circulation models. Part I: from cyclostrophic super-rotation to geostrophic turbulence. Quarterly Journal of the Royal Meteorological Society. 2018;144(717):2537–2557. https://doi.org/10.1002/qj.3350.
10. A. Sánchez-Lavega, S. Lebonnois, T. Imamura, P. Read, D. Luz The atmospheric dynamics of Venus. Space Science Reviews.. 2017;212(3–4):1541–1616. https://doi.org/10.1007/s11214-017-0389-x.
11. A.P. Showman, L.M. Polvani The Matsuno-Gill model and equatorial superrotation. Geophysical Research Letters.. 2010;37(18). https://doi.org/10.1029/2010GL044343.

12.   Imamura T., Mitchell J., Lebonnois S., Kaspi Y., Showman A.P., Korablev O. Superrotation in planetary atmospheres. Space Science Reviews. 216(5).

13.   D.W. Waugh Fluid dynamics of polar vortices on Earth, Mars, and Titan. Annual Review of Fluid Mechanics.. 2023;55(1):265–289. https://doi.org/10.1146/annurev-fluid-120720-032208.

14.   R.T. Clancy, B.J. Sandor, M.J. Wolff, et al. An intercomparison of ground-based millimeter, MGS TES, and Viking atmospheric temperature measurements: seasonal and interannual variability of temperatures and dust loading in the global Mars atmosphere. Journal of Geophysical Research: Planets. 2000;105(E4):9553–9571. https://doi.org/10.1029/1999je001089.

15.   D. Smith Michael Interannual variability in TES atmospheric observations of Mars during 1999–2003. Icarus.. 2004;167(1):148–165. https://doi.org/10.1016/j.icarus.2003.09.010.

16.   D.J. McCleese, N.G. Heavens, J.T. Schofield, et al. Structure and dynamics of the Martian lower and middle atmosphere as observed by the Mars climate sounder: seasonal variations in zonal mean temperature, dust, and water ice aerosols. Journal of Geophysical Research: Planets.. 2010;115(12). https://doi.org/10.1029/2010JE003677.

17.   L. Montabone, K. Marsh, S.R. Lewis, et al. The mars analysis correction data assimilation (MACDA) dataset version 1.0. Geoscience Data Journal.. 2014;1(2):129–139. https://doi.org/10.1002/gdj3.13.

18.   S.J. Greybush, E. Kalnay, R.J. Wilson, et al. The ensemble Mars atmosphere reanalysis system (EMARS) version 1.0. Geoscience Data Journal.. 2019;6(2):137–150. https://doi.org/10.1002/gdj3.77.

19.   J.A. Holmes, S.R. Lewis, M.R. Patel OpenMARS: a global record of martian weather from 1999 to 2015. Planetary and Space Science.. 2020;188. https://doi.org/10.1016/j.pss.2020.104962.

20.   T. Navarro, F. Forget, E. Millour, S.J. Greybush, E. Kalnay, T. Miyoshi The challenge of atmospheric data assimilation on Mars. Earth and Space Science.. 2017;4(12):690–722. https://doi.org/10.1002/2017ea000274.

21.   J.E. Tillman, R.M. Henry, S.L. Hess Frontal systems during passage of the Martian north polar hood over the Viking Lander 2 site prior to the first 1977 dust storm. Journal of Geophysical Research: Solid Earth.. 1979;84(B6):2947–2955. https://doi.org/10.1029/jb084ib06p02947.

22.   J.R. Barnes Time spectral analysis of mid-latitude disturbances in the Martian atmosphere. Journal of the Atmospheric Sciences. 1980;37(9):2002–2015. doi:10.1175/1520-0469(1980)037<2002:tsaomd>2.0.co;2.

23.   R.M. Haberle, J. Gõmez-Elvira, M. De La Torre Juárez, et al. Preliminary interpretation of the REMS pressure data from the first 100 sols of the MSL mission. Journal of Geophysical Research: Planets.. 2014;119(3):440–453. https://doi.org/10.1002/2013JE004488.

24.   P.L. Read, S.R. Lewis, D.P. Mulholland The physics of Martian weather and climate: a review. Reports on Progress in Physics.. 2015;78(12). https://doi.org/10.1088/0034-4885/78/12/125901.

25.   M. Haberle Robert, B. Pollack James, R. Barnes Jeffrey, et al. Mars atmospheric dynamics as simulated by the NASA Ames general circulation model: 1 The zonal-mean circulation. Journal of Geophysical Research: Planets. 1993;98(E2):3093–3123. https://doi.org/10.1029/92je02946.

26.   R.M. Haberle, H. Houben, J.R. Barnes, R.E. Young A simplified three-dimensional model for Martian climate studies. Journal of Geophysical Research: Planets. 1997;102(E4):9051–9067. https://doi.org/10.1029/97je00383.

27.   I. Guendelman, Y. Kaspi The key factors controlling the seasonality of planetary climate. AGU Advances.. 2022;3(5). https://doi.org/10.1029/2022av000684.

28.   J.R. Barnes, R.M. Haberle, R.J. Wilson, S.R. Lewis, J.R. Murphy, P.L. Read The Global Circulation. Cambridge University Press (CUP); 2017:229–294. 10.1017/9781139060172.009.

29.   T. Kuroda, A.S. Medvedev, P. Hartogh, M. Takahashi On forcing the winter polar warmings in the Martian middle atmosphere during dust storms. Journal of the Meteorological Society of Japan Ser II.. 2009;87(5):913–921. https://doi.org/10.2151/jmsj.87.913.

30.   D.J. McCleese, J.T. Schofield, F.W. Taylor, et al. Intense polar temperature inversion in the middle atmosphere on Mars. Nature Geoscience.. 2008;1(11):745–749. https://doi.org/10.1038/ngeo332.

31.   A.S. Medvedev, E. Yiğit, P. Hartogh, E. Becker Influence of gravity waves on the Martian atmosphere: general circulation modeling. Journal of Geophysical Research.. 2011;116(E10). https://doi.org/10.1029/2011je003848.

32.   A.D. Toigo, C. Lee, C.E. Newman, M.I. Richardson The impact of resolution on the dynamics of the martian global atmosphere: varying resolution studies with the MarsWRF GCM. Icarus.. 2012;221(1):276–288. https://doi.org/10.1016/j.icarus.2012.07.020.

33.   T. Kuroda, A.S. Medvedev, E. Yiğit, P. Hartogh A global view of gravity waves in the Martian atmosphere inferred from a high-resolution general circulation model. Geophysical Research Letters. 2015;42(21):9213–9222. https://doi.org/10.1002/2015gl066332.

34.   T. Kuroda, A.S. Medvedev, E. Yiğit, P. Hartogh Global distribution of gravity wave sources and fields in the Martian atmosphere during equinox and solstice inferred from a high-resolution general circulation model. Journal of the Atmospheric Sciences.. 2016;73(12):4895–4909. https://doi.org/10.1175/jas-d-16-0142.1.

35.   C.B. Leovy The martian lower atmosphere. Nature. 1981;294(5839):310–311. https://doi.org/10.1038/294310a0.

36.   Z. Wu, T. Li, N.G. Heavens, et al. Earth-like thermal and dynamical coupling processes in the Martian climate system. Earth-Science Reviews.. 2022;229. https://doi.org/10.1016/j.earscirev.2022.104023.

37.   D.W. Waugh, A.D. Toigo, S.D. Guzewich, S.J. Greybush, R.J. Wilson, L. Montabone Martian polar vortices: comparison of reanalyses. Journal of Geophysical Research: Planets.. 2016;121(9):1770–1785. https://doi.org/10.1002/2016JE005093.

38.   K. Rajendran, S.R. Lewis, J.A. Holmes, P.M. Streeter, A.A. Fedorova, M.R. Patel Enhanced super-rotation before and during the 2018 Martian global dust storm. Geophysical Research Letters.. 2021;48(16). https://doi.org/10.1029/2021GL094634.

39.   M.I. Richardson, R.J. Wilson Investigation of the nature and stability of the Martian seasonal water cycle with a general circulation model. Journal of Geophysical Research: Planets.. 2002;107(E5). https://doi.org/10.1029/2001je001536.

40.   A.M. Zalucha, R.A. Plumb, R.J. Wilson An analysis of the effect of topography on the Martian Hadley cells. Journal of the

Atmospheric Sciences.. 2010;67(3):673–693. https://doi.org/10.1175/2009jas3130.1.

41. D. Banfield, B.J. Conrath, P.J. Gierasch, R.J. Wilson, M.D. Smith Traveling waves in the martian atmosphere from MGS TES Nadir data. Icarus.. 2004;170(2):365–403. https://doi.org/10.1016/j.icarus.2004.03.015.

42. D.M. Mitchell, L. Montabone, S. Thomson, P.L. Read Polar vortices on Earth and Mars: a comparative study of the climatology and variability from reanalyses. Quarterly Journal of the Royal Meteorological Society.. 2015;141(687):550–562. https://doi.org/10.1002/qj.2376.

43. D. Guzewich Scott, A.D. Toigo, D.W. Waugh The effect of dust on the martian polar vortices. Icarus.. 2016;278:100–118. https://doi.org/10.1016/j.icarus.2016.06.009.

44. A.D. Toigo, D.W. Waugh, S.D. Guzewich What causes Mars' annular polar vortices? Geophysical Research Letters.. 2017;44(1):71–78. https://doi.org/10.1002/2016gl071857.

45. E.R. Ball, D.M. Mitchell, W.J.M. Seviour, S.I. Thomson, G.K. Vallis The roles of latent heating and dust in the structure and variability of the Northern Martian polar vortex. The Planetary Science Journal.. 2021;2(5). https://doi.org/10.3847/psj/ac1ba2.

46. P.M. Streeter, S.R. Lewis, M.R. Patel, J.A. Holmes, K. Rajendran An eight-year climatology of the martian northern polar vortex. Icarus.. 2024;409. https://doi.org/10.1016/j.icarus.2023.115864.

47. P.M. Streeter, S.R. Lewis, M.R. Patel, et al. Asymmetric impacts on Mars' polar vortices from an equinoctial global dust storm. Journal of Geophysical Research: Planets. 2021;126(5). https://doi.org/10.1029/2020JE006774.

48. J.M. Seviour William, W. Waugh Darryn, K. Scott Richard The stability of Mars's annular polar vortex. Journal of the Atmospheric Sciences.. 2017;74(5):1533–1547. https://doi.org/10.1175/jas-d-16-0293.1.

49. F. Tabataba-Vakili, P.L. Read, S.R. Lewis, et al. A Lorenz/Boer energy budget for the atmosphere of Mars from a "reanalysis" of spacecraft observations. Geophysical Research Letters. 2015;42(20):8320–8327. https://doi.org/10.1002/2015gl065659.

50. J. Greybush Steven, E. Kalnay, M.J. Hoffman, R.J. Wilson Identifying Martian atmospheric instabilities and their physical origins using bred vectors. Quarterly Journal of the Royal Meteorological Society.. 2013;139(672):639–653. https://doi.org/10.1002/qj.1990.

51. M. Battalio, I. Szunyogh, M. Lemmon Energetics of the martian atmosphere using the Mars Analysis correction data assimilation (MACDA) dataset. Icarus.. 2016;276:1–20. https://doi.org/10.1016/j.icarus.2016.04.028.

52. M. Battalio, I. Szunyogh, M. Lemmon Wave energetic of the southern hemisphere of Mars. Icarus.. 2018;309:220–240. https://doi.org/10.1016/j.icarus.2018.03.015.

53. J.M. Battalio Transient eddy kinetic energetics on Mars in three reanalysis datasets. Journal of the Atmospheric Sciences.. 2022;79(2):361–382. https://doi.org/10.1175/jas-d-21-0038.1.

54. R.J. Wilson, D. Banfield, B.J. Conrath, M.D. Smith Traveling waves in the Northern Hemisphere of Mars. Geophysical Research Letters.. 2002;29(14). https://doi.org/10.1029/2002gl014866.

55. T.A. Mooring, R.J. Wilson Transient eddies in the MACDA Mars reanalysis. Journal of Geophysical Research: Planets.. 2015;120(10):1671–1696. https://doi.org/10.1002/2015je004824.

56. S.R. Lewis, D.P. Mulholland, P.L. Read, L. Montabone, R.J. Wilson, M.D. Smith The solstitial pause on Mars: 1. A planetary wave reanalysis. Icarus.. 2016;264:456–464. https://doi.org/10.1016/j.icarus.2015.08.039.

57. M. Haberle R., Juárez Manuel de la Torre, M.A. Kahre, et al. Detection of Northern Hemisphere transient eddies at gale crater mars. Icarus.. 2018;307:150–160. https://doi.org/10.1016/j.icarus.2018.02.013.

58. D. Banfield, A. Spiga, C. Newman, et al. The atmosphere of Mars as observed by InSight. Nature Geoscience. 2020;13(3):190–198. https://doi.org/10.1038/s41561-020-0534-0.

59. M.G. Battalio M., N.C. Jackson de Juárez Torre, A. Sánchez-Lavega, D. Víudez-Moreiras Planetary waves traveling between Mars science laboratory and Insight 2020. Geophysical Research Letters.. 2022;49(21).

60. S. Zurita-Zurita, J.M. de la Torre, C.E. Newman, et al. Mars surface pressure oscillations as precursors of large dust storms reaching gale. Journal of Geophysical Research: Planets.. 2022;127(8).

61. M. Collins, S.R. Lewis, P.L. Read, F. Hourdin Baroclinic wave transitions in the Martian atmosphere. Icarus.. 1996;120(2):344–357. https://doi.org/10.1006/icar.1996.0055.

62. S.J. Greybush, J.E. Gillespie, R.J. Wilson Transient eddies in the TES/MCS ensemble Mars atmosphere reanalysis system (EMARS). Icarus.. 2019;317:158–181. https://doi.org/10.1016/j.icarus.2018.07.001.

63. J.L. Hollingsworth, R.M. Haberle, J.R. Barnes, et al. Orographic control of storm zones on Mars. Nature.. 1996;380(6573):413–416. https://doi.org/10.1038/380413a0.

64. J.L. Hollingsworth, R.M. Haberle, J. Schaeffer Seasonal variations of storm zones on Mars. Advances in Space Research.. 1997;19(8):1237–1240. https://doi.org/10.1016/s0273-1177(97)00275-5.

65. J.L. Hollingsworth, J.R. Barnes Forced stationary planetary waves in Mars's winter atmosphere. Journal of the Atmospheric Sciences. 1996;53(3):428–448. doi:10.1175/1520-0469(1996)053<0428:fspwim>2.0.co;2.

66. H. Wang, M.I. Richardson, R.J. Wilson, A.P. Ingersoll, A.D. Toigo, R.W. Zurek Cyclones, tides, and the origin of a cross-equatorial dust storm on Mars. Geophysical Research Letters. 2003;30(9). https://doi.org/10.1029/2002gl016828.

67. A. Cantor Bruce MOC observations of the 2001 Mars planet-encircling dust storm. Icarus.. 2007;186(1):60–96. https://doi.org/10.1016/j.icarus.2006.08.019.

68. J.L. Hollingsworth, M.A. Kahre Extratropical cyclones, frontal waves, and Mars dust: modeling and considerations. Geophysical Research Letters.. 2010;37(22). https://doi.org/10.1029/2010gl044262.

69. D.P. Hinson, H. Wang Further observations of regional dust storms and baroclinic eddies in the northern hemisphere of Mars. Icarus.. 2010;206(1):290–305. https://doi.org/10.1016/j.icarus.2009.08.019.

70. D.P. Hinson, H. Wang, M.D. Smith A multiyear survey of dynamics near the surface in the northern hemisphere of Mars: short-period baroclinic waves and dust storms. Icarus.. 2012;219(1):307–320. https://doi.org/10.1016/j.icarus.2012.03.001.

71. H. Wang, M.I. Richardson The origin, evolution, and trajectory of large dust storms on Mars during Mars years 24–30

(1999–2011). Icarus.. 2015;251:112–127. https://doi.org/10.1016/j.icarus.2013.10.033.

72. X. Jing, C. Kim-Chiu, C. Kwing-lam Dynamical processes of dust lifting in the northern mid-latitude region of Mars during the dust storm season. Icarus.. 2019;317:94–103. https://doi.org/10.1016/j.icarus.2018.07.020.

73. H. Wang, M. Saidel, M.I. Richardson, A.D. Toigo, J.M. Battalio Martian dust storm distribution and annual cycle from Mars daily global map observations. Icarus.. 2023;394. https://doi.org/10.1016/j.icarus.2022.115416.

74. J.M. Battalio, H. Wang, M.I. Richardson, A.D. Toigo, M. Saidel Spatial extent of dust storm boundaries in the Mars dust activity database. Icarus.. 2023;400. https://doi.org/10.1016/j.icarus.2023.115567.

75. C. Gebhardt, B.K. Guha, R.M.B. Young, M.J. Wolff A frontal dust storm in the Northern Hemisphere at solar longitude 97—an unusual observation by the Emirates Mars mission. Geophysical Research Letters.. 2022;49(20). https://doi.org/10.1029/2022GL099528.

76. S.D. Guzewich, A.D. Toigo, H. Wang An investigation of dust storms observed with the Mars color imager. Icarus.. 2017;289:199–213. https://doi.org/10.1016/j.icarus.2017.02.020.

77. S.D. Guzewich, A.D. Toigo, L. Kulowski, H. Wang Mars orbiter camera climatology of textured dust storms. Icarus.. 2015;258:1–13. https://doi.org/10.1016/j.icarus.2015.06.023.

78. J.B. Madeleine, F. Forget, E. Millour, L. Montabone, M.J. Wolff Revisiting the radiative impact of dust on Mars using the LMD global climate model. Journal of Geophysical Research: Planets. 2011;116(11). https://doi.org/10.1029/2011JE003855.

79. L. Montabone, F. Forget, E. Millour, et al. Eight-year climatology of dust optical depth on Mars. Icarus.. 2015;251:65–95. https://doi.org/10.1016/j.icarus.2014.12.034.

80. D.M. Kass, A. Kleinböhl, D.J. McCleese, J.T. Schofield, M.D. Smith Interannual similarity in the Martian atmosphere during the dust storm season. Geophysical Research Letters.. 2016;43(12):6111–6118. https://doi.org/10.1002/2016gl068978.

81. H. Nakamura Midwinter suppression of baroclinic wave activity in the pacific. Journal of the Atmospheric Sciences. 1992;49(17):1629–1642. doi:10.1175/1520-0469(1992)049<1629:msobwa>2.0.co;2.

82. T. Kuroda, A.S. Medvedev, P. Hartogh, M. Takahashi Seasonal changes of the baroclinic wave activity in the northern hemisphere of Mars simulated with a GCM. Geophysical Research Letters.. 2007;34(9). https://doi.org/10.1029/2006gl028816.

83. D.P. Mulholland, S.R. Lewis, P.L. Read, J.B. Madeleine, F. Forget The solsticial pause on Mars: 2 modelling and investigation of causes. Icarus.. 2016;264:465–477. https://doi.org/10.1016/j.icarus.2015.08.038.

84. C. Lee, M.I. Richardson, C.E. Newman, M.A. Mischna The sensitivity of solsticial pauses to atmospheric ice and dust in the MarsWRF general circulation model. Icarus. 2018;311:23–34. https://doi.org/10.1016/j.icarus.2018.03.019.

85. D.P. Hinson, R.J. Wilson Baroclinic waves in the northern hemisphere of Mars as observed by the MRO Mars climate sounder and the MGS thermal emission spectrometer. Icarus.. 2021;357. https://doi.org/10.1016/j.icarus.2020.114152.

86. R.M. Haberle, M.A. Kahre, J.L. Hollingsworth, et al. Documentation of the NASA/Ames legacy Mars global climate model: simulations of the present seasonal water cycle. Icarus.. 2019;333:130–164. https://doi.org/10.1016/j.icarus.2019.03.026.

87. Kahre M.A., Haberle R.M. Hollingsworth J.L., Wolff M.J. MARCI-observed clouds in the Hellas Basin during northern hemisphere summer on Mars: interpretation with the NASA/Ames legacy Mars global climate model. Icarus. 1135;338.

88. P. Drossart, G. Piccioni, A. Adriani, et al. Scientific goals for the observation of Venus by VIRTIS on ESA/Venus express mission. Planetary and Space Science.. 2007;55(12):1653–1672. https://doi.org/10.1016/j.pss.2007.01.003.

89. M. Nakamura, T. Imamura, N. Ishii, et al. AKATSUKI returns to Venus. Earth, Planets and Space. 2016;68(1).

90. N. Sugimoto, A. Yamazaki, T. Kouyama, H. Kashimura, T. Enomoto, M. Takagi Development of an ensemble Kalman filter data assimilation system for the Venusian atmosphere. Scientific Reports.. 2017;7(1). https://doi.org/10.1038/s41598-017-09461-1.

91. Y.L. Yung, W.B. DeMore Photochemistry of the stratosphere of Venus: implications for atmospheric evolution. Icarus.. 1982;51(2):199–247. https://doi.org/10.1016/0019-1035(82)90080-x.

92. K. McGouldrick, O.B. Toon An investigation of possible causes of the holes in the condensational Venus cloud using a microphysical cloud model with a radiative-dynamical feedback. Icarus.. 2007;191(1):1–24. https://doi.org/10.1016/j.icarus.2007.04.007.

93. P. Gao, X. Zhang, D. Crisp, C.G. Bardeen, Y.L. Yung Bimodal distribution of sulfuric acid aerosols in the upper haze of Venus. Icarus.. 2014;231:83–98. https://doi.org/10.1016/j.icarus.2013.10.013.

94. D.V. Titov, W.J. Markiewicz, N.I. Ignatiev, et al. Morphology of the cloud tops as observed by the Venus express monitoring camera. Icarus.. 2012;217(2):682–701. https://doi.org/10.1016/j.icarus.2011.06.020.

95. H. Ando, Y. Fujisawa, N. Sugimoto, M. Takagi, Y. Matsuda Cold collar reproduced by a Venus GCM with the Akatsuki horizontal wind assimilation. Journal of Geophysical Research: Planets.. 2023;128(4). https://doi.org/10.1029/2022je007689.

96. R. Hueso, J. Peralta, I. Garate-Lopez, T.V. Bandos, A. Sánchez-Lavega Six years of Venus winds at the upper cloud level from UV, visible and near infrared observations from VIRTIS on Venus Express. Planetary and Space Science.. 2015;113–114:78–99. https://doi.org/10.1016/j.pss.2014.12.010.

97. T. Horinouchi, Y.-Y. Hayashi, S. Watanabe, et al. How waves and turbulence maintain the superrotation of Venus' atmosphere. Science.. 2020;368(6489):405–409. https://doi.org/10.1126/science.aaz4439.

98. S. Lebonnois, N. Sugimoto, G. Gilli Wave analysis in the atmosphere of Venus below 100-km altitude, simulated by the LMD Venus GCM. Icarus.. 2016;278:38–51. https://doi.org/10.1016/j.icarus.2016.06.004.

99. N. Sugimoto, Y. Fujisawa, M. Shirasaka, et al. Kelvin wave and its impact on the Venus atmosphere tested by observing system simulation experiment. Atmosphere. 2022;13(2). https://doi.org/10.3390/atmos13020182.

100. M. Yamamoto, T. Hirose, K. Ikeda, M. Takahashi, M. Satoh Shortperiod planetary-scale waves in a Venus general circulation model: rotational and divergent component structures and energy conversions. Icarus.. 2023;392.

101. P.J. Gierasch Meridional circulation and the maintenance of the Venus atmospheric rotation. Journal of the Atmospheric Sciences. 1975;32(6):1038–1044. doi:10.1175/1520-0469(1975)032<1038:mcatmo>2.0.co;2.

102. W.B. Rossow, G.P. Williams Large-scale motion in the Venus stratosphere. Journal of the Atmospheric Sciences.

1979;36(3):377–389. doi:10.1175/1520-0469(1979)036<0377:lsmitv>2.0.co;2.

103. I. Garate-Lopez, S. Lebonnois Latitudinal variation of clouds' structure responsible for Venus' cold collar. Icarus.. 2018;314:1–11. https://doi.org/10.1016/j.icarus.2018.05.011.

104. A.D. Del Genio, W.B. Rossow Planetary-scale waves and the cyclic nature of cloud top dynamics on Venus. Journal of the Atmospheric Sciences. 1990;47(3):293–318. doi:10.1175/1520-0469(1990)047<0293:pswatc>2.0.co;2.

105. M. Imai, Y. Takahashi, M. Watanabe, et al. Ground-based observation of the cyclic nature and temporal variability of planetary-scale UV features at the Venus cloud top level. Icarus.. 2016;278:204–214. https://doi.org/10.1016/j.icarus.2016.06.011.

106. J. Peralta, K. Muto, R. Hueso, et al. Nightside winds at the lower clouds of Venus with Akatsuki/IR2: longitudinal, local time, and decadal variations from comparison with previous measurements. Astrophysical Journal, Supplement Series.. 2018;239(2). https://doi.org/10.3847/1538-4365/aae844.

107. M. Yamamoto, M. Takahashi Superrotation and equatorial waves in a 3-D Venus-like AGCM. Geophysical Research Letters. 2003;30(9). https://doi.org/10.1029/2003gl016924.

108. T. Imamura Meridional propagation of planetary-scale waves in vertical shear: implication for the Venus atmosphere. Journal of the Atmospheric Sciences.. 2006;63(6):1623–1636. https://doi.org/10.1175/jas3684.1.

109. N. Sugimoto, M. Takagi, Y. Matsuda Waves in a Venus general circulation model. Geophysical Research Letters.. 2014;41(21):7461–7467. https://doi.org/10.1002/2014gl061807.

110. B. Pollack James, B. Toon Owen, C. Whitten Robert, et al. Distribution and source of the UV absorption in Venus' atmosphere. Journal of Geophysical Research: Space Physics.. 1980;85(A13):8141–8150. https://doi.org/10.1029/ja085ia13p08141.

111. M. Yamamoto, M. Takahashi A parametric study of atmospheric superrotation on Venus-like planets: effects of oblique angle of planetary rotation axis. Geophysical Research Letters. 2007;34(16). https://doi.org/10.1029/2007gl030220.

112. T. Kouyama, T. Imamura, M. Nakamura, T. Satoh, Y. Futaana Vertical propagation of planetary-scale waves in variable background winds in the upper cloud region of Venus. Icarus.. 2015;248:560–568. https://doi.org/10.1016/j.icarus.2014.07.011.

113. A. Sánchez-Lavega, J. Peralta, J.M. Gomez-Forrellad, et al. Venus cloud morphology and motions from ground-based images at the time of the Akatsuki Orbit insertion. The Astrophysical Journal.. 2016;833(1). https://doi.org/10.3847/2041-8205/833/1/l7.

114. I. Lunine Jonathan, K. Atreya Sushil The methane cycle on Titan. Nature Geoscience.. 2008;1(3):159–164. https://doi.org/10.1038/ngeo125.

115. I. Lunine Jonathan, D. Lorenz Ralph Rivers, lakes, dunes, and rain: crustal processes in Titan's Methane cycle. Annual Review of Earth and Planetary Sciences. 2009;37(1):299–320. https://doi.org/10.1146/annurev.earth.031208.100142.

116. L. Mitchell Jonathan, M. Lora Juan The climate of Titan. Annual Review of Earth and Planetary Sciences.. 2016;44(1):353–380. https://doi.org/10.1146/annurev-earth-060115-012428.

117. A.G. Hayes, R.D. Lorenz, J.I. Lunine A post-Cassini view of Titan's methane-based hydrologic cycle. Nature Geoscience.. 2018;11(5):306–313. https://doi.org/10.1038/s41561-018-0103-y.

118. T. Tokano Meteorological assessment of the surface temperatures on Titan: constraints on the surface type. Icarus.. 2005;173(1):222–242. https://doi.org/10.1016/j.icarus.2004.08.019.

119. S.M. MacKenzie, J.M. Lora, R.D. Lorenz A thermal inertia map of Titan. Journal of Geophysical Research: Planets.. 2019;124(7):1728–1742. https://doi.org/10.1029/2019je005930.

120. F.M. Flasar, R.K. Achterberg The structure and dynamics of Titan's middle atmosphere. Philosophical Transactions of the Royal Society A: Mathematical, Physical and Engineering Sciences. 1889;367:649–664.

121. N.A. Teanby, B. Bézard, S. Vinatier, et al. The formation and evolution of Titan's winter polar vortex. Nature Communications.. 2017;8(1). https://doi.org/10.1038/s41467-017-01839-z.

122. N.A. Teanby, M. Sylvestre, J. Sharkey, C.A. Nixon, S. Vinatier, P.G.J. Irwin Seasonal evolution of Titan's stratosphere during the Cassini mission. Geophysical Research Letters.. 2019;46(6):3079–3089. https://doi.org/10.1029/2018gl081401.

123. J. Sharkey, N.A. Teanby, M. Sylvestre, et al. Potential vorticity structure of Titan's polar vortices from Cassini CIRS observations. Icarus. 2021;354. https://doi.org/10.1016/j.icarus.2020.114030.

124. F. Hourdin, F. Forget, O. Talagrand The sensitivity of the Martian surface pressure and atmospheric mass budget to various parameters: a comparison between numerical simulations and Viking observations. Journal of Geophysical Research: Planets.. 1995;100(E3):5501–5523. https://doi.org/10.1029/94je03079.

125. C.E. Newman, C. Lee, Y. Lian, M.I. Richardson, A.D. Toigo Stratospheric superrotation in the TitanWRF model. Icarus. 2011;213(2):636–654. 10.1016/j.icarus.2011.03.025.

126. S. Lebonnois, C. Covey, A. Grossman, et al. Angular momentum budget in general circulation models of superrotating atmospheres: a critical diagnostic. Journal of Geophysical Research: Planets.. 2012;117(E12). https://doi.org/10.1029/2012je004223.

127. N.A. Lombardo, J.M. Lora Influence of observed seasonally varying composition on Titan's stratospheric circulation. Icarus.. 2023;390. https://doi.org/10.1016/j.icarus.2022.115291.

128. N.T. Lewis, N.A. Lombardo, P.L. Read, J.M. Lora Equatorial waves and superrotation in the stratosphere of a Titan general circulation model. The Planetary Science Journal.. 2023;4(8). https://doi.org/10.3847/psj/ace76f.

129. J.M. Lora, J.I. Lunine, J.L. Russell GCM simulations of Titan's middle and lower atmosphere and comparison to observations. Icarus.. 2015;250:516–528. https://doi.org/10.1016/j.icarus.2014.12.030.

130. J.M. Lora, J.M. Battalio, M. Yap, C. Baciocco Topographic and orbital forcing of Titan's hydroclimate. Icarus. 2022;384. https://doi.org/10.1016/j.icarus.2022.115095.

131. M.K. Bird, M. Allison, S.W. Asmar, et al. The vertical profile of winds on Titan. Nature.. 2005;438(7069):800–802. https://doi.org/10.1038/nature04060.

132. J.L. Mitchell, R.T. Pierrehumbert, D.M.W. Frierson, R. Caballero The dynamics behind Titan's methane clouds. Proceedings of the National Academy of Sciences. 2006;103(49):18421–18426. https://doi.org/10.1073/pnas.0605074103.

133. H.B. Niemann, S.K. Atreya, J.E. Demick, et al. Composition of Titan's lower atmosphere and simple surface volatiles as measured by the Cassini–Huygens probe gas chromatograph mass spectrometer experiment. Journal of Geophysical Research E: Planets. 2010;115(12):1–22.

134. C.A. Nixon, R.D. Lorenz, R.K. Achterberg, et al. Titan's cold case files - outstanding questions after Cassini–Huygens. Planetary and Space Science.. 2018;155:50–72. https://doi.org/10.1016/j.pss.2018.02.009.

135. M.E. Brown, A.H. Bouchez, C.A. Griffith Direct detection of variable tropospheric clouds near Titan's south pole. Nature.. 2002;420(6917):795–797. https://doi.org/10.1038/nature01302.

136. H.G. Roe, I. de Pater, B.A. Macintosh, C.P. McKay Titan's clouds from gemini and keck adaptive optics imaging. The Astrophysical Journal.. 2002;581(2):1399–1406. https://doi.org/10.1086/344403.

137. E.L. Schaller, H.G. Roe, T. Schneider, M.E. Brown Storms in the tropics of Titan. Nature.. 2009;460(7257):873–875. https://doi.org/10.1038/nature08193.

138. E.P. Turtle, J.E. Perry, J.M. Barbara, et al. Titan's meteorology over the Cassini mission: evidence for extensive subsurface methane reservoirs. Geophysical Research Letters.. 2018;45(11):5320–5328. https://doi.org/10.1029/2018gl078170.

139. E.P. Turtle, A.D. Del Genio, J.M. Barbara, et al. Seasonal changes in Titan's meteorology. Geophysical Research Letters.. 2011;38(3):1–5.

140. J.L. Mitchell, M. Ádámkovics, R. Caballero, E.P. Turtle Locally enhanced precipitation organized by planetary-scale waves on Titan. Nature Geoscience.. 2011;4(9):589–592. https://doi.org/10.1038/ngeo1219.

141. S.M. Hörst Titan's atmosphere and climate. Journal of Geophysical Research: Planets. 2017;122(3):432–482. https://doi.org/10.1002/2016je005240.

142. P. Lavvas, C.A. Griffith, R.V. Yelle Condensation in Titan's atmosphere at the Huygens landing site. Icarus.. 2011;215(2):732–750. https://doi.org/10.1016/j.icarus.2011.06.040.

143. P. Lavvas, R.V. Yelle, T. Koskinen, et al. Aerosol growth in Titan's ionosphere. Proceedings of the National Academy of Sciences.. 2013;110(8):2729–2734. https://doi.org/10.1073/pnas.1217059110.

144. C.P. McKay, J.B. Pollack, R. Courtin The thermal structure of Titan's atmosphere. Icarus.. 1989;80(1):23–53. https://doi.org/10.1016/0019-1035(89)90160-7.

145. C.P. McKay, J.B. Pollack, R. Courtin The greenhouse and antigreenhouse effects on Titan. Science.. 1991;253(5024):1118–1121. https://doi.org/10.1126/science.11538492.

146. M.G. Tomasko, L. Doose, S. Engel, et al. A model of Titan's aerosols based on measurements made inside the atmosphere. Planetary and Space Science.. 2008;56(5):669–707. https://doi.org/10.1016/j.pss.2007.11.019.

147. G.F. Lindal, G.E. Wood, H.B. Hotz, D.N. Sweetnam, V.R. Eshleman, G.L. Tyler The atmosphere of Titan: an analysis of the Voyager 1 radio occultation measurements. Icarus.. 1983;53(2):348–363. https://doi.org/10.1016/0019-1035(83)90155-0.

148. M. Fulchignoni, F. Ferri, F. Angrilli, et al. In situ measurements of the physical characteristics of Titan's environment. Nature.. 2005;438(7069):785–791. https://doi.org/10.1038/nature04314.

149. B.J. Conrath Influence of planetary-scale topography on the diurnal thermal tide during the 1971 Martian dust storm. Journal of the Atmospheric Sciences. 1976;33(12):2430–2439. doi:10.1175/1520-0469(1976)033<2430:iopsto>2.0.co;2.

150. B. Leovy Conway, W. Jakosky Richard Thermal tides and Martian dust storms: direct evidence for coupling. Journal of Geophysical Research: Solid Earth.. 1979;84(B6):2956–2968. https://doi.org/10.1029/jb084ib06p02956.

151. B. Leovy Conway Observations of Martian tides over two annual cycles. Journal of the Atmospheric Sciences. 1981;38(1):30–39. doi:10.1175/1520-0469(1981)038<0030:oomtot>2.0.co;2.

152. R.J. Wilson, K. Hamilton Comprehensive model simulation of thermal tides in the Martian atmosphere. Journal of the Atmospheric Sciences. 1996;53(9):1290–1326. doi:10.1175/1520-0469(1996)053<1290:cmsott>2.0.co;2.

153. A.F.C. Bridger, J.R. Murphy Mars' surface pressure tides and their behavior during global dust storms. Journal of Geophysical Research: Planets.. 1998;103(E4):8587–8601. https://doi.org/10.1029/98je00242.

154. D. Banfield, B. Conrath, J.C. Pearl, M.D. Smith, P. Christensen Thermal tides and stationary waves on Mars as revealed by Mars global surveyor thermal emission spectrometer. Journal of Geophysical Research: Planets.. 2000;105(E4):9521–9537. https://doi.org/10.1029/1999je001161.

155. R.J. Wilson Evidence for diurnal period Kelvin waves in the Martian atmosphere from Mars global surveyor TES data. Geophysical Research Letters.. 2000;27(23):3889–3892. https://doi.org/10.1029/2000gl012028.

156. D.P. Hinson, R.J. Wilson Temperature inversions, thermal tides, and water ice clouds in the Martian tropics. Journal of Geophysical Research: Planets.. 2004;109(1). https://doi.org/10.1029/2003je002129 E01002-E01002.

157. S.R. Lewis, P.R. Barker Atmospheric tides in a Mars general circulation model with data assimilation. Advances in Space Research.. 2005;36(11):2162–2168. https://doi.org/10.1016/j.asr.2005.05.122.

158. K.L. Cahoy, D.P. Hinson, G.L. Tyler Characterization of a semidiurnal eastward-propagating tide at high northern latitudes with Mars Global Surveyor electron density profiles. Geophysical Research Letters.. 2007;34(15). https://doi.org/10.1029/2007GL030449.

159. C. Lee, W.G. Lawson, M.I. Richardson, et al. Thermal tides in the martian middle atmosphere as seen by the mars climate sounder. Journal of Geophysical Research: Planets. 2009;114(3). https://doi.org/10.1029/2008JE003285.

160. P. Withers, D.C. Catling Observations of atmospheric tides on Mars at the season and latitude of the Phoenix atmospheric entry. Geophysical Research Letters.. 2010;37(24). https://doi.org/10.1029/2010gl045382.

161. T.M. Sato, H. Fujiwara, Y.O. Takahashi, et al. Tidal variations in the Martian lower atmosphere inferred from Mars express planetary fourier spectrometer temperature data. Geophysical Research Letters.. 2011;38(24). https://doi.org/10.1029/2011gl050348.

162. Wilson R.J. (2012). The role of thermal tides in the Martian dust cycle. Vol 7. European Planetary Science Congress.

163. D. Guzewich Scott, R. Talaat Elsayed, W. Waugh Darryn Observations of planetary waves and nonmigrating tides by the Mars

climate sounder. Journal of Geophysical Research: Planets.. 2012;117(E3). https://doi.org/10.1029/2011je003924.

164. A. Kleinböhl, R.J. Wilson, D. Kass, J.T. Schofield, D.J. McCleese The semidiurnal tide in the middle atmosphere of Mars. Geophysical Research Letters.. 2013;40(10):1952–1959. https://doi.org/10.1002/grl.50497.

165. S.D. Guzewich, R.J. Wilson, T.H. McConnochie, A.D. Toigo, D.J. Banfield, M.D. Smith Thermal tides during the 2001 Martian global-scale dust storm. Journal of Geophysical Research: Planets. 2014;119(3):506–519. https://doi.org/10.1002/2013je004502.

166. Z. Wu, T. Li, X. Dou Seasonal variation of Martian middle atmosphere tides observed by the Mars climate sounder. Journal of Geophysical Research: Planets.. 2015;120(12):2206–2223. https://doi.org/10.1002/2015je004922.

167. S.L. England, G. Liu, P. Withers, et al. Simultaneous observations of atmospheric tides from combined in situ and remote observations at Mars from the MAVEN spacecraft. Journal of Geophysical Research: Planets. 2016;121(4):594–607. https://doi.org/10.1002/2016je004997.

168. Z. Wu, T. Li, X. Zhang, J. Li, J. Cui Dust tides and rapid meridional motions in the Martian atmosphere during major dust storms. Nature Communications.. 2020;11(1). https://doi.org/10.1038/s41467-020-14510-x.

169. L.J. Steele, A. Kleinböhl, D.M. Kass, R.W. Zurek Aerosols and tides in the Martian tropics during southern hemisphere spring equinox from Mars climate sounder data. Journal of Geophysical Research: Planets.. 2021;126(4). https://doi.org/10.1029/2020je006776.

170. M. Slipski, A. Kleinböhl, D.M. Kass Role of thermal tides and gravity waves in Mars equatorial mesospheric cloud formation revealed by Mars climate sounder observations. Geophysical Research Letters.. 2022;49(24). https://doi.org/10.1029/2022gl100607.

171. S. Fan, F. Forget, M.D. Smith, et al. Migrating thermal tides in the Martian atmosphere during aphelion season observed by EMM/EMIRS. Geophysical Research Letters.. 2022;49(19). https://doi.org/10.1029/2022GL099494.

172. J. Peralta, D. Luz, D.L. Berry, et al. Solar migrating atmospheric tides in the winds of the polar region of Venus. Icarus.. 2012;220(2):958–970. https://doi.org/10.1016/j.icarus.2012.06.015.

173. J.R. Barnes Linear baroclinic instability in the Martian atmosphere. Journal of the Atmospheric Sciences. 1984;41(9):1536–1550. doi:10.1175/1520-0469(1984)041<1536:lbiitm>2.0.co;2.

174. P. Kopparla, Y.J. Lee, T. Imamura, A. Yamazaki Principal components of short-term variability in the ultraviolet albedo of Venus. Astronomy and Astrophysics.. 2019;626. https://doi.org/10.1051/0004-6361/201935388.

175. Y. Nara, T. Imamura, K. Masunaga, et al. Vertical coupling between the cloud-level atmosphere and the thermosphere of Venus inferred from the simultaneous observations by Hisaki and Akatsuki. Journal of Geophysical Research: Planets.. 2020;125(3). https://doi.org/10.1029/2019JE006192.

176. H. Ando, M. Takagi, H. Sagawa, N. Sugimoto, M. Sekiguchi, Y. Matsuda Quasi-periodic variation of the lower equatorial cloud induced by atmospheric waves on Venus. Journal of Geophysical Research: Planets.. 2021;126(6). https://doi.org/10.1029/2020JE006781.

177. D. Lai, T. Li Long-term variation of the quasi-five-day wave in the top layer of Venus clouds. Journal of Geophysical Research: Planets.. 2023;128(4). https://doi.org/10.1029/2022JE007596.

178. Y.J. Lee, A. García Muñoz, T. Imamura, et al. Brightness modulations of our nearest terrestrial planet Venus reveal atmospheric superrotation rather than surface features. Nature Communications.. 2020;11(1). https://doi.org/10.1038/s41467-020-19385-6.

179. J. Peralta, T. Navarro, C.W. Ortun, et al. A long-lived sharp disruption on the lower clouds of Venus. Geophysical Research Letters.. 2020;47(11). https://doi.org/10.1029/2020GL087221.

180. N. Kajiwara, T. Imamura, M. Taguchi, T. Kouyama Planetary-scale waves seen in thermal infrared images of Venusian cloud top. Journal of Geophysical Research: Planets. 2021;126(12). https://doi.org/10.1029/2021JE007047.

181. M. Yamamoto, M. Takahashi Venusian middle-atmospheric dynamics in the presence of a strong planetary-scale 5.5-day wave. Icarus.. 2012;217(2):702–713. https://doi.org/10.1016/j.icarus.2011.06.017.

182. J. Peralta, A. Sánchez-Lavega, M.A. López-Valverde, D. Luz, P. Machado Venus's major cloud feature as an equatorially trapped wave distorted by the wind. Geophysical Research Letters. 2015;42(3):705–711. https://doi.org/10.1002/2014gl062280.

183. Y. Nara, T. Imamura, S. Murakami, et al. Formation of the Y feature at the Venusian cloud Top by planetary-scale waves and the mean circulation: analysis of Venus express VMC images. Journal of Geophysical Research: Planets. 2019;124(5):1143–1156. https://doi.org/10.1029/2018je005779.

184. T. Fukuhara, M. Futaguchi, G.L. Hashimoto, et al. Large stationary gravity wave in the atmosphere of Venus. Nature Geoscience.. 2017;10(2):85–88. https://doi.org/10.1038/ngeo2873.

185. Y. Kaspi, A.P. Showman Atmospheric dynamics of terrestrial explanets over a wide range of orbital and atmospheric parameters. The Astrophysical Journal.. 2015;804(1). https://doi.org/10.1088/0004-637x/804/1/60.

186. I.V. Khatuntsev, M.V. Patsaeva, D.V. Titov, L.V. Zasova, N.I. Ignatiev, D.A. Gorinov Twelve-year cycle in the cloud top winds derived from VMC/Venus express and UVI/Akatsuki imaging. Atmosphere.. 2022;13(12). https://doi.org/10.3390/atmos13122023.

187. L.J. Martin Clearing the Martian air: the troubled history of dust storms. Icarus.. 1984;57(3):317–321. https://doi.org/10.1016/0019-1035(84)90120-9.

188. L.J. Martin, R.W. Zurek An analysis of the history of dust activity on Mars. Journal of Geophysical Research.. 1993;98(2):3221–3246. https://doi.org/10.1029/92JE02937.

189. R.W. Zurek, L.J. Martin Interannual variability of planet-encircling dust storms on Mars. Journal of Geophysical Research.. 1993;98(2):3247–3259. https://doi.org/10.1029/92JE02936.

190. J.R. Murphy, O.B. Toon, R.M. Haberle, J.B. Pollack Numerical simulations of the decay of Martian global dust storms. Journal of Geophysical Research: Solid Earth.. 1990;95(B9):14629–14648. https://doi.org/10.1029/jb095ib09p14629.

191. M.J. Strausberg, H. Wang, M.I. Richardson, S.P. Ewald, A.D. Toigo Observations of the initiation and evolution of the 2001 Mars global dust storm. Journal of Geophysical Research: Planets.. 2005;110(E2). https://doi.org/10.1029/2004je002361.

192. R. Todd Clancy, M.J. Wolff, B.A. Whitney, B.A. Cantor, M.D. Smith, T.H. McConnochie Extension of atmospheric dust loading to high altitudes during the 2001 Mars dust storm: MGS TES limb observations. Icarus.. 2010;207(1):98–109. https://doi.org/10.1016/j.icarus.2009.10.011.

193. A. Sánchez-Lavega, T. del Río-Gaztelurrutia, J. Hernández-Bernal, M. Delcroix The onset and growth of the 2018 Martian global dust storm. Geophysical Research Letters. 2019;46(11):6101–6108. https://doi.org/10.1029/2019gl083207.

194. J.H. Shirley, C.E. Newman, M.A. Mischna, M.I. Richardson Replication of the historic record of martian global dust storm occurrence in an atmospheric general circulation model. Icarus.. 2019;317:197–208. https://doi.org/10.1016/j.icarus.2018.07.024.

195. J.H. Shirley, R.J. McKim, J.M. Battalio, D.M. Kass Orbit-spin coupling and the triggering of the Martian planet-encircling dust storm of 2018. Journal of Geophysical Research: Planets.. 2020;125(6). https://doi.org/10.1029/2019JE006077.

196. P. Wolkenberg, M. Giuranna, M.D. Smith, D. Grassi, M. Amoroso Similarities and differences of global dust storms in MY 25, 28, and 34. Journal of Geophysical Research: Planets.. 2020;125(3). https://doi.org/10.1029/2019je006104.

197. D.M. Kass, J.T. Schofield, A. Kleinböhl, et al. Mars climate sounder observation of Mars' 2018 global dust storm. Geophysical Research Letters.. 2018;47(23):1–9.

198. Montabone L., Spiga A., Kass D.M., A. Kleinböhl, F. Forget and E. Millour. Martian Year 34 column dust climatology from Mars climate sounder observations: reconstructed maps and model simulations. Journal of Geophysical Research: Planets. 125(8).

199. H.E. Gillespie, S.J. Greybush, R.J. Wilson An investigation of the encirclement of Mars by dust in the 2018 global dust storm using EMARS. Journal of Geophysical Research: Planets.. 2020;125(7). https://doi.org/10.1029/2019je006106.

200. E.P. Gerber, D.W.J. Thompson What makes an annular mode "Annular"? Journal of the Atmospheric Sciences. 2017;74(2):317–332. https://doi.org/10.1175/jas-d-16-0191.1.

201. D.W.J. Thompson, J.M. Wallace Annular modes in the extratropical circulation. Part i: month-to-month variability*. Journal of Climate. 2000;13(5):1000–1016. doi:10.1175/1520-0442(2000)013<1000:amitec>2.0.co;2.

202. P. Hassanzadeh, Z. Kuang Quantifying the annular mode dynamics in an idealized atmosphere. Journal of the Atmospheric Sciences.. 2019;76(4):1107–1124. https://doi.org/10.1175/jas-d-18-0268.1.

203. K.E. Trenberth, D.A. Paolino Characteristic patterns of variability of sea level pressure in the Northern Hemisphere. Monthly Weather Review. 1981;109(6):1169–1189. doi:10.1175/1520-0493(1981)109<1169:cpovos>2.0.co;2.

204. D.L. Hartmann, F. Lo Wave-driven zonal flow vacillation in the Southern Hemisphere. Journal of the Atmospheric Sciences. 1998;55(8):1303–1315. doi:10.1175/1520-0469(1998)055<1303:wdzfvi>2.0.co;2.

205. D.L. Hartmann, J.M. Wallace, V. Limpasuvan, D.W.J. Thompson, J.R. Holton Can ozone depletion and global warming interact to produce rapid climate change? Proceedings of the National Academy of Sciences. 2000;97(4):1412–1417. https://doi.org/10.1073/pnas.97.4.1412.

206. D.W.J. Thompson, J.M. Wallace The arctic oscillation signature in the wintertime geopotential height and temperature fields. Geophysical Research Letters.. 1998;25(9):1297–1300. https://doi.org/10.1029/98gl00950.

207. D.J. Lorenz, D.L. Hartmann Eddy–zonal flow feedback in the Southern Hemisphere. Journal of the Atmospheric Sciences. 2001;58(21):3312–3327. doi:10.1175/1520-0469(2001)058<3312:ezffit>2.0.co;2.

208. J.W. Kidson Interannual variations in the Southern Hemisphere circulation. Journal of Climate. 1988;1(12):1177–1198. doi:10.1175/1520-0442(1988)001<1177:ivitsh>2.0.co;2.

209. G.R. North, T.L. Bell, R.F. Cahalan, F.J. Moeng Sampling errors in the estimation of empirical orthogonal functions. Monthly Weather Review.. 1982;110(7):699–706. doi:10.1175/1520-0493(1982)110<0699:seiteo>2.0.co;2.

210. A. Hannachi, I.T. Jolliffe, D.B. Stephenson Empirical orthogonal functions and related techniques in atmospheric science: a review. International Journal of Climatology.. 2007;27(9):1119–1152. https://doi.org/10.1002/joc.1499.

211. M.P. Baldwin Annular modes in global daily surface pressure. Geophysical Research Letters.. 2001;28(21):4115–4118. https://doi.org/10.1029/2001GL013564.

212. L. Boljka, T.G. Shepherd, M. Blackburn On the coupling between barotropic and baroclinic modes of extratropical atmospheric variability. Journal of the Atmospheric Sciences.. 2018;75(6):1853–1871. https://doi.org/10.1175/jas-d-17-0370.1.

213. S.W. Lubis, P. Hassanzadeh The intrinsic 150-day periodicity of the Southern Hemisphere extratropical large-scale atmospheric circulation. AGU Advances.. 2023;4(3).

214. D.W.J. Thompson, E.A. Barnes Periodic variability in the large-scale Southern Hemisphere atmospheric circulation. Science.. 2014;343(6171):641–645. https://doi.org/10.1126/science.1247660.

215. D.J. Karoly The role of transient eddies in low-frequency zonal variations of the Southern Hemisphere circulation. Tellus, Series A. 1990;42(1):41–50. https://doi.org/10.3402/tellusa.v42i1.11858.

216. V. Limpasuvan, D.L. Hartmann Wave-maintained annular modes of climate variability*. Journal of Climate. 2000;13(24):4414–4429. doi:10.1175/1520-0442(2000)013<4414:wmamoc>2.0.co;2.

217. D.W.J. Thompson, J.D. Woodworth Barotropic and baroclinic annular variability in the Southern Hemisphere. Journal of the Atmospheric Sciences.. 2014;71(4):1480–1493. https://doi.org/10.1175/jas-d-13-0185.1.

218. A.J. Simmons, B.J. Hoskins The life cycles of some nonlinear baroclinic waves. Journal of the Atmospheric Sciences. 1978;35(3):414–432. doi:10.1175/1520-0469(1978)035<0414:tlcosn>2.0.co;2.

219. D.W.J. Thompson, Y. Li Baroclinic and barotropic annular variability in the Northern Hemisphere. Journal of the Atmospheric Sciences.. 2015;72(3):1117–1136. https://doi.org/10.1175/jas-d-14-0104.1.

220. R.L. Fogt, G.J. Marshall The southern annular mode: variability, trends, and climate impacts across the Southern Hemisphere. WIREs Climate Change.. 2020;11(4). https://doi.org/10.1002/wcc.652.

221. E.W. Doddridge, J. Marshall Modulation of the seasonal cycle of antarctic sea ice extent related to the southern annular mode. Geophysical Research Letters.. 2017;44(19):9761–9768. https://doi.org/10.1002/2017gl074319.

222. Y. Li, D.W.J. Thompson, Y. Huang, M. Zhang Observed linkages between the northern annular mode/North Atlantic Oscillation,

cloud incidence, and cloud radiative forcing. Geophysical Research Letters.. 2014;41(5):1681–1688. https://doi.org/10.1002/2013gl059113.

223. Y. Li, D.W.J. Thompson Observed signatures of the barotropic and baroclinic annular modes in cloud vertical structure and cloud radiative effects. Journal of Climate.. 2016;29(13):4723–4740. https://doi.org/10.1175/jcli-d-15-0692.1.

224. J. Nie, P. Wang, W. Yang, B. Tan Northern hemisphere storm tracks in strong AO anomaly winters. Atmospheric Science Letters.. 2008;9(3):153–159. https://doi.org/10.1002/asl.186.

225. J. Kidston, D.M.W. Frierson, J.A. Renwick, G.K. Vallis Observations, simulations, and dynamics of jet stream variability and annular modes. Journal of Climate.. 2010;23(23):6186–6199. https://doi.org/10.1175/2010jcli3235.1.

226. C. Strong, G. Magnusdottir Tropospheric Rossby wave breaking and the NAO/NAM. Journal of the Atmospheric Sciences.. 2008;65(9):2861–2876. https://doi.org/10.1175/2008jas2632.1.

227. G. Rivière, I. Orlanski Characteristics of the atlantic storm-track eddy activity and its relation with the North Atlantic oscillation. Journal of the Atmospheric Sciences.. 2007;64(2):241–266. https://doi.org/10.1175/jas3850.1.

228. G. Rivière Effect of latitudinal variations in low-level baroclinicity on eddy life cycles and upper-tropospheric wave-breaking processes. Journal of the Atmospheric Sciences.. 2009;66(6):1569–1592. https://doi.org/10.1175/2008jas2919.1.

229. G. Rivière, A. Laîné, G. Lapeyre, D. Salas-Mélia, M. Kageyama Links between Rossby wave breaking and the North Atlantic oscillation–arctic oscillation in present-day and last glacial maximum climate simulations. Journal of Climate.. 2010;23(11):2987–3008. https://doi.org/10.1175/2010jcli3372.1.

230. T. Woollings, A. Hannachi, B. Hoskins Variability of the North Atlantic eddy-driven jet stream. Quarterly Journal of the Royal Meteorological Society.. 2010;136(649):856–868. https://doi.org/10.1002/qj.625.

231. M. Drouard, G. Rivière, P. Arbogast The link between the North Pacific climate variability and the North Atlantic oscillation via downstream propagation of synoptic waves. Journal of Climate.. 2015;28(10):3957–3976. https://doi.org/10.1175/jcli-d-14-00552.1.

232. J.M. Wallace North atlantic oscillatiodannular mode: two paradigms—one phenomenon. Quarterly Journal of the Royal Meteorological Society.. 2000;126(564):791–805. https://doi.org/10.1002/qj.49712656402.

233. M.H.P. Ambaum, B.J. Hoskins, D.B. Stephenson Arctic oscillation or North Atlantic oscillation? Journal of Climate. 2001;14(16):3495–3507. doi:10.1175/1520-0442(2001)014<3495:aoonao>2.0.co;2.

234. W.A. Robinson A baroclinic mechanism for the eddy feedback on the zonal index. Journal of the Atmospheric Sciences. 2000;57(3):415–422. doi:10.1175/1520-0469(2000)057<0415:abmfte>2.0.co;2.

235. S.W. Lubis, P. Hassanzadeh An eddy–zonal flow feedback model for propagating annular modes. Journal of the Atmospheric Sciences.. 2021;78(1):249–267. https://doi.org/10.1175/jas-d-20-0214.1.

236. S.B. Feldstein An observational study of the intraseasonal poleward propagation of zonal mean flow anomalies. Journal of the Atmospheric Sciences. 1998;55(15):2516–2529. doi:10.1175/1520-0469(1998)055<2516:aosoti>2.0.co;2.

237. A. Sheshadri, R.A. Plumb Propagating annular modes: empirical orthogonal functions, principal oscillation patterns, and time scales. Journal of the Atmospheric Sciences.. 2017;74(5):1345–1361. https://doi.org/10.1175/jas-d-16-0291.1.

238. S.S. Leroy, Y.L. Yung, M.I. Richardson, R.J. Wilson Principal modes of variability of Martian atmospheric surface pressure. Geophysical Research Letters.. 2003;30(13). https://doi.org/10.1029/2002gl015909.

239. Y. Yamashita, T. Kuroda, M. Takahashi Maintenance of zonal wind variability associated with the annular mode on Mars. Geophysical Research Letters.. 2007;34(16). https://doi.org/10.1029/2007gl030069.

240. K. Yamazaki, Y. Shinya Analysis of the arctic oscillation simulated by AGCM. Journal of the Meteorological Society of Japan Ser II.. 1999;77(6):1287–1298. https://doi.org/10.2151/jmsj1965.77.6_1287.

241. Y. Yamashita, H.L. Tanaka, M. Takahashi Observational analysis of the local structure of the wave activity flux associated with maintenances of the arctic oscillation index. SOLA.. 2005;1:53–56. https://doi.org/10.2151/sola.2005-015.

242. V. Limpasuvan, D.L. Hartmann Eddies and the annular modes of climate variability. Geophysical Research Letters.. 1999;26(20):3133–3136. https://doi.org/10.1029/1999gl010478.

243. M.J. Kavulich, I. Szunyogh, G. Gyarmati, R.J. Wilson Local dynamics of baroclinic waves in the Martian atmosphere. Journal of the Atmospheric Sciences.. 2013;70(11):3415–3447. https://doi.org/10.1175/jas-d-12-0262.1.

244. L. Nayvelt, P.J. Gierasch, K.H. Cook Modeling and observations of Martian stationary waves. Journal of the Atmospheric Sciences.. 1997;54(8):986–1013. doi:10.1175/1520-0469(1997)054<0986:maooms>2.0.co;2.

245. D. Banfield, B.J. Conrath, M.D. Smith, P.R. Christensen, R.J. Wilson Forced waves in the martian atmosphere from MGS TES nadir data. Icarus. 2003;161(2):319–345. https://doi.org/10.1016/s0019-1035(02)00044-1.

246. R.J. Wilson Stationary planetary waves in the atmosphere of Mars during southern winter. Journal of Geophysical Research.. 2003;108(E1). https://doi.org/10.1029/2002je001949.

247. R.M. Haberle, M.A. Kahre, J.R. Barnes, J.L. Hollingsworth, M.J. Wolff MARCI observations of a wavenumber-2 large-scale feature in the north polar hood of Mars: Interpretation with the NASA/Ames legacy global climate model. Icarus. 2020;335. https://doi.org/10.1016/j.icarus.2019.07.001.

248. C. Chung, S. Nigam Weighting of geophysical data in principal component analysis. Journal of Geophysical Research: Atmospheres. 1999;104(D14):16925–16928. https://doi.org/10.1029/1999jd900234.

249. A. Kleinböhl, J.T. Schofield, D.M. Kass, et al. Mars climate sounder limb profile retrieval of atmospheric temperature, pressure, and dust and water ice opacity. Journal of Geophysical Research: Planets.. 2009;114(E10). https://doi.org/10.1029/2009je003358.

250. R.D. Lorenz, M.T. Lemmon, P.H. Smith, G.W. Lockwood Seasonal change on Titan observed with the hubble space telescope WFPC-2. Icarus.. 1999;142(2):391–401. https://doi.org/10.1006/icar.1999.6225.

251. R.D. Lorenz, P.H. Smith, M.T. Lemmon, E. Karkoschka, G.W. Lockwood, J. Caldwell Titan's north-south asymmetry from HST and voyager imaging: comparison with models and ground-based photometry. Icarus.. 1997;127(1):173–189. https://doi.org/10.1006/icar.1997.5687.

252. R.D. Lorenz, E.F. Young, M.T. Lemmon Titan's smile and collar: HST observations of seasonal change 1994-2000. Geophysical Research Letters.. 2001;28(23):4453–4456. https://doi.org/10.1029/2001GL013728.

253. L.A. Sromovsky, V.E. Suomi, J.B. Pollack, et al. Implications of Titan's north-south brightness asymmetry. Nature.. 1981;292(5825):698–702. https://doi.org/10.1038/292698a0.

254. R. de Kok, P.G.J. Irwin, N.A. Teanby, et al. A tropical haze band in Titan's stratosphere. Icarus.. 2010;207(1):485–490. https://doi.org/10.1016/j.icarus.2009.10.021.

255. C.C. Porco, E. Baker, J. Barbara, et al. Imaging of Titan from the Cassini spacecraft. Nature.. 2005;434(7030):159–168. https://doi.org/10.1038/nature03436.

256. F. Nichols-Fleming, P. Corlies, A.G. Hayes, et al. Tracking short-term variations in the haze distribution of titan's atmosphere with SINFONI VLT. Planetary Science Journal. 2021;2(5). https://doi.org/10.3847/PSJ/abffd7.

257. N.W. Kutsop, A.G. Hayes, P.M. Corlies, et al. Titan stratospheric haze bands observed in Cassini VIMS as tracers of meridional circulation. The Planetary Science Journal.. 2022;3(5). https://doi.org/10.3847/psj/ac582d.

258. D.E. Jennings, R.K. Achterberg, V. Cottini, et al. Evolution of the far-infrared cloud at Titan's south pole. Astrophysical Journal Letters.. 2015;804(2). https://doi.org/10.1088/2041-8205/804/2/L34.

259. S. Le Mouélic, S. Rodriguez, R. Robidel, et al. Mapping polar atmospheric features on Titan with VIMS: from the dissipation of the northern cloud to the onset of a southern polar vortex. Icarus.. 2018;311:371–383. https://doi.org/10.1016/j.icarus.2018.04.028.

260. P. Rannou, S. Le Mouélic, C. Sotin, R.H. Brown Cloud and haze in the winter polar region of Titan observed with the visual and infrared mapping spectrometer onboard Cassini. The Astrophysical Journal. 2012;748(1):4. https://doi.org/10.1088/0004-637x/748/1/4.

261. S.P. Faulk, J.M. Lora, J.L. Mitchell, P.C.D. Milly Titan's climate patterns and surface methane distribution due to the coupling of land hydrology and atmosphere. Nature Astronomy. 2020;4(4):390–398. https://doi.org/10.1038/s41550-019-0963-0.

262. J.M. Battalio, J.M. Lora, S. Rafkin, A. Soto The interaction of deep convection with the general circulation in Titan's atmosphere. Part 2: impacts on the climate. Icarus.. 2022;373. https://doi.org/10.1016/j.icarus.2021.114623.

263. L. Wang, N. Nakamura Covariation of finite-amplitude wave activity and the zonal mean flow in the midlatitude troposphere: 1. theory and application to the Southern Hemisphere summer. Geophysical Research Letters.. 2015;42(19):8192–8200. https://doi.org/10.1002/2015GL065830.

264. L. Wang, N. Nakamura Covariation of finite-amplitude wave activity and the zonal-mean flow in the midlatitude troposphere. part ii: eddy forcing spectra and the periodic behavior in the Southern Hemisphere Summer. Journal of the Atmospheric Sciences.. 2016;73(12):4731–4752. https://doi.org/10.1175/jas-d-16-0091.1.

265. K. Swanson, R.T. Pierrehumbert Nonlinear wave packet evolution on a baroclinicaily unstable jet. Journal of the Atmospheric Sciences. 1994;51(3):384–396. doi:10.1175/1520-0469(1994)051<0384:dccisf>2.0.co;2.

266. I. Orlanski, E.K.M. Chang Ageostrophic geopotential fluxes in downstream and upstream development of baroclinic waves. Journal of the Atmospheric Sciences. 1993;50(2):212–225. doi:10.1175/1520-0469(1993)050<0212:agfida>2.0.co;2.

267. I. Orlanski, J. Sheldon A case of downstream baroclinic development over Western North America. Monthly Weather Review. 1993;121(11):2929–2950. doi:10.1175/1520-0493(1993)121<2929:acodbd>2.0.co;2.

268. K.M. Chang Edmund Downstream development of baroclinic waves as inferred from regression analysis. Journal of the Atmospheric Sciences. 1993;50(13):2038–2053. doi:10.1175/1520-0469(1993)050<2038:ddobwa>2.0.co;2.

269. I. Orlanski, J.P. Sheldon Stages in the energetics of baroclinic systems. Tellus A.. 1995;47(5):605–628. https://doi.org/10.1034/j.1600-0870.1995.00108.x.

270. E.K.M. Chang, S. Lee, K.L. Swanson Storm track dynamics. Journal of Climate. 2002;15(16):2163–2183. doi:10.1175/1520-0442(2002)015<02163:std>2.0.co;2.

271. M. Nakayama, H. Nakamura, F. Ogawa Modulations of storm-track activity associated with the baroclinic annular mode. Journal of Climate.. 2023;36(12):4219–4234. https://doi.org/10.1175/jcli-d-22-0377.1.

272. M. Nakayama, H. Nakamura, F. Ogawa Impacts of a midlatitude oceanic frontal zone for the baroclinic annular mode in the southern hemisphere. Journal of Climate.. 2021;34(18):7389–7408. https://doi.org/10.1175/jcli-d-20-0359.1.

273. R.K. Scott, W.J.M. Seviour, D.W. Waugh Forcing of the Martian polar annulus by Hadley cell transport and latent heating. Quarterly Journal of the Royal Meteorological Society.. 2020;146(730):2174–2190. https://doi.org/10.1002/qj.3786.

274. D.W.J. Thompson, B.R. Crow, E.A. Barnes Intraseasonal periodicity in the Southern Hemisphere circulation on regional spatial scales. Journal of the Atmospheric Sciences.. 2017;74(3):865–877. https://doi.org/10.1175/jas-d-16-0094.1.

275. S. Xue, J. Lu, Y. Qian, Y. Zhang Evidence for coupling between the subseasonal oscillations in the Southern Hemisphere midlatitude ocean and atmosphere. Journal of Geophysical Research: Atmospheres.. 2021;126(4). https://doi.org/10.1029/2020jd033872.

276. Z. Liu, L. Wang Regional features of the 20–30 day periodic behavior in the Southern Hemisphere summer circulation. Geophysical Research Letters.. 2023;50(18).

277. P.L. Read, S.R. Lewis The Martian Climate Revisited—Atmosphere and Environment of a Desert Planet. Springer-Verlag; 2004.

278. G.J. Marshall, D.W.J. Thompson, M.R. van den Broeke The signature of Southern Hemisphere atmospheric circulation patterns in antarctic precipitation. Geophysical Research Letters.. 2017;44(22). https://doi.org/10.1002/2017gl075998.

279. H. Wang Cross-equatorial flushing dust storms and Northern Hemisphere transient eddies: an analysis for Mars year 24. Journal of Geophysical Research: Planets. 2018;123(7):1732–1745. https://doi.org/10.1029/2018je005623.

280. A.D. Toigo, M.I. Richardson, H. Wang, S.D. Guzewich, C.E. Newman The cascade from local to global dust storms on Mars: temporal and spatial thresholds on thermal and dynamical feedback. Icarus.. 2018;302:514–536. https://doi.org/10.1016/j.icarus.2017.11.032.

281. A. El-Said, S.R. Lewis, M.R. Patel Quantifying the atmospheric impact of local dust storms using a martian global circulation

model. Icarus.. 2020;336. https://doi.org/10.1016/j.icarus.2019.113470.

282. J.G. Charney The dynamics of long waves in a baroclinic westerly current. Journal of Meteorology. 1947;4(5):136–162. doi:10.1175/1520-0469(1947)004<0136:tdolwi>2.0.co;2.

283. R. Lorenz The longevity and aspect ratio of dust devils: effects on detection efficiencies and comparison of landed and orbital imaging at Mars. Icarus.. 2013;226(1):964–970. https://doi.org/10.1016/j.icarus.2013.06.031.

284. R.D. Lorenz The weather on Titan. Science.. 2000;290(5491):467–468. https://doi.org/10.1126/science.290.5491.467.

285. R.D. Lorenz, C.A. Griffith, J.I. Lunine, C.P. McKay, N.O. Rennò Convective plumes and the scarcity of Titan's clouds. Geophysical Research Letters.. 2005;32(1):1–4. https://doi.org/10.1029/2004GL021415.

286. E.P. Turtle, J.E. Perry, A.G. Hayes, et al. Rapid and extensive surface changes near Titan's equator: evidence of April showers. Science.. 2011;331(6023):1414–1417. https://doi.org/10.1126/science.1201063.

287. S.P. Faulk, J.L. Mitchell, S. Moon, J.M. Lora Regional patterns of extreme precipitation on Titan consistent with observed alluvial fan distribution. Nature Geoscience.. 2017;10(11):827–831. https://doi.org/10.1038/NGEO3043.

288. Spaulding-Astudillo F.E., Mitchell J.L. (2023). The emergence of relaxation-oscillator convection on Earth and Titan. arXiv. June. <https://arxiv.org>

289. J.T. Seeley, R.D. Wordsworth Episodic deluges in simulated hothouse climates. Nature.. 2021;599(7883):74–79. https://doi.org/10.1038/s41586-021-03919-z.

290. N.J. Lutsko, M.C. Hell Moisture and the persistence of annular modes. Journal of the Atmospheric Sciences.. 2021;78(12):3951–3964. https://doi.org/10.1175/JAS-D-21-0055.1.

291. H. Karyu, T. Kuroda, K. Itoh, et al. Vertical wind-induced cloud opacity variation in low latitudes simulated by a venus GCM. Journal of Geophysical Research.. 2023;128(2).

292. G.P. Williams Jovian dynamics. part iii: multiple, migrating, and equatorial jets. Journal of the Atmospheric Sciences. 2003;60(10):1270–1296. doi:10.1175/1520-0469(2003)60<1270:jdpimm>2.0.co;2.

293. Y. Kaspi, G.R. Flierl Formation of jets by baroclinic instability on gas planet atmospheres. Journal of the Atmospheric Sciences.. 2007;64(9):3177–3194. https://doi.org/10.1175/jas4009.1.

294. T. Schneider, J. Liu Formation of jets and equatorial superrotation on jupiter. Journal of the Atmospheric Sciences.. 2009;66(3):579–601. https://doi.org/10.1175/2008jas2798.1.

295. S.I. Thomson, M.E. McIntyre Jupiter's unearthly jets: a new turbulent model exhibiting statistical steadiness without large-scale dissipation*. Journal of the Atmospheric Sciences. 2016;73(3):1119–1141. https://doi.org/10.1175/jas-d-14-0370.1.

296. Y. Kaspi, E. Galanti, W.B. Hubbard, et al. Jupiter's atmospheric jet streams extend thousands of kilometres deep. Nature.. 2018;555(7695):223–226. https://doi.org/10.1038/nature25793.

297. T. Kuroda, A.S. Medvedev, P. Hartogh, M. Takahashi Semiannual oscillations in the atmosphere of Mars. Geophysical Research Letters.. 2008;35(23). https://doi.org/10.1029/2008gl036061.

298. D. Smith Michael, C. Pearl John, J. Conrath Barney, R. Christensen Philip Thermal Emission Spectrometer results: Mars atmospheric thermal structure and aerosol distribution. Journal of Geophysical Research: Planets.. 2001;106(E10):23929–23945. https://doi.org/10.1029/2000JE001321.

299. R.R. Garcia, T.J. Dunkerton, R.S. Lieberman, R.A. Vincent Climatology of the semiannual oscillation of the tropical middle atmosphere. Journal of Geophysical Research: Atmospheres.. 1997;102(D22):26019–26032. https://doi.org/10.1029/97jd00207.

300. M.P. Baldwin, L.J. Gray, T.J. Dunkerton, et al. The quasibiennial oscillation. Reviews of Geophysics.. 2001;39(2):179–229. https://doi.org/10.1029/1999RG000073.

301. D.G. Andrews On the interpretation of the eliassen-palm flux divergence. Quarterly Journal of the Royal Meteorological Society. 1987;113(475):323–338. https://doi.org/10.1002/qj.49711347518.

302. A.K. Smith, L.A. Holt, R.R. Garcia, et al. The equatorial stratospheric semiannual oscillation and time-mean winds in QBOi models. Quarterly Journal of the Royal Meteorological Society. 2022;148(744):1593–1609. https://doi.org/10.1002/qj.3690.

303. R.J. Reed Zonal wind behavior in the equatorial stratosphere and lower mesosphere. Journal of Geophysical Research.. 1966;71(18):4223–4233. https://doi.org/10.1029/jz071i018p04223.

304. J.R. Holton, W.M. Wehrbein A numerical model of the zonal mean circulation of the middle atmosphere. Pure and Applied Geophysics PAGEOPH.. 1980;118(1):284–306. https://doi.org/10.1007/bf01586455.

305. P.L. Read, A.A. Castrejón-Pita Phase synchronization between stratospheric and tropospheric quasibiennial and semiannual oscillations. Quarterly Journal of the Royal Meteorological Society.. 2012;138(666):1338–1349. https://doi.org/10.1002/qj.1872.

306. D.G. Andrews, M.E. McIntyre Generalized Eliaseen-Palm and Charney-Drazin theorems for waves on axisymmetric mean flows in compressible atmospheres. Journal of the Atmospheric Sciences.. 1978;35(2):175–185.

307. E.A. Ray, M.J. Alexander, J.R. Holton An analysis of the structure and forcing of the equatorial semiannual oscillation in zonal wind. Journal of Geophysical Research Atmospheres.. 1998;103(2):1759–1774. https://doi.org/10.1029/97JD02679.

308. F. Sassi, R.R. Garcia The role of equatorial waves forced by convection in the tropical semiannual oscillation. Journal of the Atmospheric Sciences. 1997;54(15):1925–1942. doi:10.1175/1520-0469(1997)054<1925:TROEWF>2.0.CO;2.

309. T. Kuroda, N. Hashimoto, D. Sakai, M. Takahashi Simulation of the Martian atmosphere using a ccSR/NIES AGCM. Journal of the Meteorological Society of Japan Ser II.. 2005;83(1):1–19. https://doi.org/10.2151/jmsj.83.1.

310. T. Numaguti, S. Nakajima Development of atmospheric general circulation model. Climate System Dynamics and Modeling.. 1995;1–27.

311. B. Stephen, S. Fels Richard Lindzen. The interaction of thermally excited gravity waves with mean flows. Geophysical Fluid Dynamics.. 1974;6(2):149–191.

312. T. Ruan, N.T. Lewis, S.R. Lewis, L. Montabone, P.L. Read Investigating the semiannual oscillation on Mars using data assimilation. Icarus.. 2019;333:404–414. https://doi.org/10.1016/j.icarus.2019.06.012.

313. P. Chatterjee, B.N. Goswami Structure, genesis and scale selection of the tropical quasibiweekly mode. Quarterly Journal of the

Weather Review. 1981;109(4):784–812. doi:10.1175/1520-0493(1981)109<0784:titghf>2.0.co;2.

345. R. Quadrelli, J.M. Wallace A simplified linear framework for interpreting patterns of Northern Hemisphere wintertime climate variability. Journal of Climate. 2004;17(19):3728–3744. doi:10.1175/1520-0442(2004)017<3728:aslffi>2.0.co;2.

346. O. Martínez-Alvarado, L. Montabone, S.R. Lewis, I.M. Moroz, P.L. Read Transient teleconnection event at the onset of a planet-encircling dust storm on Mars. Annales Geophysicae.. 2009;27(9):3663–3676. https://doi.org/10.5194/angeo-27-3663-2009.

347. T. Bertrand, R.J. Wilson, M.A. Kahre, R. Urata, A. Kling Simulation of the 2018 global dust storm on Mars using the NASA Ames Mars GCM: a multitracer approach. Journal of Geophysical Research: Planets.. 2020;125(7). https://doi.org/10.1029/2019je006122.

348. A.D. Del Genio, W.B. Rossow Temporal variability of ultraviolet cloud features in the Venus stratosphere. Icarus.. 1982;51(2):391–415. https://doi.org/10.1016/0019-1035(82)90091-4.

349. W.J. Markiewicz, D.V. Titov, N. Ignatiev, et al. Venus monitoring camera for Venus express. Planetary and Space Science.. 2007;55(12):1701–1711. https://doi.org/10.1016/j.pss.2007.01.004.

350. R. Hueso, J. Peralta, A. Sánchez-Lavega Assessing the long-term variability of Venus winds at cloud level from VIRTIS–Venus express. Icarus.. 2012;217(2):585–598. https://doi.org/10.1016/j.icarus.2011.04.020.

351. K. McGouldrick, C.C.C. Tsang Discovery of a 150 day period in the Venus condensational clouds. Icarus.. 2017;286:118–133. https://doi.org/10.1016/j.icarus.2016.10.005.

352. K. McGouldrick Effects of variation in coagulation and photochemistry parameters on the particle size distributions in the Venus clouds. Earth, Planets and Space.. 2017;69(1). https://doi.org/10.1186/s40623-017-0744-x.

353. A. Yamazaki, M. Yamada, Y.J. Lee, et al. Ultraviolet imager on Venus orbiter Akatsuki and its initial results. Earth, Planets and Space.. 2018;70(1). https://doi.org/10.1186/s40623-017-0772-6.

354. D. Crisp, W.M. Sinton, K.-W. Hodapp, et al. The nature of the near-infrared features on the Venus night side. Science.. 1989;246(4929):506–509. https://doi.org/10.1126/science.246.4929.506.

355. P. Kopparla, A. Seshadri, T. Imamura, Y.J. Lee A recharge oscillator model for interannual variability in Venus' clouds. Journal of Geophysical Research: Planets.. 2020;125(11). https://doi.org/10.1029/2020je006568.

356. R. Barnes Tidal locking of habitable exoplanets. Celestial Mechanics and Dynamical Astronomy.. 2017;129(4):509–536. https://doi.org/10.1007/s10569-017-9783-7.

357. S.R. Kane Atmospheric dynamics of a near tidally locked Earth-sized planet. Nature Astronomy.. 2022;6(4):420–427. https://doi.org/10.1038/s41550-022-01626-x.

358. S. Seager, ed Exoplanets.. University of Arizona Press; 2011. 2nd ed..

359. M. Perryman The Exoplanet Handbook. Cambridge University Press; 2018.

360. J.F. Kasting, D.P. Whitmire, R.T. Reynolds Habitable zones around main sequence stars. Icarus.. 1993;101(1):108–128. https://doi.org/10.1006/icar.1993.1010.

361. J. Scalo, L. Kaltenegger, A.G. Segura, et al. M stars as targets for terrestrial exoplanet searches and biosignature detection. Astrobiology.. 2007;7(1):85–166. https://doi.org/10.1089/ast.2006.0000.

362. M.J. Heath, L.R. Doyle, M.M. Joshi, R.M. Haberle Habitability of planets around red dwarf stars. Origins of Life and Evolution of the Biosphere.. 1999;29(4):405–424. https://doi.org/10.1023/A:1006596718708.

363. T.J. Henry, W.-C. Jao, J.P. Subasavage, et al. The solar neighborhood. XVII. Parallax results from the CTIOPI 0.9 m program: 20 new members of the RECONS 10 parsec sample. The Astronomical Journal. 2006;132(6):2360–2371. https://doi.org/10.1086/508233.

364. R.K. Kopparapu A revised estimate of the occurrence rate of terrestrial planets in the habitable zone around Kepler M-dwarfs. The Astrophysical Journal.. 2013;767(1). https://doi.org/10.1088/2041-8205/767/1/l8.

365. X. Bonfils, X. Delfosse, S. Udry, et al. The HARPS search for southern extra-solar planets. Astronomy & Astrophysics. 2013;549. https://doi.org/10.1051/0004-6361/201014704.

366. C.D. Dressing, D. Charbonneau The occurrence of potentially habitable planets orbiting M dwarfs estimated from the full Kepler dataset and an empirical measurement of the detection sensitivity. The Astrophysical Journal.. 2015;807(1). https://doi.org/10.1088/0004-637x/807/1/45.

367. K.K. Hardegree-Ullman, M.C. Cushing, P.S. Muirhead, J.L. Christiansen Kepler planet occurrence rates for mid-type M dwarfs as a function of spectral type. The Astronomical Journal. 2019;158(2). https://doi.org/10.3847/1538-3881/ab21d2.

368. J.-Y. Yang, J.-W. Xie, J.-L. Zhou Occurrence and architecture of Kepler planetary systems as functions of stellar mass and effective temperature. The Astronomical Journal.. 2020;159(4). https://doi.org/10.3847/1538-3881/ab7373.

369. T.M. Merlis, T. Schneider Atmospheric dynamics of earth-like tidally locked aquaplanets. Journal of Advance Model Earth System.. 2010;2(4):1–17.

370. A. Edson, S. Lee, P. Bannon, J.F. Kasting, D. Pollard Atmospheric circulations of terrestrial planets orbiting low-mass stars. Icarus.. 2011;212(1):1–13. https://doi.org/10.1016/j.icarus.2010.11.023.

371. L. Carone, R. Keppens, L. Decin Connecting the dots - II. Phase changes in the climate dynamics of tidally locked terrestrial exoplanets. Monthly Notices of the Royal Astronomical Society.. 2015;453(3):2412–2437. https://doi.org/10.1093/mnras/stv1752.

372. S. Noda, M. Ishiwatari, K. Nakajima, et al. The circulation pattern and day-night heat transport in the atmosphere of a synchronously rotating aquaplanet: dependence on planetary rotation rate. Icarus.. 2017;282:1–18. https://doi.org/10.1016/j.icarus.2016.09.004.

373. J. Haqq-Misra, E.T. Wolf, M. Joshi, X. Zhang, R.K. Kopparapu Demarcating circulation regimes of synchronously rotating terrestrial planets within the habitable zone. The Astrophysical Journal.. 2018;852(2). https://doi.org/10.3847/1538-4357/aa9f1f.

374. D.E. Sergeev, N.T. Lewis, F.H. Lambert, et al. Bistability of the atmospheric circulation on TRAPPIST-1e. The Planetary Science Journal.. 2022;3(9). https://doi.org/10.3847/psj/ac83be.

375. M. Hammond, N.T. Lewis The rotational and divergent components of atmospheric circulation on tidally locked planets. Proceedings of the National Academy of Sciences. 2021;118(13). https://doi.org/10.1073/pnas.2022705118.
376. D. Faranda, G. Messori, P. Yiou Dynamical proxies of North Atlantic predictability and extremes. Scientific Reports.. 2017;7(1). https://doi.org/10.1038/srep41278.
377. A. Hochman, P. De Luca, T.D. Komacek Greater climate sensitivity and variability on TRAPPIST-1e than Earth. The Astrophysical Journal.. 2022;938(2). https://doi.org/10.3847/1538-4357/ac866f.
378. H. Hersbach, B. Bell, P. Berrisford, et al. The ERA5 global reanalysis. Quarterly Journal of the Royal Meteorological Society.. 2020;146(730):1999–2049. https://doi.org/10.1002/qj.3803.
379. M. Cohen, M.A. Bollasina, P.I. Palmer, et al. Longitudinally asymmetric stratospheric oscillation on a tidally locked exoplanet. The Astrophysical Journal.. 2022;930(2). https://doi.org/10.3847/1538-4357/ac625d.
380. T.J. Dunkerton, D.P. Delisi Climatology of the equatorial lower stratosphere. Journal of the Atmospheric Sciences. 1985;42(4):376–396. doi:10.1175/1520-0469(1985)042<0376:cotels>2.0.co;2.
381. K. Hamilton, A. Hertzog, F. Vial, G. Stenchikov Longitudinal variation of the stratospheric quasi-biennial oscillation. Journal of the Atmospheric Sciences. 2004;61(4):383–402. doi:10.1175/1520-0469(2004)061<0383:lvotsq>2.0.co;2.
382. M. Cohen, M.A. Bollasina, D.E. Sergeev, P.I. Palmer, N.J. Mayne Traveling planetary-scale waves cause cloud variability on tidally locked aquaplanets. The Planetary Science Journal. 2023;4(4). https://doi.org/10.3847/psj/acc9c4.
383. C. Zhang, A.F. Adames, B. Khouider, B. Wang, D. Yang Four theories of the Madden-Julian oscillation. Reviews of Geophysics.. 2020;58(3).
384. J. Yang, N.B. Cowan, D.S. Abbot Stabilizing cloud feedback dramatically expands the habitable zone of tidally locked planets. The Astrophysical Journal.. 2013;771(2). https://doi.org/10.1088/2041-8205/771/2/l45.
385. D.E. Sergeev, T.J. Fauchez, M. Turbet, et al. The TRAPPIST-1 habitable atmosphere intercomparison (THAI). II. moist cases— the two waterworlds. The Planetary Science Journal. 2022;3(9). https://doi.org/10.3847/psj/ac6cf2.
386. M. Braam, P.I. Palmer, L. Decin, M. Cohen, N.J. Mayne Stratospheric dayside-to-nightside circulation drives the 3D ozone distribution on synchronously rotating rocky exoplanets. Monthly Notices of the Royal Astronomical Society.. 2023;526(1):263–278. https://doi.org/10.1093/mnras/stad2704.
387. S. Zhou, A.J. Miller The Interaction of the Madden–Julian oscillation and the arctic oscillation. Journal of Climate.. 2005;18(1):143–159. https://doi.org/10.1175/jcli3251.1.
388. T. Nakamura, Y. Tachibana, M. Honda, S. Yamane Influence of the Northern Hemisphere annular mode on ENSO by modulating westerly wind bursts. Geophysical Research Letters.. 2006;33(7). https://doi.org/10.1029/2005gl025432.
389. C. Cassou Intraseasonal interaction between the Madden–Julian oscillation and the North Atlantic Oscillation. Nature.. 2008;455(7212):523–527. https://doi.org/10.1038/nature07286.
390. M.L. L'Heureux, R.W. Higgins Boreal winter links between the Madden–Julian oscillation and the arctic oscillation. Journal of Climate. 2008;21(12):3040–3050. https://doi.org/10.1175/2007jcli1955.1.
391. H. Lin, G. Brunet, J. Derome An observed connection between the North Atlantic oscillation and the Madden–Julian oscillation. Journal of Climate.. 2009;22(2):364–380. https://doi.org/10.1175/2008jcli2515.1.
392. Z. Wu, B. Wang, J. Li, F.F. Jin An empirical seasonal prediction model of the east Asian summer monsoon using ENSO and NAO. Journal of Geophysical Research: Atmospheres. 2009;114(D18). https://doi.org/10.1029/2009jd011733.
393. S. Chen, B. Yu, W. Chen An analysis on the physical process of the influence of AO on ENSO. Climate Dynamics.. 2014;42(3–4):973–989. https://doi.org/10.1007/s00382-012-1654-z.
394. S. Chen, R. Wu, W. Chen, B. Yu Recent weakening of the linkage between the spring Arctic Oscillation and the following winter El Niño-Southern oscillation. Climate Dynamics.. 2020;54(1–2):53–67. https://doi.org/10.1007/s00382-019-04988-7.
395. R.J. Lillis, M. Mischell, L. Montabone, et al. MOSAIC: a satellite constellation to enable groundbreaking mars climate system science and prepare for human exploration. Planetary Science Journal.. 2021;2(5). https://doi.org/10.3847/PSJ/ac0538.
396. A.L. Shields The climates of other worlds: a review of the emerging field of exoplanet climatology. Astrophysical Journal, Supplement Series.. 2019;243(2). https://doi.org/10.3847/1538-4365/ab2fe7.
397. J. Lustig-Yaeger, V.S. Meadows, A.P. Lincowski The detectability and characterization of the TRAPPIST-1 exoplanet atmospheres with JWST. The Astronomical Journal. 2019;158(1). https://doi.org/10.3847/1538-3881/ab21e0.
398. Morio Nakayama, Hisashi Nakamura, Fumiaki Ogawa Impacts of a Midlatitude Oceanic Frontal Zone for the Baroclinic Annular Mode in the Southern Hemisphere. Journal of Climate. 2021;34(18):7389–7408. doi:10.1175/JCLI-D-20-0359.1.
399. Morio Nakayama, Hisashi Nakamura, Fumiaki Ogawa Modulations of Storm-Track Activity Associated with the Baroclinic Annular Mode. Journal of Climate. 2023;36(12):4219–4234. doi:10.1175/JCLI-D-22-0377.1.